Hidden Players in Marine Pollution: Investigating Polycyclic Aromatic Hydrocarbon Co-metabolism in Marine Bacteria

A Dissertation Presented for the
Doctor of Philosophy
Degree
The University of Tennessee, Knoxville

Jillian Walton
May 2025

DEDICATION

To my grandfather,

who taught me there is more to nature than meets the eye.

ACKNOWLEDGEMENTS

There are many people who I need to thank for helping me get to where I am today. I could write pages on each interaction, conversation, and experience that allowed me to end up here. I don't have endless pages, but I do have a couple.

To Alison, thank you for allowing me to join your lab and supporting my many interests. Thank you for taking a chance on my wild idea to explore PAH co-metabolism. Without your faith in me, I wouldn't be where I am today.

To my lab, specifically, April, Mustafa, Madeline, and Saloni, thank you for making me smile and laugh no matter what experiment was making me bang my head against the bench. You made the grueling hours in lab worth it and helped me leave each day with a smile on my face more often than not.

To Taylor and Ellen, mentoring both of you was the highlight of my graduate school experience. Watching you both grow into brilliant scientists motivated me to do my best as your mentor. I know you both will go on to do amazing things and I am grateful to have been part of your scientific journey.

To Dr. Zachary Burcham, I know your time in our lab was short, but I appreciated your willingness to help and collaborate with me. You brought much needed expertise to our lab, and I am grateful to have you as a co-author.

To Dr. Edward Wright, I know for a fact that this dissertation would not exist without you. Thank you for your patience with me and assistance with HPLC. No matter how stressful experiments became, you were always willing and ready to help me troubleshoot any problems.

To my committee, Dr. Todd Reynolds, Dr. Andrew Steen, and Dr. Jennifer DeBruyn, thank you for being a consistent source of encouragement, giving me your honest feedback even if it was difficult to hear, and for pushing me to live up to my potential.

To Dr. Jean Lim, without your mentorship during my undergraduate training, I wouldn't have believed that I could accomplish what I did in this dissertation. You taught me that failure comes often, success should be celebrated, and there is no problem that cannot be solved by talking it out with someone else. You inspired me to mentor undergraduates of my own, and I hope I was able to live up to your example.

To my dad, we didn't always know I would get here, but I wouldn't be here without you. Thank you for always picking up the phone not knowing if there would be tears or laughs on the other side. You have always been there when I needed you and I will never take that for granted.

To my mom, thank you for supporting my love of science. You have been one of my biggest cheerleaders throughout this entire process.

To my sisters, Jenna and Julia, thank you for being patient with me as I went through this process. Thank you for the joy, the laughs, the inside jokes, and the hugs. I promise to be better at texting back now.

And finally, to my husband, my best friend, and the love of my life, you followed me to Knoxville, leaving behind your friends and your job. You have seen me excited and devastated, curious and overwhelmed, and joyful and anxious, and never once did you leave my side. Thank you for growing with me, humoring me, and loving me.

ABSTRACT

Polycyclic aromatic hydrocarbons (PAHs) are toxic, carcinogenic pollutants that are found in nearly every environment. The recalcitrance of these pollutants makes their removal difficult, but microbial degradation has been investigated as a remediation technique. Marine environments are the final destinations for many PAHs, thus investigating marine microbes able to degrade these compounds is crucial to the mitigation of PAH pollution. While investigation into microbial PAH degraders has been conducted, most studies only focus on sole-metabolism, or the degradation of PAHs not dependent the presence of a labile carbon source. The following work investigates another PAH transformation strategy: co-metabolism. Co-metabolism, as defined in this dissertation, is the degradation of PAHs only in the presence of a labile carbon source. Despite coastal PAH pollution co-occurring with high DOC concentrations, little research has investigated co-metabolism, and even less has focused on co-metabolism within marine environments. Here, I show that PAH co-metabolism appears to be a widespread metabolic strategy among marine bacteria, with evidence from both culture collection isolates and environmental isolates. In addition, this co-metabolism appears to proceed by a different mechanism than sole-metabolism due to the lack of PAH degradation genetic biomarkers in strains capable of co-metabolism. The lack of biomarkers may explain the underrepresentation of co-metabolism PAH degraders in literature as many studies only experimentally investigate sole-metabolism and heavily rely on biomarkers to determine PAH degradation activity. Using a model marine bacterium, *Ruegeria pomeroyi* DSS-3, we found that the mechanism of co-metabolism appears to be carbon source dependent and is likely mediated by non-specific dioxygenases, one of which appears to be common in *Roseobacteraceae* PAH co-metabolizers. Furthermore, evidence in this dissertation suggests that co-metabolism degraders play an important role in natural attenuation of PAHs within non-chronically polluted environments. This dissertation provides a foundation for future research into PAH co-metabolism by establishing methods and contributing to the known diversity and ecology of marine bacterial PAH co-metabolizers.

TABLE OF CONTENTS

LIST OF TABLES

LIST OF APPENDIX TABLES

LIST OF FIGURES

LIST OF APPENDIX FIGURES

LIST OF ATTACHMENTS

Table B.3.4 Tn5 Mutant Insertion Location

(Table_B.3.4_Tn5_Mutant_Insertion_Location.xlsx)

Table B.3.6 SPO3678 BLAST Results from JGI IMG

(Table_B.3.6_SPO3678_BLAST_Results_from_JGI_IMG.txt)

Table B.3.7 FoldSeek Search Results for SPO3678 ColabFold Model

(Table_B.3.7_FoldSeek_Search_Results_for_SPO3678_ColabFold_Model.json)

Table C.4.4 Isolate Information (Table_C.4.4_Isolate_Information.xlsx)

Table C.4.5 Assembly Metrics (Table_C.4.5_Assembly Metrics.csv)

Appendix D Supplemental Materials (Appendix_D_Supplemental_Materials.docx)

CHAPTER 1 INTRODUCTION

Polycyclic aromatic hydrocarbon properties and distribution

Polycyclic aromatic hydrocarbons (PAHs) are persistent organic pollutants constructed of fused benzene rings. The pi-distributed electrons of the aromatic rings increase the stability and hydrophobicity of these pollutants. Their stability in turn decreases their bioavailability, contributing to their recalcitrance in the environment (1). PAHs are split into two categories based on the number of rings: low-molecular weight (LMW; <4 rings) and high-molecular weight (HMW; ≥4 rings) (**Figure 1.1**). Stability and hydrophobicity increase with increasing molecular weight, whereas bioavailability decreases with increasing molecular weight. PAHs are formed through pyrogenic and petrogenic processes. Pyrogenic PAHs occur from the combustion of organic carbon, whereas petrogenic PAHs originate from petroleum (2). These compounds are distributed in the atmosphere, soil, and water, and can enter the environment as byproducts of anthropogenic (e.g., crude oil, industrial wastewater, and solid waste combustion) and natural (e.g., volcanic eruptions and forest fires) processes (**Figure 1.2**) (3, 4).

Not only are these compounds recalcitrant in the environment, but many are also carcinogenic, mutagenic, and toxic. Over 100 known PAHs are present in the environment, with 16 listed on the U.S. Environmental Protection Agency's Priority Pollutant List (**Figure 1.1**) (2). In humans these compounds cause cancer, cardiovascular problems, adverse birth effects, and immune system suppression. Much like their other chemical properties, toxicity also increases with increasing molecular weight (2). While some evidence of bioaccumulation of these compounds has been reported, PAHs do not appear to undergo biomagnification in higher trophic levels due to detoxifying enzymes, such as cytochrome P450 monooxygenases able to oxidize PAHs (5, 6). In addition to the hazard of the parent PAH compounds, the degradation intermediates, such as epoxides and dihydrodiols, form covalent bonds with proteins and genetic material, leading to cell damage (2, 7). Thus, while higher trophic level organisms, such as humans, have enzymes that oxidize PAHs, the intermediates from this oxidation can cause further negative health effects rather than reducing toxicity.

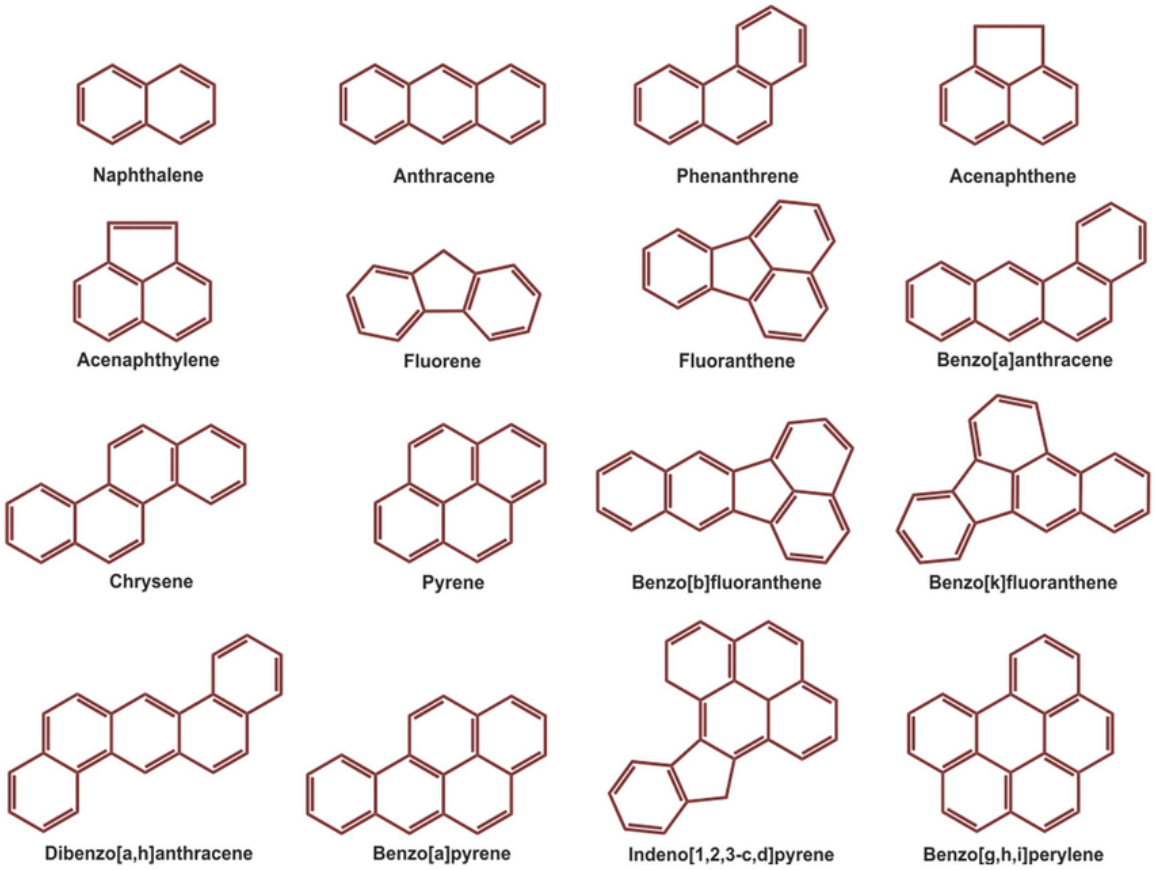

Figure 1.1: Sixteen polycyclic aromatic hydrocarbons listed on the Environmental Protection Agency's Priority Pollutant List. ("Structure of the 16 PAHs enlisted as priority pollutants by US EPA" by Ghosal et al., 2016 in Frontiers Microbiology is licensed under CC-BY 4.0; https://doi.org/10.3389/fmicb.2016.01369) (2)

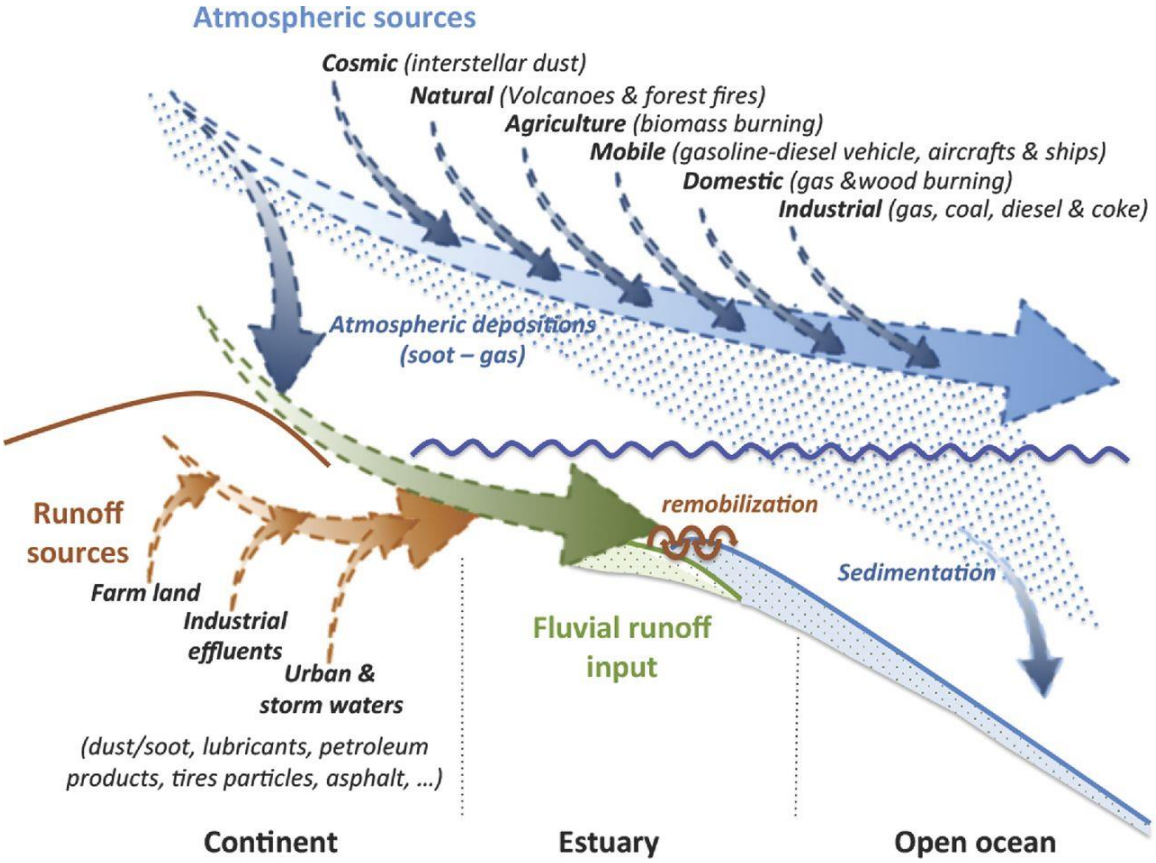

Figure 1.2: Natural and anthropogenic sources of marine pyrogenic polycyclic aromatic hydrocarbon pollution. ("Main sources of pyrogenic PAHs entering the marine environment." by Duran & Cravo-Laureau, 2019 in FEMS Microbiology Reviews is licensed under CC-BY 4.0; https://doi.org/10.1093/femsre/fuw031) (4)

Polycyclic aromatic hydrocarbons in marine ecosystems

Coastal communities, such as salt marshes, are ecologically productive areas that provide a plethora of ecosystem services (e.g., coastal protection, water purification, and carbon sequestration). Marine ecosystems act as a sink for PAH pollution with these compounds entering from terrestrial runoff, atmospheric deposition, and direct sources (e.g., industrial wastewater and oil spills). Within marine ecosystems, PAH pollution is commonly reported at oil and petroleum spill sites, since crude oil contains 0.2-7% PAHs by weight (1, 8). PAH concentration ranges from 0.0003 to 42,350 μg/L in the water column and 0 to 1.266 kg/kg in sediment in contaminated aquatic sites around the world (9). In addition to their high abundance in crude oil, higher molecular weight PAHs increase in relative abundance at these polluted sites as more bioavailable LMW compounds are degraded, leaving persistent PAH pollution in local ecosystems (10). Furthermore, PAHs are more toxic and persistent than other crude oil components, causing long-term environmental damage (11).

For marine life, PAHs can bioaccumulate in fish and bivalve species and result in similar health effects as in humans with the addition of deformities, cataracts, and reproductive cycle disruption (6, 12). Coastal PAH pollution can also cause aboveground and belowground vegetation death and decreased ecosystem recovery, ultimately resulting in habitat loss and increased shoreline erosion (10, 13). The microflora also has reports of PAH pollution affecting the community composition after exposure to PAHs. At marine crude oil spill sites, *Alcanivorax* spp. and *Cycloclasticus* spp. commonly dominate microbial communities but only *Cycloclasticus* spp. have been reported to degrade the aromatic fraction of crude oil (11). Known PAH degraders, such as *Mycobacterium* spp., *Sphingomonas* spp., *Pseudomonas* spp. and *Rhodococcus* spp. are commonly found at PAH polluted sites (14, 15). While microflora community shifts have been reported, these shifts do not describe the degradation potential of the organisms or the mechanisms of degradation that may be occurring. Since coastal marine ecosystems have constant influx of PAH through various sources, understanding natural attenuation by both abiotic and biotic means can help to sustain the longevity of these ecosystems.

While LMW PAHs, such as naphthalene readily volatize from marine surface water, most PAHs of higher molecular weight cannot volatize at ambient temperatures (7). PAHs readily adsorb to organic and inorganic particulate matter and sink to the sediment, thus increasing the

concentration of PAHs in marine sediment compared to the water column (1, 4, 16). One study that investigated PAH transport through the water column found that each day 3.1%–6.7% of particulate PAHs sank to the ocean floor in the Gulf of Mexico (17). During this vertical transport, particulate PAHs decrease due to desorption and degradation. Sediment adsorbed PAHs can also be remobilized in the water column by processes that disturb the sediment (e.g., currents, storms, bioturbation, dredging) (4). Beyond adsorption of PAHs, abiotic factors in marine environments affect PAH concentrations and bioavailability. While photooxidation of PAHs appears to happen rapidly in surface water, the sinking of PAHs prevents abiotic degradation by this process (18). Photooxidation produces oxy-PAHs, which can be more toxic than the parent compounds (4). Other than photooxidation, abiotic transformation of PAHs in marine environments has not been extensively studied. Chemical oxidation of PAHs has been studied in soils, where reactive oxygen species produced by sediment particles can transform these compounds. (19).

Microbial degradation of polycyclic aromatic hydrocarbons

While a plethora of chemical and physical removal methods have been established for PAH environmental remediation, microbial degradation of PAHs has been proposed as a more efficient, sustainable, and cost-effective solution (1). Due to the recalcitrance of PAHs, few microbes can overcome the metabolic hurdle they pose, so investigating microbes and pathways that degrade PAHs is of particular interest. PAHs can be degraded via aerobic and anaerobic metabolic processes, but the focus of this dissertation will be on aerobic (oxygen-dependent) degradation. Furthermore, while some fungi and archaea degrade PAHs, this dissertation will only discuss bacterial PAH degradation (2, 7).

Bacterial polycyclic aromatic hydrocarbon degraders

A variety of taxa have been reported to degrade PAHs as a sole carbon and energy source. *Mycobacterium* spp., *Rhodococcus* spp. *Pseudomonas* spp., *Sphingomondaceae* strains, and many others have been well studied both for their ability to degrade PAHs (e.g., enzymes and mechanisms of degradation) (20). *Mycobacterium* spp. have received significant study due to their prevalence in and contribution to PAH-degrading soil communities (20, 21). Specifically, *Mycobacterium vanbaalenii* PYR-1 was one of the first organisms found to degrade PAHs and has undergone extensive study since its isolation from sediment in a chronically polluted bay

(Figure 1.3) (22). Its complete PAH metabolic pathway has been identified; conversely other organisms have not received the same level of study (23). Thus, investigations into other bacterial degradation mechanisms and pathways are needed to explore the landscape of PAH biodegradation.

Alphaproteobacteria are metabolically versatile, thus many PAH degraders have been discovered in this phylum. Most of these bacteria belong to the *Sphingomondaceae* family (24). Within the family, the PAH degrative gene clustered differ between surface and subsurface isolates. In addition, genes involved in PAH degradation for family members are generally plasmid-associated (25). While some Betaproteobacteria have been reported to degrade PAHs, Gammaproteobacteria are more well-known for their PAH degradation ability, specifically their ability to degrade HMW PAHs (24). Several *Pseudomonas* spp. and *Cyclocasticus* spp. show high degradation efficiency of pyrene (24). Outside of Proteobacteria, much of the study of Actinobacteria has been focused on *Mycobacterium* spp. as mentioned above, but a variety of *Rhodococcus* spp. have also been shown to degrade PAHs. Specifically, the naphthalene (a LMW PAH) degradation pathway within *Rhodococcus* spp. has been well investigated and these strains rely on three structural genes for the degradation of this compound (2). Numerous *Bacillus* spp. have also been reported to degrade pyrene, a HMW PAH (24).

While utilizing a single organism for PAH degradation has shown promise, microbial consortiums of PAH degraders are also of interest as degradation efficiencies and rates can increase by utilizing multiple bacteria (2). Consortiums can have a drastic effect on PAH degradation with degradation rates increasing from ~50% degradation to nearly 100% (26, 27). Such increased degradation is attributed to cross-feeding, where PAH degradation intermediates can act as substrates for other organisms (28). Beyond PAH metabolism, mixed communities can also overcome the inhibitory effects of PAHs or increase the solubility of PAHs through biosurfactant production (26, 29). In addition, different bacterial groups can degrade different PAHs, allowing multispecies consortia to increase degradation efficiency of mixed PAHs (14, 30). Despite the plethora of bacteria and consortium investigated for their ability to degrade PAHs, most studies only focus on the ability of PAHs to be used as a primary growth substrate without considering the presence of other degradation mechanisms.

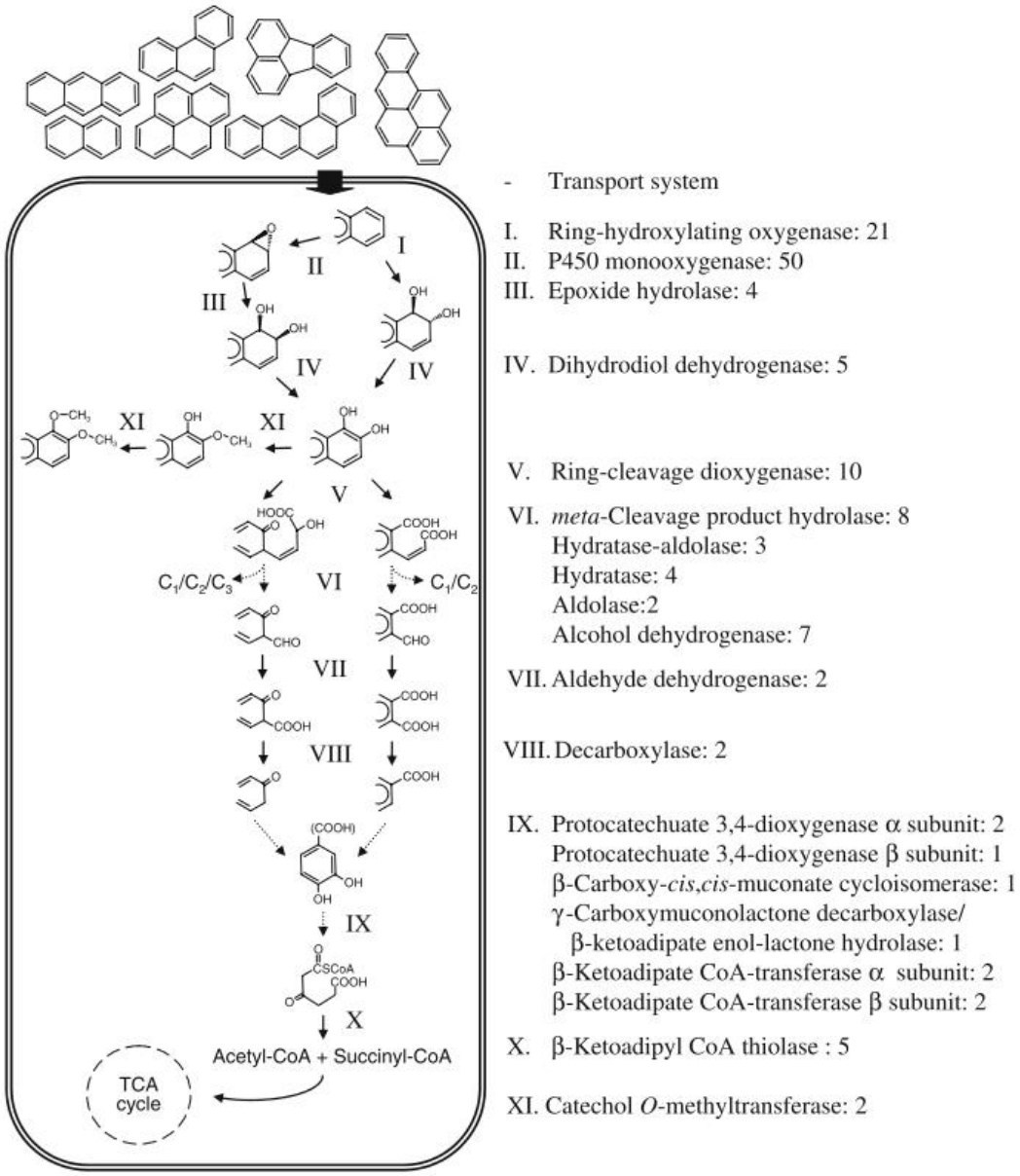

Figure 1.3: Proposed *Mycobacterium vanbaalenii* PYR-1 polycyclic aromatic hydrocarbon degradation pathway. ("Overview of degradative pathway for HMW PAHs. Solid arrows indicate one-step reactions and dashed arrows show two or more steps. Roman numbers represent enzymatic steps in the pathway. Enzyme names are shown with the number of genes identified in the PYR-1 genome." by Kim et al., 2008 in Biodegradation licensed under CCC 5899420508390) (38)

Bacterial polycyclic aromatic hydrocarbon transport

Despite the interest in bacterial PAH degradation, few studies have been conducted on how PAHs enter the cell. Unlike fungi, bacterial degradation of PAHs requires the compounds to be transported inside the cell as the enzymes that degrade these compounds are generally intracellular. From what little research has been conducted, PAHs are able to enter bacteria mainly through passive diffusion (32). Some bacteria also can actively transport PAHs into the cell through transporters, but much evidence is restricted to transcriptional analysis only. For instance, both *Burkholderia vietnamiensis* G4 and *Mycolicibacterium* spp. strains, had several transporters induced during PAH exposure and degradation (29, 31). This evidence aligns with PAH transport experiments conducted with *Arthobacter* sp. Sphe3, where its active uptake system utilizing proton motive force is induced by phenanthrene (32). While these active transport systems exist, little is known about if such transport systems are conserved among different bacterial species or not. In addition to this active transport into the cell, some bacteria also contain efflux pumps to remove PAHs from the cell. *Pseudomonas fluorescens* LP6a can passively transport PAHs into the cell, but also has an efflux pump that is dependent on the intracellular concentration of PAHs. This mainly occurs in the presence of another carbon source when PAHs are not being used as a carbon and energy source, similar to the active transport system in *Arthobacter* sp. Sphe3 (31, 33).

Bacteria also change their membrane structure in the presence of PAHs due to the accumulation of PAHs in bacterial membranes. Evidence suggests that only PAHs with fewer than six rings, regardless of configuration are capable of membrane accumulation (34). When PAHs are present in bacterial membranes, they disrupt the hydrogen and dipole-dipole bonds in the lipid bilayer, thus changing the structure and function of the membrane. To overcome this, bacteria will modify their membrane lipids to make the membrane more hydrophobic and reduce fluidity (31, 35). Specifically, such membrane changes have been well documented in *Mycobacterium* spp., where they decrease the mycolic acid and increase unsaturated fatty acid proportions of their membranes to compensate for PAH accumulation.

Bacterial polycyclic aromatic hydrocarbon degradation pathways

Three types of PAH biodegradation exist: sole-metabolism which is growth-linked degradation and results in the complete degradation of PAHs to H_2O and CO_2, co-metabolism which is non-

growth linked and requires a more labile carbon source for PAH degradation to occur, and detoxification which is non-growth linked and results in a structural change to the PAH (36). Most canonical sole-metabolism pathways, such as the one present in *M. vanbaalenii* PYR-1, follow similar degradation mechanisms. *M. vanbaalenii* PYR-1 shows the characteristic catabolic funneling effect seen in PAH and monocyclic aromatic compound degradation pathways where a limited number of ring-cleaving enzymes break down a plethora of aromatic compounds (37). A common feature of PAH degradation is initial hydroxylation of an aromatic ring (via dioxygenase or monooxygenase) and subsequent re-aromatization and ring cleavage reactions, resulting in monocyclic intermediates that can be funneled to the TCA cycle (**Figure 1.3**; **Figure 1.4**) (1). The initial ring-hydroxylation is conducted by PAH ring-hydroxylating dioxygenases with various specificities. These multimeric dioxygenases have two subunits: large iron-sulfur protein (alpha) and a small iron-sulfur protein (beta) (40). The alpha subunit is involved in substrate specificity and dioxygenases have been reported to have both wide and narrow specificity for PAHs. This initial hydroxylation is the rate limiting step of the pathway as it destabilizes the ring for further downstream enzymatic attack. After the addition of hydroxyl groups, the ring re-aromatizes before getting cleaved. Once the ring is cleaved, a substituent is removed by a PAH hydratase-aldolase (38, 41, 42). Generally, a pyruvate molecule is removed and then funneled to the TCA cycle (43). The following reactions continue until a single ring is left, generally in the form of salicylate or phthalate (2, 23). Depending on the organism, phthalate is converted to protocatechuate, proceeding down the protocatechaute (*pca*) degradation pathway, and salicylate is either converted to gentisate or catechol, proceeding down the gentisate (*gen*) or catechol (*cat*) degradation pathways, respectively. Evidence also suggests that PAHs can be broken down into benzoate or *p*-hydroxybenzoate and then funneled through the *cat* and *pca* pathways, respectively. In downstream pathways, these monocyclic aromatic compounds are converted to TCA cycle intermediates and may be used as primary growth substrates (**Figure 1.4**) (39).

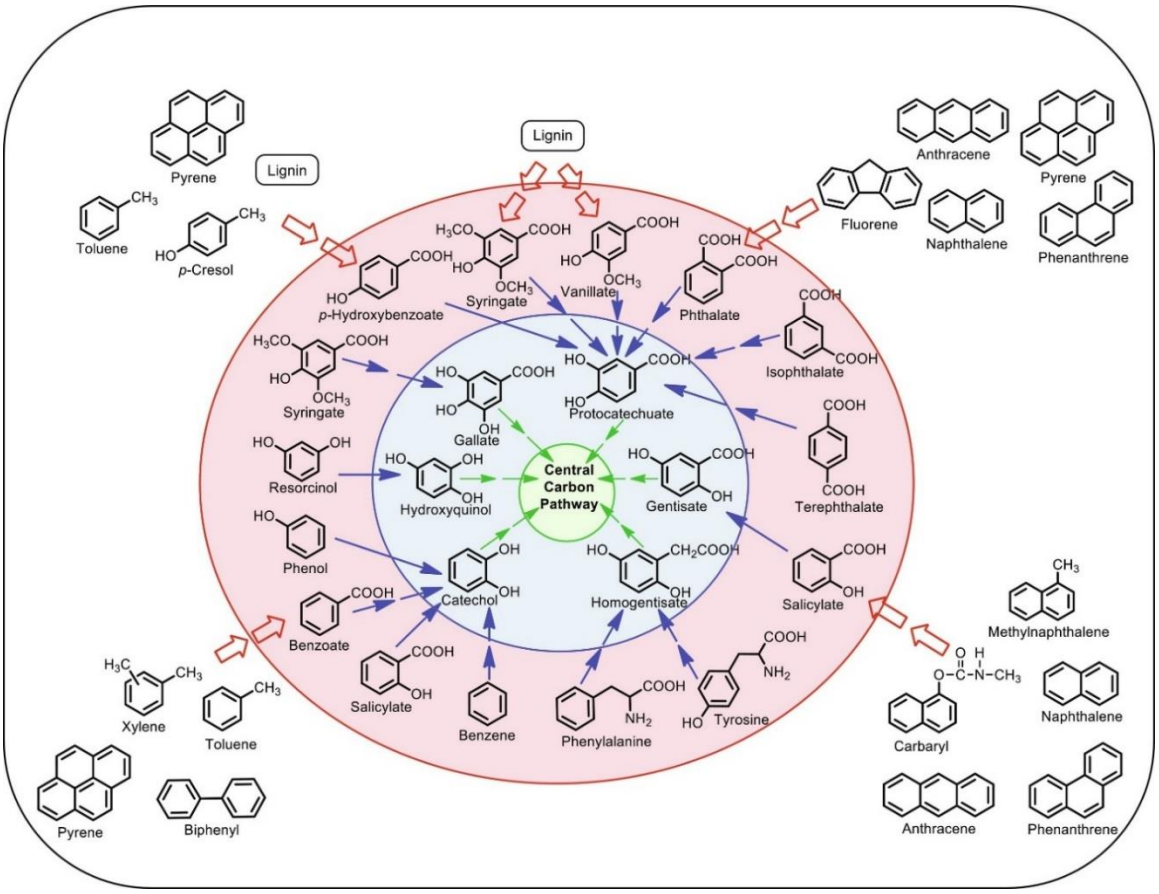

Figure 1.4: Poly- and monocyclic aromatic compound degradation through intermediate products. ("Aerobic routes for the degradation of aromatic compounds: Polycyclic aromatic compounds are metabolized to mono-aromatic intermediates (red circle and open arrow) which are further funneled through limited central common aromatic intermediates (blue circle and thick arrow) to central carbon pathway aliphatic intermediates (green circle and thin arrow)." by Phale et al., 2020 in Advances in Applied Microbiology licensed under CCC 5899421110711) (39)

Bacteria can also detoxify PAHs instead of pursing degradation via the addition of substituents to form glucuronide, reduced glutathione, sulfate, or methyl conjugates. One example of this is in *M. vanbaalenii* PYR-1 that contains a catechol *o*-methyltransferase and form an *o*-methylated PAH derivative (44). This forms a dead-end product, where oxidation cannot occur due to the methoxy groups (3). While bacterial detoxification of PAHs exists, little investigation has occurred outside of *M. vanbaalenii* PYR-1.

Even within a single microbe, diverse genetic pathways to degrade PAHs may exist, suggesting that PAH degradation pathways arise from adaptation of existing pathways (20). Even though many pathways have evolved, there are conserved genetic biomarkers for degradation: PAH ring-hydroxylating dioxygenases (RHDs), PAH hydratase-aldolases, and monocyclic aromatic compound dioxygenases (**Table 1.1**) (42, 45, 46).

PAH RHDs have been commonly used as genetic biomarkers for PAH degradation because they are the rate limiting step in PAH degradation. Most often the large alpha subunit is used as the biomarker of interest (47). Unfortunately, PAH RHDs, and even dioxygenases as a group, are highly similar despite their differences in substrate specificity, thus many dioxygenases identified as potential PAH RHDs likely act on different compounds. In terms of substrate specificity, the active site size can predict the range of PAHs it acts on. Smaller active sites generally bind LMW PAHs and larger active sites bind HMW PAHs (47). Examples of PAH RHDs include the PahA, NahA, NarA, and NidA enzymes (**Table 1.1**). Recently, PAH hydratase-aldolases involved later in the upper pathway of PAH degradation, have been suggested as a more specific and conserved biomarker for PAH degradation (42). The conservation of this enzyme may come from its function in the PAH degradation pathway, where it results in the release of at least one carbon atom containing compound to be funneled into the TCA cycle. This is the first step where the cell gains energy from the costly breakdown of PAHs (42). The distribution of this biomarker has also been shown to correlate with PAH-pollution concentration and *pahE* gene abundance was significantly positively related to PAH removal rate (48, 49). While not directly used as a biomarker, monocyclic aromatic dioxygenases, such as those involved in *cat* and *pca* pathways are used as evidence of PAH funneling to the TCA cycle. Since these enzymes act on a variety of PAH intermediates as well as plant-derived aromatic

Table 1.1: PAH biomarkers used to assess PAH degradation potential in bacteria.

Protein	Type	Substrate	Pathway	Citation
PahAc	Ring-hydroxylating dioxygenase	PAH	Upper	Liang et al., 2019 (50)
PahE	Hydratase-aldolase	(3E)-4-(2-hydroxyphenyl)-2-oxobut-3-enoate	Upper	Liang et al., 2019 (50)
NarAa	Ring-hydroxylating dioxygenase	PAH	Upper	Huang et al., 2023 (45)
NarC	Hydratase-aldolase	(3Z)-4-(2-carboxyphenyl)-2-oxobut-3-enoate	Upper	Huang et al., 2023 (45)
NidA	Ring-hydroxylating dioxygenase	PAH	Upper	Huang et al., 2023 (45)
PhdG	Hydratase-aldolase	(E)-4-(1-hydroxynaphthalen-2-yl)-2-oxobut-3-enoate	Upper	Huang et al., 2023 (45); LeVieux et al., 2016 (42)
NahAc	Ring-hydroxylating dioxygenase	PAH	Upper	Huang et al., 2023 (45)
NahE	Hydratase-aldolase	(3E)-4-(2-hydroxyphenyl)-2-oxobut-3-enoate	Upper	Huang et al., 2023 (45)
PcaH/G	Ring-cleavage dioxygenase	Protocatechuate	Lower	Zhang et al., 2019 (51)
PcaA/LigB	Ring-cleavage dioxygenase	Protocatechuate	Lower	Zhang et al., 2019 (51)
CatA	Ring-cleavage dioxygenase	Catechol	Lower	
CatE/YfiE	Ring-cleavage dioxygenase	Catechol	Lower	

compounds, their presence alone cannot determine whether an organism is able to degrade PAHs (**Table 1.1**; **Figure 1.3**) (50).

Co-metabolism, nutrient requirements, and biostimulation of PAH degradation

While the presence of another carbon source can prevent active transport of PAHs, it also can increase or stimulate PAH degradation. Recent evidence suggests that co-metabolism, or the degradation of PAHs only in the presence of a more labile carbon substrate, may be a prevalent metabolic strategy for the degradation of PAHs (36). The lack of catabolite repression in some PAH degradation pathways is unique as other aromatic compound transformations are generally under catabolite repression (39). Most studies investigating co-metabolism in bacteria have focused solely on PAHs with a LMW PAH used to increase degradation of a HMW PAH, rather than using a non-PAH carbon source (51, 52). Recently more study has focused on the ability of non-PAH carbon sources to stimulate PAH co-metabolism. Vanillate, yeast extract, tryptone, peptone, glucose, starch, sucrose, sodium succinate, and sodium citrate have all been shown to increase bacterial degradation of HMW PAHs (51, 53–55). The mechanism of this co-metabolism is currently unknown, but several explanations exist. One explanation, not considered "true" co-metabolism, is that by providing a more labile carbon source, bacterial biomass increases, thus increasing degradation (55). While some PAH degradation pathways appear to be under catabolite repression, PAH co-metabolism pathways do not appear to be regulated by catabolite repression (56–58). Other hypotheses suggest that bacteria that co-metabolically degrade PAHs likely are not receiving a direct benefit from degradation and may only be involved in the initial ring-hydroxylating step of PAH degradation (54). Another line of evidence suggests that bacterial PAH mineralization increases even with a more labile carbon source present (53). Whether this co-metabolic transformation allows bacteria to garner energy from PAHs or acts as a detoxification mechanism for PAHs is still unknown. Currently, co-metabolism appears to be a promising mechanism to stimulate PAH degradation, but further investigation into the ecology and mechanisms co-metabolism is needed.

Beyond additional carbon substrates, low nutrient concentrations (N and P) can inhibit degradation, as can high concentrations (2). Nitrogen is commonly limited in hydrocarbon contaminated environments where PAHs are commonly found, making it necessary for nitrogen amendments or nitrogen fixing by other bacteria to stimulate PAH degradation (11). An example

of this cross feeding can be seen with *Paracoccus aminovorans* HPD-2, a PAH degrading strain, and *Azotobacter chroococcum* HN, a nitrogen fixing strain, where pyrene degradation was increased in co-culture versus a *P. aminovorans* HPD-2 culture (59). Stimulating degradation by adding additional nutrients has also been shown to increase PAH degradation. Adding a general NPK fertilizer (15:15:15) increased pyrene degradation for a variety of marine strains (51). For soil bacteria and Fungi, a 10:1 C:N ratio was found to increase PAH degradation the most compared to other C:N ratios (54). A 100:10:1 C:N:P molar ratio was found to stimulate PAH degradation in both *Sphingomonas* sp. strains and *Mycobacterium* sp. strains in soil (60). Similar results were found for an enriched consortium of marine bacteria where the C:N ratio significantly affected biodegradation of phenanthrene and fluorene (61). While nutrient addition is a well-known biostimulation strategy, most of the work has been focused on soil ecosystems rather than marine ecosystems.

Biostimulation of bacteria to degrade PAHs depends on both nutrient addition as well as the addition of substrates that alter the solubility of PAHs. Humic acids have been shown to increase PAH solubility, mineralization, and diffusion of PAHs in *Mycobacterium* spp. (62, 63). Humic acids have surfactant-like properties that increase the bioavailability of PAHs (63). Surfactants, such as Tween-80 and Triton X-100, have been shown to increase PAH degradation by increasing their solubility (64). In addition to commercially produced surfactants, several bacteria produce biosurfactants, such as glycolipids, lipopeptides, surfactins, lichenyins, and phospholipids (64). Despite their ability to increase the bioavailability of PAHs, at certain concentrations they can also inhibit microbial activity or be used as a growth substrate instead of PAHs (64, 65). Surfactants have been shown to increase degradation of PAHs in a variety of bacteria, including *Mycobacterium* sp., *Sphingomonas paucimobilis* EPA 505, *Lysinibacillus* sp. AK1, *Kocuria flava* AK6, *Nocardioides* sp. AK9, *Staphylococcus* sp. A14, *Bacillus* spp., and *Arhtrobacter* sp. AK5 (65–67).

The effect of temperature, pH, salinity, and oxygen on PAH degradation

Beyond nutrient availability, surfactant production, and PAH bioavailability, PAH degradation efficiency and degradation rate depends on a variety of environmental factors (2). As temperature increases, PAH solubility increases. Higher temperatures within the optimal growth temperature range of a microbe will generally result in increased degradation of PAHs (2).

Despite warmer temperatures increasing PAH degradation, microbial PAH degradation can still occur at low temperatures (0-5°C) (68). Little research has investigated the effect of pH on PAH degradation. Of those studies, most focus on soil and sediment bacteria, so the broad effect of pH on PAH degradation is currently unknown (61, 69). Since PAHs are degraded intracellularly, it is likely that external pH does not play a large role in degradation of PAHs but could influence the bioavailability of PAHs (33). For instance, pH can influence the ability of surfactants to increase the solubility of PAHs, but the impact of pH is inconsistent in present studies (64). Despite marine environments being a sink for PAHs, PAH degradation generally decreases with increasing salinity (70, 71). Prior adaptation to environmental conditions may also lead to PAH degradation under higher salinities (61, 72). Oxygen is required for PAH RHDs in aerobic PAH degradation; thus, the availability of oxygen can further limit the rate-limiting step for PAH degradation. A common biostimulation technique involves injecting air into the contaminated site to increase biological degradation (2). Understanding how these different factors influence PAH degradation can assist in increasing PAH degradation *ex situ* and *in situ.*

***Roseobacteraceae*: A prevalent marine Alphaproteobacterial family**

Members of the *Roseobacteraceae* family of bacteria are prevalent in marine microbial communities and are most abundant in productive regions, including coastal marine ecosystems where they can make up to 25% of bacterial communities (73). While new members are constantly being identified, the family contains over 320 species and over 120 genera (74). Collectively, *Roseobacteraceae* members display tremendous metabolic and genetic diversity, even among closely related strains (74, 75). The metabolic capabilities displayed by members allow them to play a central role in marine carbon and sulfur cycles (73). As a family, *Roseobacteraceae* are found in high salinity environments, can utilize dimethylsulfoniopropionate, and have acyl-homoserine lactone-based quorum sensing systems (74).

Roseobacteraceae aromatic compound degradation

Many family members are adept at transforming aromatic compounds and possess numerous ring-cleaving pathways for their complete degradation (i.e. *pca* protocatechuate *ortho*-cleavage, *gdo* gentisate *ortho*-cleavage, *hgd* homoprotocatechuate *meta*-cleavage, *box* benzoyl-CoA, and *paa* phenylacetyl-CoA pathways). These monocyclic aromatic compounds pose a metabolic

hurdle for many bacteria due to their stability in the environment and their toxicity to bacteria. Furthermore, the degradation of these compounds proceeds through catabolic funneling, where there are few ring-cleaving enzymes with a broad substrate specificity. *Roseobacteraceae* strains typically employ these pathways to degrade plant-derived aromatic compounds (e.g., 4-hydroxybenzoate, vanillate, and coumarate); however, mounting evidence indicates that group members may also degrade anthropogenic aromatic compounds, such as PAHs (**Figure 1.4**) (39, 75, 76).

Roseobacteraceae polycyclic aromatic hydrocarbon degradation

Marine bacteria have been investigated as a potential source of diverse PAH degraders due to the stress of changing environmental conditions they must adapt to (77). Microbial adaptation can confer biodegradative ability through community composition shifts, mutations, horizontal gene transfer, and recombination events (36). Select *Roseobacteracae* members have already been investigated for their ability to degrade PAHs (**Table 1.2**). For instance, *Celeribacter indicus* P73 and *Celeribacter persicus* SBU1 showed degradation of several PAHs, suggesting that *Celeribacter* spp. strains may have adapted to degrade PAHs (78, 79). A more recent study showed pyrene, phenanthrene, and benzo[a]pyrene degradation by *Ruegeria pomeroyi* DSS-3, *Dinoroseobacter shibae* DFL 12, and *Pelagibacter bermudensis* HTCC2601, as well as several *Roseobacteraceae* environmental isolates (76). This study also revealed that some *Roseobacteraceae* members increase their PAH degradation rate in the presence of more labile carbon sources, likely attributed to PAH co-metabolism (76). Broad phenanthrene degradation capabilities and putative PAH degrading enzymes have also been identified for the *Roseovarious* genera (80). A new species of *Lutimaribacter*, *L. degradans* sp. nov, has been proposed with the identification of three strains able to degrade at least one PAH (81). Furthermore, a variety of environmental isolates with close phylogeny to this family have also shown the ability to degrade PAHs (61, 82, 83). In addition to these *ex-situ* investigations, several studies have demonstrated an increase in *Roseobacteraceace* relative abundance in areas with oil contamination, both *in situ* and *ex situ* (82, 84, 85). While several genera have been initially screened on PAHs (**Table 1.2**), the *Roseobacteraceae* family has incredible genetically and metabolically diversity, underscoring the need to investigate the PAH degrading capabilities of a plethora of genera to determine if PAH degradation is a clade-wide characteristic (86, 87).

Table 1.2: Experimentally determined *Roseobacteraceae* isolate PAH degradation.

Strain	PAH Screened	Citation
Celeribacter indicus P73	biphenyl; naphthalene; 2-methylnaphthalene; 2,6-dimethylnaphthalene; acenaphthene; anthracene; phenanthrene; dibenzothiophene; dibenzofuran; fluorene; 4-methyldibenzothiophene; fluoranthene	Cao et al., 2015 (89)
Ruegeria pomeroyi DSS-3 *Pelagibacter bermudensis* HTCC2601 *Dinoroseobacter shibae* DFL 12	pyrene; phenanthrene; benzo[a]pyrene	Zhou et al., 2020 (77)
Celeribacter persicus SBU1	fluorene; phenanthrene	Shahriari Moghadam et al., 2014 (62)
Citreicella thiooxidans DLFJ3-3 *Celeribacter neptunius* DIFJ8-2	Crude oil	Wang et al., 2014 (83)
Roseovarius sp. SCSIO 43702 *Roseovarius indicus* *Roseovarius pacificus* *Roseovarius atlanticus* *Roseovarius nanhaiticus* *Roseovarius* sp. GCL8 *Roseovarius spongiae* *Roseovarius nitrareducens* *Roseovarius salinarum*	phenanthrene	Zhang et al., 2022 (81)
Lutimaribacter degradans sp. nov EGI FJ00013	phenanthrene	Gao et al., 2023 (82)

Table 1.2 Continued

Lutimaribacter degradans sp. nov EGI FJ00014	naphthalene; benzo[b]fluorathene; benzo[a]fluoranthene; pyrene; phenanthrene	Gao et al., 2023 (82)
Lutimaribacter degradans sp. nov EGI FJ00015	2-methylnaphthalene; anthracene; benzo[b]fluorathene; benzo[a]fluoranthene; acenaphtylene; pyrene; fluorene; phenanthrene; acenaphthene	Gao et al., 2023 (82)

Despite the initial investigations into *Roseobacteraceae* PAH degradation, little is known about what genes/proteins are involved in these pathway(s). The only strain whose degradation

pathway has begun to be explored is *C. indicus* P73. This strain is reported to have 138 genes related to aromatic hydrocarbon catabolism. Based on these genes, a putative fluoranthene degradation pathway for this strain has been published and a ring-hydroxylating dioxygenase was confirmed to be involved in this fluoranthene pathway. This pathway has not been experimentally validated (88). Since the *Roseobacteraceae* family is incredibly diverse, widespread screening of strains for degradation of PAHs and investigation into their PAH degradation pathway(s) is necessary. Furthermore, as ecologically relevant and abundant bacteria, it is crucial to understand the degradation pathways of family members to understand their intrinsic PAH bioremediation potential.

Dissertation Objectives

This dissertation aims to investigate the ecology, diversity, and mechanisms of marine bacterial PAH co-metabolism, specifically focusing on the *Roseobacteraceae* family. Chapter 2 investigates the diversity of marine microbial PAH degraders and introduces PAH degradation as a widespread metabolic strategy for marine bacteria. In addition, this chapter reveals that these marine bacteria may be missing genetic biomarkers for PAH degradation, thus providing evidence for the existence of a novel PAH co-metabolism pathway. Chapter 3 builds off evidence of a novel co-metabolism pathway and attempts to study the mechanisms and genes governing the PAH co-metabolism pathway of *Ruegeria pomeroyi* DSS-3. To put the findings of Chapters 2 and 3 in context, Chapter 4 investigates the abundance and metabolic strategies of marine microbial communities using an enrichment study. This chapter presents the diversity and abundance of bacterial PAH co-metabolizers and posits their role in coastal marine systems.

REFERENCES

1. Sakshi, Haritash AK. 2020. A comprehensive review of metabolic and genomic aspects of PAH-degradation. Arch Microbiol 202:2033–2058.
2. Ghosal D, Ghosh S, Dutta TK, Ahn Y. 2016. Current State of Knowledge in Microbial Degradation of Polycyclic Aromatic Hydrocarbons (PAHs): A Review. Front Microbiol 7:1369.
3. Gupta G, Kumar V, Pal AK. 2017. Microbial Degradation of High Molecular Weight Polycyclic Aromatic Hydrocarbons with Emphasis on Pyrene. Polycycl Aromat Compd 39:124–138.
4. Duran R, Cravo-Laureau C. 2016. Role of environmental factors and microorganisms in determining the fate of polycyclic aromatic hydrocarbons in the marine environment. FEMS Microbiol Rev 40:814–830.
5. Abdel-Shafy HI, Mansour MSM. 2016. A review on polycyclic aromatic hydrocarbons: Source, environmental impact, effect on human health and remediation. Egyptian Journal of Petroleum 25:107–123.
6. Honda M, Suzuki N. 2020. Toxicities of Polycyclic Aromatic Hydrocarbons for Aquatic Animals. Int J Environ Res Public Health 17.
7. Sunanda S, Varsha V, Prajakti P, Chattopadhyay S, Sachan SG. 2023. Biodegradation of Polycyclic Aromatic Hydrocarbons and the Impact of Various Genes for their Enhanced Degradation. Lett Appl Microbiol 76.
8. Albers PH. 1995. Petroleum and Individual Polycyclic Aromatic Hydrocarbons, p. 330-335. *In* Hoffman D, Rattner B, Burton Jr. GA, Cairns Jr. A, Handbook of Ecotoxicology. Lewis Publishers, Boca Raton, FL.
9. Adeniji AO, Okoh OO, Okoh AI. 2018. Analytical Methods for Polycyclic Aromatic Hydrocarbons and their Global Trend of Distribution in Water and Sediment: A Review, p. 393–428. *In* Zoveidavianpoor, M Recent Insights in Petroleum Science and Engineering. InTech.
10. Lin Q, Mendelssohn IA, Graham SA, Hou A, Fleeger JW, Deis DR. 2016. Response of salt marshes to oiling from the Deepwater Horizon spill: Implications for plant growth,

soil surface-erosion, and shoreline stability. Science of The Total Environment 557–558:369–377.

11. Head IM, Jones DM, Röling WFM. 2006. Marine microorganisms make a meal of oil. Nat Rev Microbiol 4:173–182.
12. Logan DT. 2007. Perspective on Ecotoxicology of PAHs to Fish. Human and Ecological Risk Assessment 13:302–316.
13. Michel J, Rutherford N. 2014. Impacts, recovery rates, and treatment options for spilled oil in marshes. Mar Pollut Bull 82:19–25.
14. Zhou HW, Luan TG, Zou F, Tam NFY. 2008. Different bacterial groups for biodegradation of three- and four-ring PAHs isolated from a Hong Kong mangrove sediment. J Hazard Mater 152:1179–1185.
15. Ahmad M, Ling J, Yang Q, Sajjad W, Zhou W, Yin J, Dong J. 2021. Insight into Bacterial Community Responses to Polycyclic Aromatic Hydrocarbons and the Degradation Potentials of Three Bacterial Isolates in Seagrass Halophila ovalis Sediments. Current Microbiology 1:1–14.
16. Bacosa HP, Kamalanathan M, Cullen J, Shi D, Xu C, Schwehr KA, Hala D, Wade TL, Knap AH, Santschi PH, Quigg A. 2020. Marine Snow Aggregates are Enriched in Polycyclic Aromatic Hydrocarbons (PAHs) in Oil Contaminated Waters: Insights from a Mesocosm Study. Journal of Marine Science and Engineering 8:1-16.
17. Adhikari PL, Maiti K, Overton EB. 2015. Vertical fluxes of polycyclic aromatic hydrocarbons in the northern Gulf of Mexico. Mar Chem 168:60–68.
18. Bacosa HP, Inoue C. 2015. Polycyclic aromatic hydrocarbons (PAHs) biodegradation potential and diversity of microbial consortia enriched from tsunami sediments in Miyagi, Japan. J Hazard Mater 283:689–697.
19. Liu J, Zhang C, Jia H, Lichtfouse E, Sharma VK. 2023. Abiotic transformation of polycyclic aromatic hydrocarbons via interaction with soil components: A systematic review. Crit Rev Environ Sci Technol 53:676–699.
20. Brzeszcz J, Kaszycki P. 2018. Aerobic bacteria degrading both n-alkanes and aromatic hydrocarbons: an undervalued strategy for metabolic diversity and flexibility. Biodegradation. Springer Netherlands. https://doi.org/10.1007/s10532-018-9837-x.

21. Uyttebroek M, Breugelmans P, Janssen M, Wattiau P, Joffe B, Karlson U, Ortega-Calvo JJ, Bastiaens L, Ryngaert A, Hausner M, Springael D. 2006. Distribution of the *Mycobacterium* community and polycyclic aromatic hydrocarbons (PAHs) among different size fractions of a long-term PAH-contaminated soil. Environ Microbiol 8:836–847.
22. Heitkamp MA, Franklin W, Cerniglia CE. 1988. Microbial metabolism of polycyclic aromatic hydrocarbons: isolation and characterization of a pyrene-degrading bacterium. Appl Environ Microbiol 54:2549–2555.
23. Kim SJ, Kweon O, Jones RC, Freeman JP, Edmondson RD, Cerniglia CE. 2007. Complete and integrated pyrene degradation pathway in *Mycobacterium vanbaalenii* PYR-1 based on systems biology. J Bacteriol 189:464–472.
24. Zada S, Zhou H, Xie J, Hu Z, Ali S, Sajjad W, Wang H. 2021. Bacterial degradation of pyrene: Biochemical reactions and mechanisms. Int Biodeterior Biodegradation 162:105233.
25. Basta T, Buerger S, Stolz A. 2005. Structural and replicative diversity of large plasmids from sphingomonads that degrade polycyclic aromatic compounds and xenobiotics. Microbiology 151:2025–2037.
26. Mawad A, Albasri H, Shalkami A-G, Alamri S, Hashem M. 2021. Synergistic degradation of phenanthrene by constructed *Pseudomonas* spp. Consortium compared with pure strains. Environ Technol Innov 101942.
27. Vaidya S, Jain K, Madamwar D. 2017. Metabolism of pyrene through phthalic acid pathway by enriched bacterial consortium composed of *Pseudomonas*, *Burkholderia*, and *Rhodococcus* (PBR). 3 Biotech 7.
28. Nieto EE, Macchi M, Valacco MP, Festa S, Morelli IS, Coppotelli BM. 2023. Metaproteomic and gene expression analysis of interspecies interactions in a PAH-degrading synthetic microbial consortium constructed with the key microbes of a natural consortium. Biodegradation https://doi.org/10.1007/S10532-022-10012-3.
29. Wanapaisan P, Laothamteep N, Vejarano F, Chakraborty J, Shintani M, Muangchinda C, Morita T, Suzuki-Minakuchi C, Inoue K, Nojiri H, Pinyakong O. 2018. Synergistic

degradation of pyrene by five culturable bacteria in a mangrove sediment-derived bacterial consortium. J Hazard Mater 342:561–570.

30. Singleton DR, Adrion AC, Aitken MD. 2016. Surfactant-induced bacterial community changes correlated with increased polycyclic aromatic hydrocarbon degradation in contaminated soil. Appl Microbiol Biotechnol 100:10165–10177.
31. Cauduro GP, Leal AL, Lopes TF, Marmitt M, Valiati VH. 2020. Differential Expression and PAH Degradation: What *Burkholderia vietnamiensis* G4 Can Tell Us? Int J Microbiol 2020.
32. Kallimanis A, Frillingos S, Drainas C, Koukkou AI. 2007. Taxonomic identification, phenanthrene uptake activity, and membrane lipid alterations of the PAH degrading *Arthrobacter* sp. strain Sphe3. Appl Microbiol Biotechnol 76:709–717.
33. Bugg T, Foght JM, Pickard MA, Gray MR. 2000. Uptake and active efflux of polycyclic aromatic hydrocarbons by *Pseudomonas fluorescens* LP6a. Appl Environ Microbiol 66:5387–5392.
34. Broniatowski M, Binczycka M, Wójcik A, Flasiński M, Wydro P. 2017. Polycyclic aromatic hydrocarbons in model bacterial membranes – Langmuir monolayer studies. Biochimica et Biophysica Acta (BBA) - Biomembranes 1859:2402–2412.
35. Certik M, Dercová K, Sejáková ZS. 2003. Effect of polyaromatic hydrocarbons (PAHs) on the membrane lipids of bacterial cell. Biologia 58:1111–1117.
36. Poursat BAJ, van Spanning RJM, de Voogt P, Parsons JR. 2019. Implications of microbial adaptation for the assessment of environmental persistence of chemicals. Crit Rev Environ Sci Technol 49:2220–2255.
37. Kweon O, Kim SJ, Holland RD, Chen H, Kim DW, Gao Y, Yu LR, Baek S, Baek DH, Ahn H, Cerniglia CE. 2011. Polycyclic aromatic hydrocarbon metabolic network in *Mycobacterium vanbaalenii* PYR-1. J Bacteriol 193:4326–4337.
38. Parales RE, Resnick SM. 2006. Aromatic Ring Hydroxylating Dioxygenases, p. 287–340. *In* Pseudomonas. Springer, Boston, MA.
39. Kim SJ, Kweon O, Jones RC, Edmondson RD, Cerniglia CE. 2008. Genomic analysis of polycyclic aromatic hydrocarbon degradation in *Mycobacterium vanbaalenii* PYR-1. Biodegradation 19:859–881.

40. Kiyohara H, Torigoe S, Kaida N, Asaki T, Iida T. 1994. Cloning and Characterization of a Chromosomal Gene Cluster, *pah*, That Encodes the Upper Pathway for Phenanthrene and Naphthalene Utilization by *Pseudomonas putida* OUS82. J Bacteriol 176:2439–2443.
41. Liang C, Huang Y, Wang H. 2019. *pahE*, a Functional Marker Gene for Polycyclic Aromatic Hydrocarbon-Degrading Bacteria. Appl Environ Microbiol 85.
42. LeVieux JA, Johnson WH, Erwin K, Li W, Jessie Zhang Y, Whitman CP. 2016. The bacterial catabolism of polycyclic aromatic hydrocarbons: Characterization of three hydratase-aldolase-catalyzed reactions. Perspect Sci 9:33–41.
43. Phale PS, Malhotra H, Shah BA. 2020. Degradation strategies and associated regulatory mechanisms/features for aromatic compound metabolism in bacteria. Adv Appl Microbiol 112:1–65.
44. Kim YH, Moody JD, Freeman JP, Brezna B, Engesser KH, Cerniglia CE. 2004. Evidence for the existence of PAH-quinone reductase and catechol-O-methyltransferase in *Mycobacterium vanbaalenii* PYR-1. J Ind Microbiol Biotechnol 31:507–516.
45. Huang Y, Li L, Yin X, Zhang T. 2023. Polycyclic aromatic hydrocarbon (PAH) biodegradation capacity revealed by a genome-function relationship approach. Environ Microbiome 18:1–13.
46. Haruhiko Nakata RD. 2015. Isolation and Evaluation of PAH Degrading Bacteria. J Bioremediat Biodegrad 06:1–7.
47. Cébron A, Norini MP, Beguiristain T, Leyval C. 2008. Real-Time PCR quantification of PAH-ring hydroxylating dioxygenase (PAH-RHDα) genes from Gram positive and Gram negative bacteria in soil and sediment samples. J Microbiol Methods 73:148–159.
48. Rodríguez A, Zárate SG, Bastida A. 2022. Identification of New Dioxygenases Able to Recognize Polycyclic Aromatic Hydrocarbons with High Aromaticity. Catalysts 12:279.
49. Liang C, Ye Q, Huang Y, Wang Y, Zhang Z, Wang H. 2022. Shifts of the new functional marker gene (*pahE*) of polycyclic aromatic hydrocarbons (PAHs) degrading bacterial population and its relationship with PAHs biodegradation. J Hazard Mater 437.
50. Liang C, Ye Q, Huang Y, Zhang Z, Wang C, Wang Y, Wang H. 2022. Distribution of the new functional marker gene (*pahE*) of aerobic polycyclic aromatic hydrocarbon (PAHs)

degrading bacteria in different ecosystems. Science of The Total Environment 865:161233.

51. Zhang S, Hu Z, Wang H. 2019. Metagenomic analysis exhibited the co-metabolism of polycyclic aromatic hydrocarbons by bacterial community from estuarine sediment. Environ Int 129:308–319.
52. Ahmad M, Ling J, Yin J, Chen L, Yang Q, Zhou W, Zhang Y, Huang X, Khan I, Dong J. 2023. Evaluation of the Different Nutritional and Environmental Parameters on Microbial Pyrene Degradation by Mangrove Culturable Bacteria. Int J Mol Sci 24:8282.
53. Jiang J, Tian W, Lu Z, Chu M, Cao H, Zhang D. 2023. Cometabolic degradation of pyrene with phenanthrene as substrate: assisted by halophilic *Pseudomonas stutzeri* DJP1. Biodegradation 2023 1–14.
54. Rao L, Gu D, Xiang X, Zeng J, Wu Y, Lin X, Christie P. 2023. Impact of lignin constituents on the bacterial community and polycyclic aromatic hydrocarbon co-metabolism in an agricultural soil. Environmental Pollution 333:122105.
55. Teng Y, Luo Y, Ping L, Zou D, Li Z, Christie P. 2010. Effects of soil amendment with different carbon sources and other factors on the bioremediation of an aged PAH-contaminated soil. Biodegradation 21:167–178.
56. Li J, Chen W, Zhou W, Wang Y, Deng M, Zhou S. 2021. Synergistic degradation of pyrene by *Pseudomonas aeruginos*a PA06 and *Achromobacter* sp. AC15 with sodium citrate as the co-metabolic carbon source. Ecotoxicology 30:1487–1498.
57. Vandera E, Samiotaki M, Parapouli M, Panayotou G, Koukkou AI. 2015. Comparative proteomic analysis of *Arthrobacter phenanthrenivorans* Sphe3 on phenanthrene, phthalate and glucose. J Proteomics 113:73–89.
58. Rojo F. 2021. A new global regulator that facilitates the co-metabolization of polyaromatic hydrocarbons and other nutrients in *Novosphingobium*. Environ Microbiol 23:2875–2877.
59. Chen SH, Aitken MD. 1998. Salicylate Stimulates the Degradation of High-Molecular Weight Polycyclic Aromatic Hydrocarbons by *Pseudomonas saccharophila* P15. Environ Sci Technol 33:435–439.

60. Wang X, Teng Y, Wang X, Xu Y, Li R, Sun Y, Dai S, Hu W, Wang H, Li Y, Fang Y, Luo Y. 2023. Nitrogen transfer and cross-feeding between *Azotobacter chroococcum* and *Paracoccus aminovorans* promotes pyrene degradation. The ISME Journal 1–13.
61. Leys NM, Bastiaens L, Verstraete W, Springael D. 2005. Influence of the carbon/nitrogen/phosphorus ratio on polycyclic aromatic hydrocarbon degradation by Mycobacterium and Sphingomonas in soil. Appl Microbiol Biotechnol 66:726–736.
62. Shahriari Moghadam M, Ebrahimipour G, Abtahi B, Ghassempour A, Seyed Hashtroudi M. 2014. Biodegradation of polycyclic aromatic hydrocarbons by a bacterial consortium enriched from mangrove sediments. J Environ Health Sci Eng 12:1–9.
63. Tejeda-Agredano MC, Mayer P, Ortega-Calvo JJ. 2014. The effect of humic acids on biodegradation of polycyclic aromatic hydrocarbons depends on the exposure regime. Environmental Pollution 184:435–442.
64. Li X, Liu H, Yang W, Sheng H, Wang F, Harindintwali JD, Herath HMSK, Zhang Y. 2022. Humic acid enhanced pyrene degradation by *Mycobacterium* sp. NJS-1. Chemosphere 288.
65. Lamichhane S, Bal Krishna KC, Sarukkalige R. 2017. Surfactant-enhanced remediation of polycyclic aromatic hydrocarbons: A review. J Environ Manage 199:46–61.
66. Tiehm A. 1994. Degradation of polycyclic aromatic hydrocarbons in the presence of synthetic surfactants. Appl Environ Microbiol 60:258–263.
67. Luning Prak DJ, Pritchard PH. 2011. Degradation of polycyclic aromatic hydrocarbons dissolved in Tween 80 surfactant solutions by *Sphingomonas paucimobilis* EPA 505. https://doi.org/101139/w02-004 48:151–158.
68. Khandelwal A, Nain L, Singh SB, Varghese E, Sharma A, Gupta S, Singh N. 2021. Bacteria and fungi mediated degradation of poly aromatic hydrocarbons and effect of surfactant Tween-80. https://doi.org/101080/0306731920212015584 1–16.
69. Brakstad OG, Bonaunet K. 2006. Biodegradation of petroleum hydrocarbons in seawater at low temperatures (0-5°C) and bacterial communities associated with degradation. Biodegradation 17:71–82.

70. Kästner M, Breuer-Jammali M, Mahro B. 1998. Impact of inoculation protocols, salinity, and pH on the degradation of polycyclic aromatic hydrocarbons (PAHs) and survival of PAH-degrading bacteria introduced into soil. Appl Environ Microbiol 64:359–362.
71. Minai-Tehrani D, Minoui S, Herfatmanesh A. 2009. Effect of salinity on biodegradation of polycyclic aromatic hydrocarbons (PAHs) of heavy crude oil in soil. Bull Environ Contam Toxicol 82:179–184.
72. Li D, Li K, Liu Y, Wang L, Liu N, Huang S. 2022. Synergistic PAH biodegradation by a mixed bacterial consortium: based on a multi-substrate enrichment approach. Environmental Science and Pollution Research 2022 1:1–11.
73. Wang C, Guo G, Huang Y, Hao H, Wang H. 2017. Salt Adaptation and Evolutionary Implication of a Nah-related PAHs Dioxygenase cloned from a Halophilic Phenanthrene Degrading Consortium. Sci Rep 7.
74. Wagner-Döbler I, Biebl H. 2006. Environmental biology of the marine Roseobacter lineage. Annu Rev Microbiol 60:255–280.
75. Liang HK, Orata FD, Boucher Y, Case RJ. 2021. Roseobacters in a Sea of Poly- and Paraphyly: Whole Genome-Based Taxonomy of the Family *Rhodobacteraceae* and the Proposal for the Split of the "Roseobacter Clade" Into a Novel Family, *Roseobacteraceae* fam. nov. Front Microbiol 12.
76. Buchan A, González JM, Chua MJ. 2019. Aerobic Hydrocarbon-Degrading Alphaproteobacteria: *Rhodobacteraceae* (Roseobacter), p. 93–104. *In* McGenity, TJ (ed.), Taxonomy, Genomics and Ecophysiology of Hydrocarbon-Degrading Microbes. Springer International Publishing.
77. Zhou H, Zhang S, Xie J, Wei H, Hu Z, Wang H. 2020. Pyrene biodegradation and its potential pathway involving Roseobacter clade bacteria. Int Biodeterior Biodegradation 150:104961.
78. Dash HR, Mangwani N, Chakraborty J, Kumari S, Das S. 2013. Marine bacteria: Potential candidates for enhanced bioremediation. Appl Microbiol Biotechnol 97:561–571.
79. Jami M, Lai Q, Ghanbari M Moghadam MS, Kneifel W, Domig KJ. 2016. *Celeribacter persicus* sp. nov., a polycyclic-aromatic-hydrocarbon-degrading bacterium isolated from mangrove soil. Int J Syst Evol Microbiol 66:1875–1880.

80. Lai Q, Cao J, Yuan J, Li F, Shao Z. 2014. *Celeribacter indicus* sp. nov., a polycyclic aromatic hydrocarbon-degrading bacterium from deep-sea sediment and reclassification of *Huaishuia halophila* as *Celeribacter halophilus* comb. nov. Int J Syst Evol Microbiol 64:4160–4167.
81. Zhang YH, Dong JD, Wang YS, Gu JD, Yin JP, Ahmad M, Ling J. 2022. Comparative genomics reveals the evidence of aromatic hydrocarbons degradation potential in genus *Roseovarius* in marine environment. Int Biodeterior Biodegradation 171:105408.
82. Gao L, Fang BZ, Liu YH, Jiao JY, Li MM, Alkhalifah DHM, Hozzein WN, Li WJ. 2023. Comparative genomic analyses of *Lutimaribacter degradans* sp. nov. With the ability to PAHs-biodegradation and transformation. Int Biodeterior Biodegradation 176:105505.
83. Wang W, Zhong R, Shan D, Shao Z. 2014. Indigenous oil-degrading bacteria in crude oil-contaminated seawater of the Yellow sea, China. Appl Microbiol Biotechnol 98:7253–7269.
84. Zhou HW, Wong AHY, Yu RMK, Park YD, Wong YS, Tam NFY. 2009. Polycyclic aromatic hydrocarbon-induced Structural shift of bacterial communities in mangrove sediment. Microb Ecol 58:153–160.
85. Yang T, Speare K, McKay L, MacGregor BJ, Joye SB, Teske A. 2016. Distinct Bacterial Communities in Surficial Seafloor Sediments Following the 2010 Deepwater Horizon Blowout. Front Microbiol 7.
86. Jiménez N, Viñas M, Guiu-Aragonés C, Bayona JM, Albaigés J, Solanas AM. 2011. Polyphasic approach for assessing changes in an autochthonous marine bacterial community in the presence of Prestige fuel oil and its biodegradation potential. Appl Microbiol Biotechnol 91:823–834.
87. Simon M, Scheuner C, Meier-Kolthoff JP, Brinkhoff T, Wagner-Döbler I, Ulbrich M, Klenk HP, Schomburg D, Petersen J, Göker M. 2017. Phylogenomics of *Rhodobacteraceae* reveals evolutionary adaptation to marine and non-marine habitats. The ISME Journal 2017 11:6 11:1483–1499.
88. Voget S, Wemheuer B, Brinkhoff T, Vollmers J, Dietrich S, Giebel H-A, Beardsley C, Sardemann C, Bakenhus I, Billerbeck S, Daniel R, Simon M. 2014. Adaptation of an

abundant Roseobacter RCA organism to pelagic systems revealed by genomic and transcriptomic analyses. The ISME Journal 9:2 9:371–384.

89. Cao J, Lai Q, Yuan J, Shao Z. 2015. Genomic and metabolic analysis of fluoranthene degradation pathway in *Celeribacter indicus* P73 T. Sci Rep 5:1–12.

CHAPTER 2

EVIDENCE FOR NOVEL POLYCYCLIC AROMATIC HYDROCARBON DEGRADATION PATHWAYS IN CULTURABLE MARINE ISOLATES

A version of this chapter was originally published by Jillian Walton and Alison Buchan:
Walton, JL. & Buchan, A. 2023. Evidence for novel polycyclic aromatic hydrocarbon degradation pathways in culturable marine isolates. *Microbiol Spectr* 12:e03409-23.
Contribution statement: JW conceived the project, conducted experiments, analyzed results, created figures, and wrote the article; AB supervised the project and provided feedback on the article.

Abstract

Polycyclic aromatic hydrocarbons (PAHs) are common toxic and carcinogenic pollutants in marine ecosystems. Despite their prevalence in these habitats, relatively little is known about the natural microflora and biochemical pathways that contribute to their degradation. Approaches to investigate marine microbial PAH degraders often heavily rely on genetic biomarkers, which requires prior knowledge of specific degradative enzymes and genes encoding them. As such, these biomarker-reliant approaches cannot efficiently identify novel degradation pathways nor degraders. Here, we screen 18 marine bacterial strains representing the Pseudomonadota, Bacillota, and Bacteroidota phyla for degradation of two model PAHs, pyrene (HMW) and phenanthrene (LMW). Using a qualitative PAH plate screening assay, we determined 16 of 18 strains show some ability to degrade either or both compounds. Degradative ability was subsequently confirmed with a quantitative HPLC approach, where an additional strain showed some degradation in liquid culture. Several members of the prominent marine *Roseobacteraceae* family degraded pyrene and phenanthrene with varying efficiency (1.2-29.6% and 5.2-52.2%, respectively) over 26 days. Described PAH genetic biomarkers were absent in all PAH degrading strains for which genome sequences are available, suggesting that these strains harbor novel transformation pathways. These results demonstrate the utility of culture-based approaches in expanding the knowledge landscape concerning PAH degradation in marine systems.

Introduction

Polycyclic aromatic hydrocarbons (PAHs) are pollutants generated from incomplete combustion of organic compounds, such as wood, coal, petroleum oil, and municipal solid waste, that are ubiquitously found in atmospheric, terrestrial, and aquatic environments (1, 2). PAHs are composed of fused aromatic rings and are classified based on their molecular weight: low (<4 rings; LMW) and high molecular weight (>4 rings; HMW). These compounds are toxic and

carcinogenic, presenting a hazard to both human and environmental health (2). The removal of these compounds from the environment is difficult due to their stability, hydrophobicity, and low bioavailability (2). Because of their recalcitrance and hazardous nature, the U.S. EPA has designated 16 PAHs as priority pollutants (3). HMW PAHs are of particular concern as the recalcitrance of these chemicals increases with number of aromatic rings (4). While chemical and physical methods have been designed to remove PAHs from the environment, many of these methods have low degradation efficiency and high costs relative to biological removal methods, including microbial degradation (4).

Marine ecosystems are frequently final destinations for PAHs through terrestrial run-off, atmospheric deposition, industrial discharge, and oil spills (2, 5, 6). Despite the abundance of PAHs in marine ecosystems, relatively few marine bacteria have been investigated for their PAH biodegradation pathways. In contrast, significant research has been conducted with soil and freshwater PAH degrading bacteria, including *Mycobacterium* spp., *Pseudomonas* spp., and *Sphingomonas* spp. (7). While, in principle, these bacteria can be applied to marine environments for bioaugmentation, such approaches have challenges, most notably bacterial survival and the ability to degrade a compound in non-native environments (8). Additionally, halophilic and halotolerant marine bacteria may be useful in remediation of high salinity waste effluents that commonly contain PAH contaminants, such as industrial wastewaters (9, 10). To effectively remediate marine environments and high salinity wastes, marine bacteria isolated from ecosystems of interest should be investigated for ability to degrade PAHs.

Bacteria are capable of transforming PAHs in various ways. The marine sediment bacterium *Mycobacterium vanbaalenii* PYR-1 was one of the first strains demonstrated to utilize pyrene, a HMW PAH, as a sole carbon source. The enzymes required for the complete mineralization of several PAHs have been characterized in this strain (11–13). Most other characterized PAH degraders employ similar enzymatic reactions to those identified in *M. vanbaalenii* PYR-1. Accordingly, the *M. vanbaalenii* PYR-1 pathway and highly homologous pathways form the basis for identification of PAH degradation capabilities in both isolated strains and in culture-independent gene surveys. In general, complete PAH catabolism is initiated by hydroxylation of an aromatic ring (via a dioxygenase or monooxygenase), followed by subsequent re-aromatization and ring cleavage reactions, resulting in monocyclic intermediates that are

funneled to central metabolism (i.e., TCA cycle). Not all PAH degraders are capable of complete mineralization, instead, transforming these compounds into less toxic intermediates, such as the addition of methoxy groups (12). Metabolically, these intermediates are dead-end products and further degradation is generally prevented due to the methylation of hydroxyl groups (1). Finally, co-metabolism of PAHs is increasingly observed in diverse bacteria. This phenomenon usually occurs with LMW and HMW PAH mixtures, where the presence of more labile LMW PAH increases the rate or efficiency of HMW PAH degradation (4, 14, 15). While some evidence exists that other labile carbon sources (e.g., starch and yeast extract) can be used for co-metabolism of PAHs, less information is available about the mechanism of co-metabolism and which compounds effectively induce co-metabolism (16, 17).

Several genetic biomarkers for PAH degradation have been established. First, is the initial ring-hydroxylating dioxygenase (RHD), which catalyzes the initial rate-limiting step for PAH degradation: hydroxylation of an aromatic ring. These enzymes (e.g., PahA, NidA) have been reported to be substrate specific but may be able to hydroxylate several different ring structures (13, 18). Specifically, the alpha subunit of this enzyme is responsible for substrate specificity and is used as a biomarker for PAH degradation. Second, the PAH hydratase-aldolase (*pahE*), has been shown to be the most specific and conserved biomarker within conventional PAH degradation pathways. This is the first step from which an organism may gain energy from the breakdown of PAHs through liberation of substrates feeding into the TCA cycle (19). Third, the final ring cleaving reaction acts on the monocyclic aromatic derivatives to produce TCA cycle intermediates, supporting growth. Generally, PAHs are converted into the monoaromatic central intermediates, protocatechuate or catechol, and funneled through their respective catabolic pathways (20). Each of these three steps provides a necessary reaction for complete PAH mineralization in conventional degradation pathways.

A variety of culture-independent approaches are used to probe for PAH degraders in marine environments, including PCR amplification of biomarker genes (most often PAH RHD), 16S rRNA gene libraries of PAH enrichments, and biomarker homology and identity searches in metagenomes and genomes (21–23). These approaches have broadened the view of PAH degradation in marine habitats by increasing the number of predicted PAH degraders, identifying phylogenetic distribution of genetic biomarkers, and discovering diverse genetic organization of

pathways (19, 24, 25). For example, a recent study demonstrated the utility and specificity of *pahE* as a genetic biomarker and used an amplicon-based library to recover sequences that led to the prediction of PAH degradative abilities for several previously unreported taxa (e.g., *Nevskia ramose* DSM 11499 and *Rhodovulum* sp. N122) (19). While these culture-independent approaches have increased our knowledge of the genetic diversity and distribution of putative PAH degraders, these efforts frequently fail to: (i) link functionality to specific organisms and (ii) identify novel pathways for PAH degradation. Additionally, the focus on only those isolates capable of using PAHs (single or mixed) as a sole carbon source limits our understanding of strains that may play critical roles in co-metabolic transformation of PAHs in the environment. To aid in expanding the landscape of known marine PAH degraders and pathways, we screened 18 diverse marine bacterial isolates for the ability to degrade pyrene and/or phenanthrene. After our initial screen, we focused our efforts on members of the marine *Roseobacteraceae* family as prior studies have indicated that representatives (e.g., *Roseovarius* species, *Ruegeria pomeroyi* DSS-3, and *Celeribacter indicus* P73) of this abundant and active group of bacteria are able to degrade both LMW and HMW PAHs, including pyrene, phenanthrene, and fluoranthene (17, 24, 26). From this work, we hypothesize that some marine bacteria: (i) harbor novel pathways for PAH degradation and (ii) may likely not degrade PAHs as a sole carbon source, explaining the limited marine bacterial PAH degraders and pathways identified via omics-based approaches and culture-based approaches that investigate sole metabolism of PAHs.

Results

PAH degradative abilities identified in diverse marine bacteria

An initial panel of 12 marine bacteria representing three phyla (Pseudomonadota, Bacillota, and Bacteroidota) abundant in marine ecosystems were subjected to a qualitative PAH degradation assay using pyrene and phenanthrene top agar plates (*Marinobacterium georgiense* DSM 11526, *Bacillus-Clostridium* strain SE165, *Bacillus-Clostridium* strain SE98, *Alteromonas macleodii* EZ55, *Vibrio natriegens* ATCC 14048, *Rhodospirillaceae* strain EZ35, *Flavobacteriaceae* strain EZ40, *Alcanivorax* sp. strain EZ46, *Ruegeria pomeroyi* DSS-3, *Citreicella* sp. SE45, and *Sagittula stellata* E-37). *R. pomeroyi* DSS-3 has previously been shown to degrade PAHs, thus this screening confirmed its degradative ability (17). Except for *Alcanivorax* sp. strain EZ46 and *M. georgiense* DSM 11526, all tested strains showed clearing zones, indicative of degradation,

on both pyrene and/or phenanthrene top agar plates containing complex medium after 7 days (**Table 2.1; Figure 2.1**). In contrast, no convincing indication of degradation was evident for strains on the PAH top agar plates containing minimal medium, suggesting that these strains could not utilize PAHs as sole carbon sources (**Table 2.1; Figure A.2.1**). *Citreicella* sp. SE45 did show clearing zones on the PAH top agar plates with minimal medium, however, this was attributed to the strains ability to use the acetone solvent as a carbon source (data not shown). Following the initial screen, efforts were focused on members of the marine *Roseobacteraceae* family, an abundant and active group of heterotrophic bacteria with known abilities to degrade lignin-derived aromatic compounds (27) (**Figure A.2.2**). Three PAH degradation positive strains from the initial screen are family members (*R. pomeroyi* DSS-3, *Citreicella* sp. SE45, and *S. stellata* E-37). Several additional *Roseobacteraceae* were subsequently screened (*Sulfitobacter* sp. EE-36, *Sulfitobacter* sp. NAS-14.1, *Ruegeria* sp. TM1040, *Roseovarius* sp. 217, *Roseovarius nubinhibens* ISM, Rhodobacterales strain Y4I, *Sulfitobacter pontiacus* CB-D) using the PAH top agar plate assay with complex medium (**Table 2.2**). All showed clearing zones on the pyrene-containing complex medium plates, and all but one (*R. nubinhibens* ISM) showed definitive clearing on phenanthrene-containing complex medium plates. Rhodobacterales strain Y4I, produces a blue pigment that stains the agar, obfuscating any clearing. To assess the PAH degradation of this organism using the PAH top agar assay, the assay was repeated with an unpigmented variant (*igiD*::Tn5) (28). This strain showed clearing zones on both pyrene and phenanthrene top agar plates with complex medium (**Figure A.2.3**).

Quantitative assessment of PAH degradative ability

For all strains, excluding *Alcanivorax* sp. EZ46, PAH loss was quantified using HPLC (**Figure 2.2**). All results were consistent with the PAH top agar assay, except *M. georgiense* DSM 11526, which, despite not showing clearing zones on the PAH top agar plates, showed 6% and 16.4% degradation of pyrene and phenanthrene, respectively, in liquid culture. The extent of pyrene degradation for the marine strains ranged from 6% to 16.1% with *Rhodospirillaceae* strain EZ35, *Bacillus-Clostridium* strain SE165, and *Flavobacteriaceae* strain EZ40 showing the highest average pyrene degradation at 14.7%, 14.8%, and 16.1% loss, respectively. Phenanthrene degradation ranged from 0.7% to 24% with *M. georgiense* DSM 11526, *Alteromonas macleodii*

Table 2.1: Screening of marine strains using pyrene and phenanthrene top agar plate assay.

Bacterial Strain	**Taxonomic Phyla/Class**	**Complex + Pyrene**	**Complex + Phenanthrene**	**Minimal + Pyrene**	**Minimal + Phenanthrene**
Marinobacterium georgiense DSM 11526	Gammaproteobacteria	-	-	-	-
Bacillus-Clostridium strain SE165	Firmicutes	+	+	-	-
Bacillus-Clostridium strain SE98	Firmicutes	+	+	-	-
Alteromonas macleodii EZ55	Gammaproteobacteria	+	+	-	-
Vibrio natriegens ATCC 14048	Gammaproteobacteria	+	+	-	-
Rhodospirillaceae strain EZ35	Alphaproteobacteria	+	+	-	-
Flavobacteriaceae strain EZ40	Bacteroidetes	+	+/-	-	-
Alcanivorax sp. strain EZ46	Gammaproteobacteria	-	-	-	-
Ruegeria pomeroyi DSS-3	Alphaproteobacteria	+	+	-	-
Citreicella sp. SE45	Alphaproteobacteria	+	+	+	+
Sagittula stellata E-37	Alphaproteobacteria	+	+	-	-
Escherichia coli DH5α	Gammaproteobacteria	-	-	-	-

+ clearing zones evident by day 7 or 14

- no clearing zones evident by day 7 or 14

+/- inconclusive clearing zone

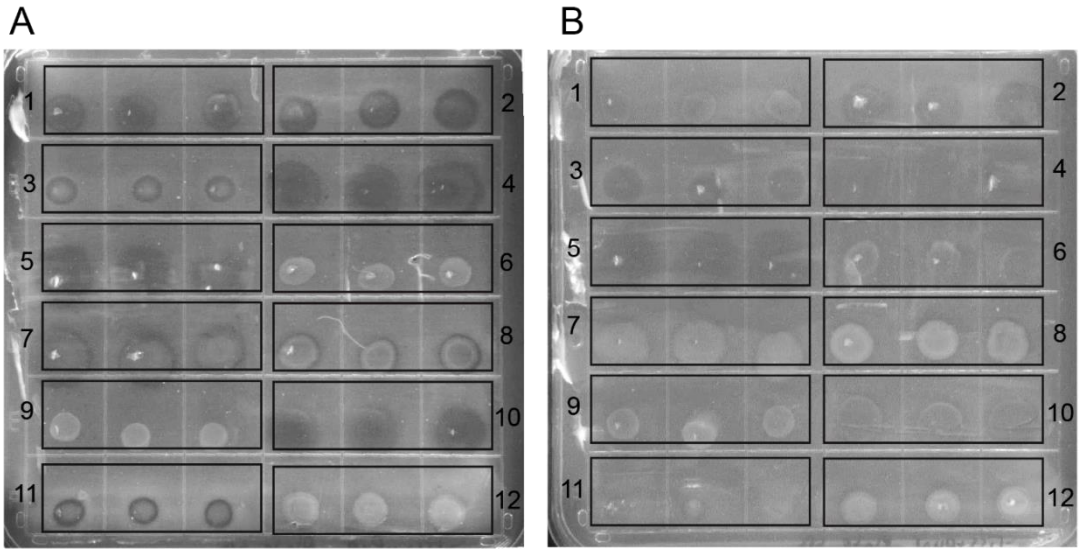

Figure 2.1: (A) Pyrene + complex medium and (B) Phenanthrene + complex medium top agar assay plate after 5 days of incubation. For each strain, three replicate bacterial spots were plated as follows: 1) *R. pomeroyi* DSS-3, 2) *Citreicella* sp. SE45, 3) *S. stellata* E-37, 4) *Bacillus-Clostridium* strain SE165, 5) *Bacillus-Clostridium* strain SE98, 6) *M. georgiense* DSM 11526, 7) V. *natriegens* ATCC 14048, 8) *Rhodospirillaceae* strain EZ35, 9) *Alcanivorax* sp. strain EZ46, 10) *A. macleodii* EZ55, 11) *Flavobacteriaceae* strain EZ40, and 12) *E. coli* DH5α. Clearing zones appear as dark circles on the media and are visualized after colonies are scraped from the top agar.

Table 2.2: Screening of *Roseobacteraceae* strains using pyrene and phenanthrene top agar plate assay.

***Roseobacteraceae* Strains**	**Complex + Pyrene**	**Complex + Phenanthrene**
Ruegeria sp. TM1040	+	+
Ruegeria pomeroyi DSS-3	+	+
Sulfitobacter sp. EE-36	+	+
Sulfitobacter sp. NAS-14.1	+	+
Sulfitobacter sp. CB-D	+	+
Roseovarius nubinhibens ISM	+	+/-
Roseovarius sp. 217	+	+
Rhodobacterales strain Y4I (*igiD*::Tn5)	+	+
Citreicella sp. SE45	+	+
Sagittula stellata E-37	+	+
Escherichia coli DH5α	-	-

+ clearing zones evident by day 7

- no clearing zone evident by day 7

+/- inconclusive clearing zone

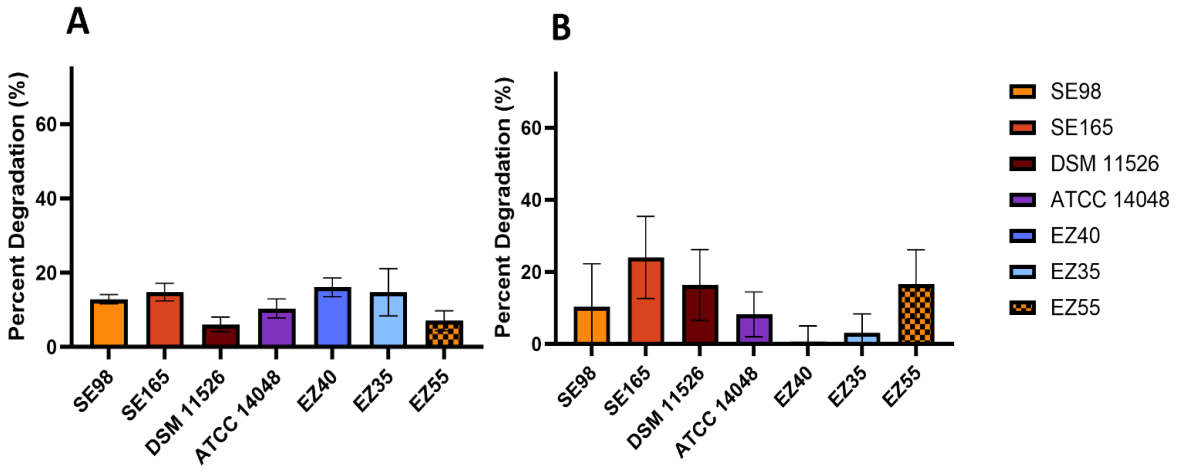

Figure 2.2: Degradation of (A) pyrene and (B) phenanthrene by marine strains after 26 days. Percent degradation is relative to T0 culture and accounts for deviation from uninoculated controls. Standard error was calculated three replicate cultures. Strain designations are indicated on x-axis.

EZ55, and *Bacillus-Clostridium* strain SE165 having the highest average phenanthrene degradation at 16.4%, 16.6%, and 24% loss, respectively. While *Flavobacteriaceae* strain EZ40 showed the greatest degradation of pyrene, it exhibited the lowest for phenanthrene in agreement with the PAH top agar assay. Only three strains, *Bacillus-Clostridium* strain SE165, *M. georgiense* DSM 11526, and *Alteromonas macleodii* EZ55, showed greater degradation of phenanthrene relative to pyrene.

For *Roseobacteraceae* strains, pyrene degradation ranged from 1.2% to 29.6% (**Figure 2.3**). *R. pomeroyi* DSS-3, *S. stellata* E-37, and *Citreicella* sp. SE45 had the highest pyrene degradation at 23.8%, 24.6%, and 29.6%, respectively. Most of the *Roseobacteraceae* strains showed greater degradation of phenanthrene degradation relative to pyrene ranging from 5.2% to 52.2%. Notably, *Ruegeria* sp. TM1040 showed the greatest difference from 12.4% loss of pyrene to 52.2% loss of phenanthrene. *Citreicella* sp. SE45, *Sulfitobacter* sp. EE-36, and *Ruegeria* sp. TM1040 had the highest phenanthrene degradation averaging 33.1%, 34.4%, and 52.2%, respectively. The *Roseobacteraceae* strains also appeared to have a greater range of degradation for both pyrene and phenanthrene relative to other marine strains.

PAH degradation protein identity in marine strains

An analysis of putative PAH degradation pathways and genes was conducted for strains with available genome sequences: *M. georgiense* DSM 11526, *A. macleodii* EZ55, *V. natriegens* ATCC 14048, *R. pomeroyi* DSS-3, *Citreicella* sp. SE45, *S. stellata* E-37, *Sulfitobacter* sp. EE-36, *Sulfitobacter* sp. NAS-14.1, *Sulfitobacter* sp. CB-D, *Roseovarius* sp. 217, *Ruegeria* sp. TM1040, *Roseovarius nubinhibens* ISM, and Rhodobacterales strain Y4I. *E. coli* DH5α, a non-PAH degrader was included for reference (**Figure 2.4**). The analysis was focused on conserved reactions common to most characterized PAH degradation pathways (i) initial PAH ring-hydroxylation via RHD; (ii) TCA substrate liberation via PAH hydratase-aldolase; (iii) monocyclic aromatic hydrocarbon catabolism via RHD) (11, 12, 29). Protein sequence alignment searches were conducted with representative protein sequences using BLASTP® and results returning an E-value below $1e^{-10}$ were further considered (**Table A.2.2 & A.2.3; Figure 2.4**). NidA (Gram + PAH/Phthalate RHD), PobA (Group I RHD), AntA (Group II RHD), PahAc (Group III RHD), BphA1 (Group IV RHD), and NagG (Salicylate RHD) were chosen to represent the known diversity of aromatic ring-hydroxylating dioxygenases involved in the first

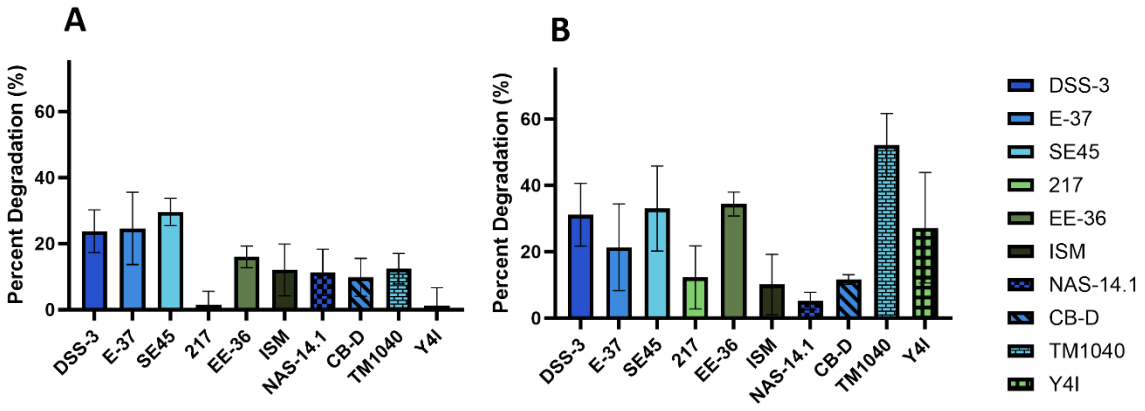

Figure 2.3: Degradation of (A) pyrene and (B) phenanthrene by *Roseobacteraceae* strains after 26 days. Percent degradation is calculated relative to T0 culture and accounts for deviation from uninoculated controls. Standard error was calculated three replicate cultures. Strain designations are indicated on x-axis.

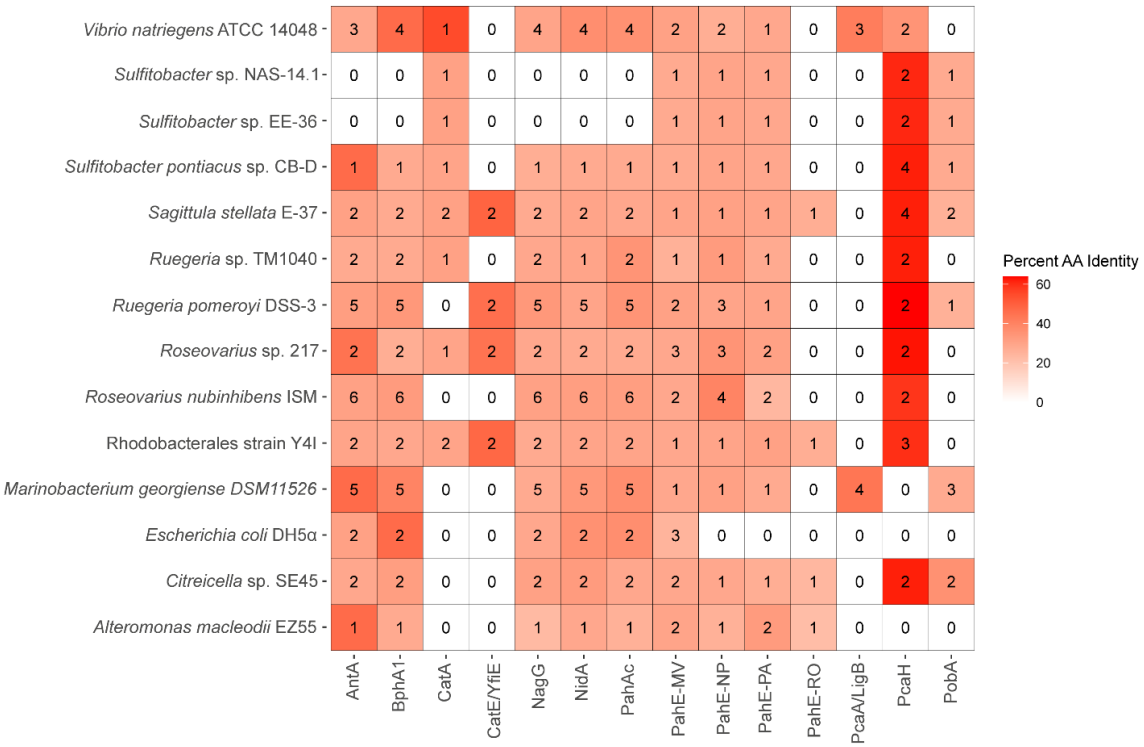

Figure 2.4: Summary of PAH protein BLASTP protein identity searches. Boxes are color-coded based on the highest percent identity of the protein hits from each strain. The numbers in the boxes indicate protein hits for each query sequence below an E-value of $1e^{-10}$. White boxes with a 0 indicate no hits with an E-value below $1e^{-10}$. Protein query sequences are named either as the protein abbreviation or as the protein abbreviation with the first letter of the genus and species from which the query sequence originated from, as indicated in the text. Detailed results from the protein identity searches are in **Table A.2.2.**

conserved reaction (30). PahE protein sequences from *Novosphingobium pentaromativorans* US6-1 (PahE-NP), *Rhodococcus opacus* B4 (PahE-RO), *Mycobacterium vanbaalenii* PYR-1 (PahE-MV), and *Pseudomonas aeruginosa* PaK1 (PahE-PA) were chosen as representatives of PAH hydratase-aldolase diversity (the second conserved reaction). Four different monocyclic aromatic dioxygenases were chosen, two from pathways that degrade protocatechuate (PcaH and PcaA/LigB) and two from pathways that degrade catechol (CatA and CatE/YfiE). To complement this analysis, HMMs for proteins in the upper PAH degradation pathway (PAH RHDs – NahAc, NarAa, NidA; PAH hydratase-aldolase – NahE, NarC, PhdG) were used to further assess potential protein homologs.All strains appeared to be missing proteins involved in PAH-specific degradation (**Figure 2.4; Figure 2.5**). Most strains encode putative protein sequences with an E-value below $1e^{-10}$ for non-PAH specific RHD groups, with identities ranging from 22% to 36% for Group I (PobA), 22% to 47% for Group II (AntA), and 24% to 47% for Group IV (BphA1). The Salicylate Group RHD, NagX, had no strong protein hits. For NidA (Gram + PAH/Phthalate RHD) and PahAc (Group
III RHD) query sequences, *E. coli* DH5α had a higher identity than almost all protein hits for both of these query sequences, with 36% (E-value $1E^{-91}$) and 37% (E-value $2E^{-88}$) identity respectively (**Table A.2.3**). When compared to NahAc, NarAa, and NidA HMMs, *E. coli* DH5α had the highest bit scores for all, with *V. natriegens* ATCC 14048 and *Marinobacterium georgiense* having bit scores closer to *E. coli* DH5α than other strains, similar to the results for the PAH RHD query sequences. None of the strains appear to encode a putative PahE protein, most showing <30% sequence identity or a bit score of <120. Interestingly, for the query sequences only *R. nubinhibens* ISM had any PahE identity greater than 35%, but all strains had a higher bit score than *E. coli* DH5α for the NahE and NarC HMMs. Most of the putative PahE results were annotated as dihydropicolinate synthases or related enzymes, which are commonly found in microorganisms where they are expected to play a role in lysine biosynthesis (31). The PcaA/LigB, PcaH, CatE/YfiE, and CatA proteins are involved in the lower pathway of PAH degradation, steps that occur after monocyclic aromatic compounds are formed.

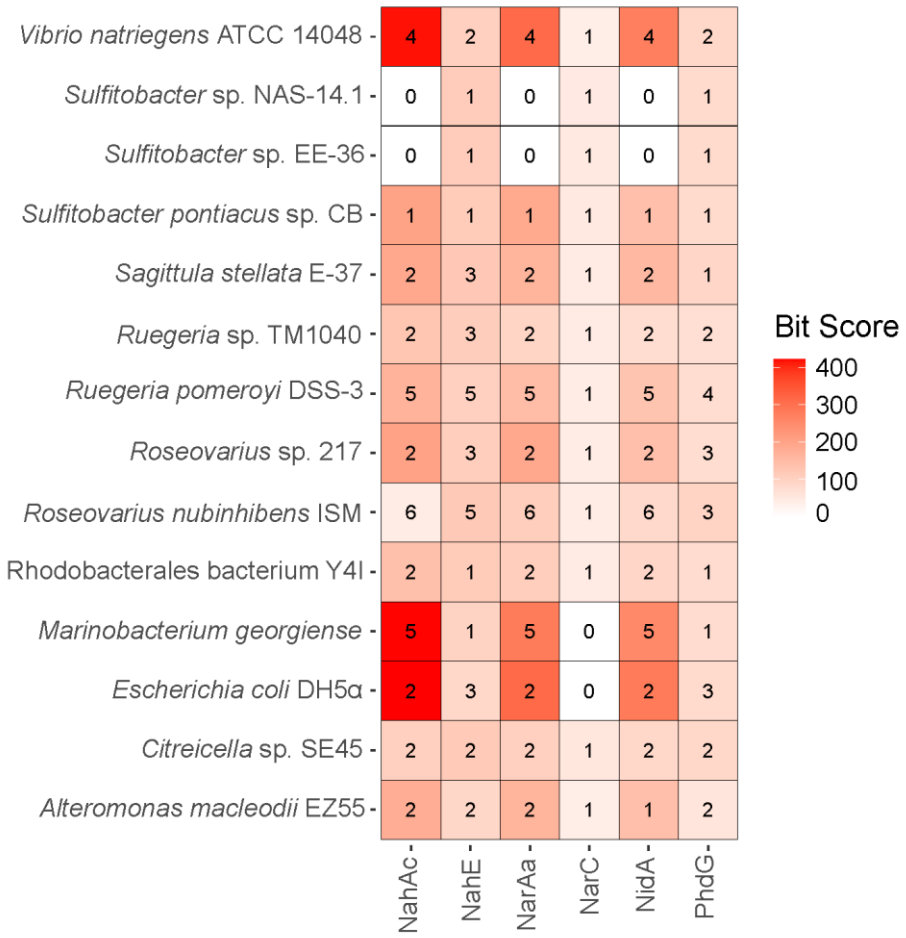

Figure 2.5: Summary of HMM searches for available strain genomes. Boxes are color-coded by the highest bit score of the protein hits for each strain. The numbers in the boxes indicate protein hits for each query sequence below an E-value of $1e^{-10}$. White boxes with a 0 indicate no hits with an E-value below $1e^{-10}$. Each HMM on the x-axis is named after the proteins that the model was constructed from. Detailed results from the protein identity searches are available from the KBase narrative (https://narrative.kbase.us/narrative/175164).

Roseobacteraceae strains encode similar proteins to PcaH (≤59% identity) (32). Other than the *Roseobacteraceae* strains, only *V. natriegens* ATCC 14048 encoded proteins with similarity to PcaH (35%; E-value ≥$1E^{-18}$). No *Roseobacteraceae* strains had any similar proteins for PcaA/LigB, whereas *V. natriegens* ATCC 14048, *E. coli* DH5α, and *M. georgiense* DSM 11526 all showed proteins with >30% identity to PcaA/LigB. Thus, of the strains with genomes analyzed, only *A. macleodii* EZ55 appears to be missing enzymes involved in protocatechuate degradation. Of the catechol dioxygenases, Rhodobacterales strain Y4I, *Roseovarius* sp. 217, and *S. stellata* E-37 had protein hits for both investigated dioxygenases (CatA and CatE/YfiE) with ≤31% and ≤49% percent identities, respectively. Out of the non-*Roseobacteraceae* strains, only *V. natriegens* ATCC 14048 had a protein hit for CatA. While no strains showed strong similarity to proteins specific to upper PAH degradation pathway proteins (i.e., PahE, NahE, NarC, NidA, NahAc, NahE, PhdG, and PahAc), proteins involved in lower PAH degradation pathways strains had much higher protein identities.

Roseobacteraceae PahE biomarker homology

To further explore the *Roseobacteraceae* family and their potential PAH degradation ability, over 750 *Roseobacteraceae* genomes were searched for PahE proteins. Only 7 genomes had >50% percent amino acid identity (E-value ≤ 2E-133) to the PahE from Pseudomonas aeruginosa PaK1 (UniProt ACN P0A142) (**Figure 2.6**). Of the *Roseobacteraceae* collection analyzed, all possessed at least 1 similar protein but at low identity (≤31%). Clear phylogenetic differences appear between these two groups of bacteria. *Roseobacteraceae* strains with over 50% identity to PahE had several bacteria previously reported to degrade PAHs (**Figure 2.6**) (26, 33–36). Additionally, putative PahE homologs of *Roseobacteraceae* strains screened in this study were investigated for the presence of conserved residues that would support activity of these enzymes in PAH degradation. This analysis revealed that the putative PahE homologs are missing several active site residues although some strains possess the catalytic residue (**Figure A.2.4**).

Discussion

To expand the knowledge of bacterial PAH degradation in marine systems, 18 strains representing diverse bacterial taxa were screened for their ability to transform phenanthrene (a LMW PAH) and pyrene (a HMW PAH). From an initial collection of 12 strains, three

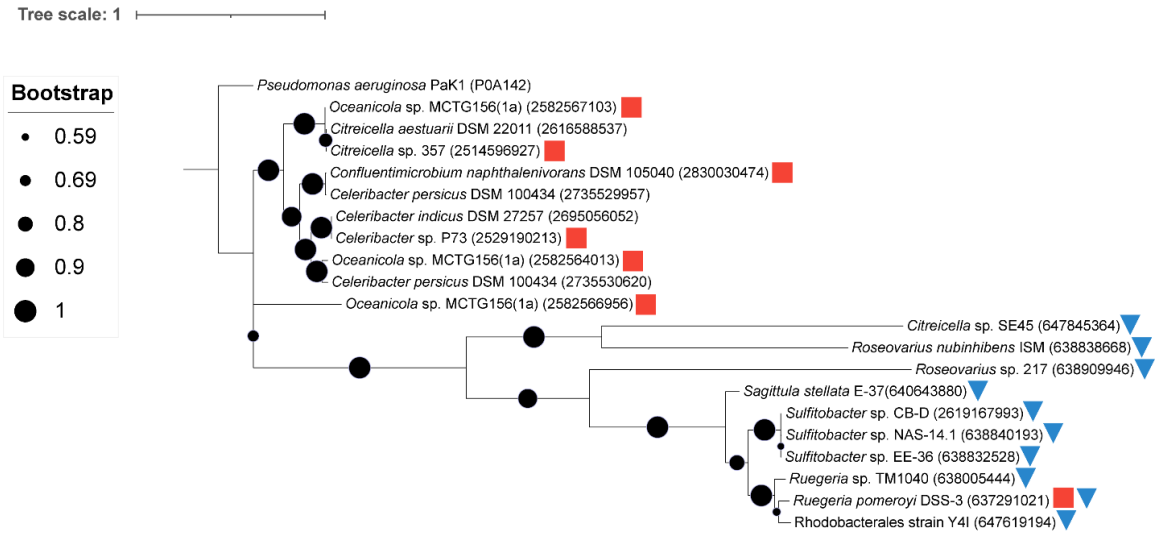

Figure 2.6: Maximum likelihood phylogenetic tree of select *Roseobacteraceae* to PahE homologs. Red squares indicate prior reports of PAH degradation for a given strain (17, 19, 26, 35). Blue triangles indicate strains for which PAH degradation ability was demonstrated in this study. Protein accession numbers are provided in parentheses. Bootstrap values (1000 iterations) are shown at branch nodes with circle size corresponding to the value as indicated in the key. Tree scale represents branch length (the number of substitutions per site generated from the Jones-Taylor-Thornton model). *P. aeruginosa* PaK1 was used included as the original query sequence that identified the putative PahE proteins.

Roseobacteraceae strains demonstrated the highest degradation of PAHs (~20% degradation by 26 days relative to < 20% for the remaining taxa) in a quantitative assay. As such, additional

family members were included in subsequent quantitative analyses. Despite the fact that none of the strains assayed here were derived from PAH enrichments nor from contaminated sites, all but one (*Alcanivorax* sp. strain EZ46), showed evidence of pyrene and/or phenanthrene transformation was found under the cultivation conditions used. *Roseobacteraceae* family members are well-known for their ability to degrade lignin-derived monocyclic aromatic compounds and recent evidence suggests that some strains can transform PAHs (17, 21, 22, 35). For example, *R. pomeroyi* DSS-3 has been previously reported to degrade phenanthrene, pyrene, and benzo[a]pyrene in complex media containing additional carbon sources (tryptone and yeast extract)(17). Similarly, *Flavobacteriaceae* and marine *Alteromonas* strains have been strongly implicated in PAH as well as oil degradation due to the appearance of strains in enrichment cultures (5, 37, 38). Consistent with prior reports of numerous *Bacillus* species, the two *Bacillus-Clostridium* strains examined in this study were able to degrade pyrene and phenanthrene (39, 40). In contrast, reports of PAH degradation by other Gammaproteobacterial genera (*Vibrio, Rhodospirillaceae*, and *Marinobacterium*) included in the collection screened here are scant. A *Vibrio cyclotrophicus* strain has been shown to degrade LMW PAHs but not use them as a growth substrate (41). *Rhodospirillaceae* strains have been identified in PAH enrichment experiments, but little specific information exists regarding their ability to transform PAHs (42, 43). *Marinobacterium georgienes* isolate (IAM 1419T) was found in a PAH enriched microbial consortium, but no confirmation of its degradation has been reported (42). Finally, *Alcanivorax* species are known degraders of n-alkanes from oil hydrocarbons, but little evidence exists regarding their ability to degrade PAHs, aligning with the findings of this study (56, 57). Marine bacteria are recognized to possess high metabolic and physiological diversity amongst closely related strains, thus variation in PAH degradation abilities is unsurprising (44–46). However, it does highlight the necessity of documenting PAH degradation ability of marine isolates, even within closely related strains, if we are to improve our understanding of the ecology and evolution of these degraders.

While none of the strains were able to utilize PAHs as a sole carbon source, nearly all strains showed PAH degradation when also provided labile carbon substrates in the complex medium (yeast extract and tryptone), suggestive of co-metabolism of pyrene and phenanthrene amongst

this cohort of marine bacteria. Co-metabolism, the synergistic degradation of two carbon sources, is a common feature among PAH degraders, with most studies reporting the synergistic breakdown of HMW PAHs and LMW PAHs (47, 48). Co-metabolism of PAHs with non-aromatic, labile carbon sources is recognized, but often not considered in PAH degradation studies (16, 49). This study emphasizes the need to assess both sole-metabolism and co-metabolism of PAHs to identify contributing degraders in natural environments. In addition to the carbon source provided, growth mode appears to also influence degradative abilities in some strains. For example, *M. georgienes* DSM 11526 showed degradation only in liquid culture and not with PAH overlay plates. Exploring co-metabolic growth substrates as well as growth conditions will provide further evidence for the role of marine microbes in natural attenuation of PAHs.

While a plethora of strains have been found to degrade LMW PAHs, fewer degraders have been discovered that transform HMW PAHs, presumably due to their decreased bioavailability and increased stability. All but one strain analyzed here showed some ability to degrade both a HMW PAH and a LMW PAH, with many strains demonstrating greater degradation of LMW PAHs. While these compounds are generally degraded by substrate specific RHDs, flexibility in these enzymes is evident with some acting on both LMW and HMW PAHs (13, 18). The available genomes analyzed revealed that strains encoded genes with low similarity to PAH-specific RHDs, suggesting that non-PAH specific RHDs act on these compounds. For conciseness, ‘similarity’ will be used to refer to both the % identity and HMM bit score results. This is consistent with evidence that some marine bacteria use various RHDs, with broad substrate ranges, to degrade PAHs (26, 50). We suggest enzymes involved in the degradation of other aromatic compounds may act on PAHs, as has been demonstrated for the *Roseobacteraceae* member, *Celeribacter indicus* P73 (26). All *Roseobacteraceae* members possessed proteins with high protein identity to PcaH, a marker for protocatechuate degradation (32). Additionally, of the remaining strains, both *M. georgiense* and *V. natrigens* are predicted to encode enzymes that may be required for lower pathways of PAH degradation. It is important to recognize, however, that enzymes involved in the lower pathway of PAH degradation lack the specificity to solely be used as PAH degradation biomarkers due to the plethora of compounds that are funneled through these pathways (51). It is also relevant to highlight that high protein

identity to specific RHDs does not necessarily indicate an ability to degrade PAHs. For example, *E. coli* DH5α had proteins more similar to PAH RHDs than most strains tested in this study, yet this strain showed no evidence for degradation in the assays. Collectively, these findings indicate that strains may use different enzymes than those present in conventional PAH degradation pathways. Finally, further studies are needed to assess whether any strains utilize PAH-derived carbon for biosynthetic or energetic purposes.

PahE has been recently implicated as a biomarker due to its specificity for PAH degradation and its conservation across taxonomically diverse organisms but could not reliably indicate PAH degradation ability with strains in this study (19, 48, 52). To consider the utility of this gene as an indicator for PAH degradation, a broader analysis of 750 *Roseobacteraceae* genomes showed low sequence identity and an absence of conserved residues to validate PahE proteins. This approach was also unable to identify many known *Roseobacteraceae* PAH degraders from this study and others (17, 24). Due to the lack of PahE, it is possible that these strains have novel pathways for biodegradation of PAHs that are not currently detected by bioinformatic approaches that rely on such biomarkers as indications of PAH degradation ability.

PAHs are common pollutants in marine ecosystems and degradation of these pollutants frequently occurs via native bacteria, albeit at limited rates (6, 37). Consequently, PAH degraders are crucial to systems subject to contamination and serve as potential candidates for remediation purposes and indicators of active PAH biodegradation. Bioinformatic and omics-based research depend on prior culture-based work to define genetic biomarkers for PAH degradation. Current biomarkers have challenges with specificity for PAH degradation pathways and the ability to identify novel pathways and/or PAH degraders. The evidence presented by this study suggests that we have yet to uncover the full diversity of bacterial PAH degraders as well as biochemical pathways employed to transform these compounds. Bridging the gap between culture-based investigations and modern bioinformatic approaches holds the key to elucidating the full landscape of PAH biodegradation in marine ecosystems.

Methods

Bacterial strains

The following eighteen strains were analyzed in this study: *Marinobacterium georgiense* DSM 11526 (53), *Bacillus-Clostridium* strain SE165 (54), *Bacillus-Clostridium* strain SE98 (54),

Alteromonas macleodii EZ55 (55), *Vibrio natriegens* ATCC 14048 (56), *Rhodospirillaceae* strain EZ35 (55), *Flavobacteriaceae* strain EZ40 (55), *Alcanivorax* sp. strain EZ46 (55), *Ruegeria pomeroyi* DSS-3 (57), *Citreicella* sp. SE45 (54), *Sagittula stellata* E-37 (58), *Sulfitobacter* sp. EE-36 (59), *Sulfitobacter* NAS-14.1(60), *Ruegeria* sp. TM1040 (46), *Roseovarius* sp. 217 (61), *Roseovarius nubinhibens* ISM (57), Rhodobacterales strain Y4I (28), *Sulfitobacter pontiacus* CB-D (62), and *Escherichia coli* DH5α (See **Table A.2.1** for strain descriptions). These strains were routinely grown on YTSS (Yeast Tryptone Sea Salt) agar [per liter: 15 g Instant Ocean (Thermo Fisher Scientific), 15 g agar (Thermo Fisher Scientific), 4 g tryptone, 2.5 g yeast extract] or YTSS broth at 30°C in the dark, unless otherwise noted.

PAH degradation screening plates

To screen for PAH degradation, a modification of the plate screening assay described in Bogardt & Hemmingsen was used (63). For this modified screening assay, strains were inoculated on top of a PAH-containing top agar rather than within the top agar layer. This allows colonies to be scraped off the agar surface to evaluate clearing zones directly beneath the colonies. In addition, we decided to use a complex medium to screen marine strains for co-metabolism in conjunction with screening initial marine strains for degradation of PAHs as a sole growth substrate (17). For PAH co-metabolism screening, YTSS agar was used as a complex medium base layer, and, for PAH degradation as a sole carbon source, Aromatic Basal Media (ABM) agar (ABM - per liter 8.7 mM KCl, 8.7 mM $CaCl_2$, 43.5 mM $MgSO_4$, and 174 mM NaCl with 225 uM K_2HPO_4, 13.35 mM NH_4Cl, 71 mM Tris-HCl [pH 7.5], 15 g agar (Thermo Fisher Scientific), 68 uM Fe-EDTA, trace metals [7.85 mM nitriloacetic acid, 0.53 mM $MnSO_4{*}H_2O$, 0.42 mM $CoCl_2 {*}6H_2O$, 0.35 mM $ZnSO_4 {*}7H_2O$, 0.038 mM $CuSO_4$, 0.11 mM $NiCl_2 {*}6H_20$, 1.16 mM Na_2SeO_3, 0.41 mM $Na_2MoO_4{*}2H_2O$, 0.33 mM $Na_2WO_4{*}2H_2O$, 0.25 mM $Na_2SiO_3{*}9H_2O$] and trace vitamins [0.0020% vitamin H (Biotin), 0.0020% folic acid, 0.0100% pyridoxine-HCl (B6), 0.0050% riboflavin (B2), 0.0050% thiamine (B1), 0.0050% nicotinic acid, 0.0050% pantothenic acid (B5), 0.0001% cyanocobalamin (B12), 0.0050% *p*-aminobenzoic acid]) was used as a minimal medium base layer. The PAH top-agar overlay was constructed using 5 mg/ml stock solutions of pyrene or phenanthrene dissolved in acetone (Thermo Fisher Scientific, ≥99.5%) and 5 ml of 0.7% top agar, using either agar (Thermo Fisher Scientific) for complex or Agar Noble (Difco™) for minimal media. The final concentration of pyrene (Millipore Sigma, 98%) and phenanthrene

(Millipore Sigma, 98%) in the agar overlay was 286 µg/mL and 430 µg/mL, respectively. Due to the difference in solubility of phenanthrene relative to pyrene, a higher concentration of phenanthrene was added to the top agar to ensure precipitation. The top agar was mixed and poured evenly on the base layer plate. PAH top agar plates were left in a fume hood for at least 2 hours to allow residual acetone to vaporize.

To prepare strains for the PAH top agar screening assay, all strains were grown to stationary phase in YTSS broth and densities adjusted to OD_{540} ~1.6. For PAH top agar complex medium plates, 5 µl of each strain was directly spotted onto plates in triplicate. For PAH top agar minimal medium plates, 1 mL aliquots were first gently centrifuged (2200 x g for 5 min.) and washed twice with ABM broth prior to inoculating plates with 5 µl of each strain in triplicate. Plates were incubated at 30°C in a polypropylene humidity chamber to prevent plates from drying out. PAH top agar complex medium plates were incubated for 7 days with 2 technical replicate plates scraped per day for each PAH (**Figure 2.1**). PAH top agar minimal medium plates were incubated for 14 days with 2 technical replicate plates scraped after 7 days and after 14 days. One strain (*Citreicella* sp. SE45) was able to use acetone as a carbon source, complicating our ability to ascertain its ability to use PAHs as a sole carbon source. Only PAH top agar plates with complex medium were used for the *Roseobacteraceae* screen as all marine bacteria showed degradation only via co-metabolism and previous results suggested that *Roseobacteraceae* members used in this study could not degrade PAHs as a sole carbon source (17). *E. coli* DH5α, previously reported to not degrade PAHs, was used as a negative control (19).

HPLC quantification of pyrene and phenanthrene degradation

Marine and *Roseobacteraceae* strains (triplicates), except for *Alcanivorax* sp. EZ46, were inoculated into 10 mL 5% YTSS and grown overnight, shaking at 200 rpm. *Alcanivorax* sp. EZ46 was excluded as it would not grow in liquid culture conditions. Densities were adjusted to an OD_{540} of ~1.6 in 5% YTSS prior to inoculation (100 µl) in 9.9 mL 5% YTSS with 25 µg/mL pyrene or phenanthrene. Before inoculation, 5% YTSS and PAH tubes were incubated overnight at 30°C to evaporate off residual acetone. A subset of cultures were immediately extracted (T0 controls) and the remaining cultures were incubated for 26 days. Uninoculated controls were incubated and processed in parallel. PAHs were extracted as follows:10 mL of HPLC-grade ethyl acetate (Thermo Fisher Scientific) was added to each tube, mixed, and allowed to separate. The

top aqueous layer was transferred to a 15mL polypropylene conical tube and directly injected into an Agilent 1100 High Performance Liquid Chromatography System (Agilent Technologies Co. Ltd.). The following conditions were used with an injection volume of 20 µl: A C18 column (Acclaim™ PolarAdvantage II C18 5µm 120Å 4.6 X 250 mm, Thermo Fisher Scientific Inc.) was operated at 30 °C with methanol as the mobile phase at a flow rate of 1 mL min^{-1} (17). Both pyrene and phenanthrene were detected using a UV detector at 254 nm. Peak area was compared to the initial inoculum and peak area was normalized to uninoculated controls.

Genomic analyses

For strain with available genome sequences: *M. georgiense* DSM 11526, *A. macleodii* EZ55, *V. natriegens* ATCC 14048, *R. pomeroyi* DSS-3, *Citreicella* sp. SE45, *S. stellata* E-37, *Sulfitobacter* sp. EE-36, *Sulfitobacter* NAS-14.1, *Ruegeria* sp. TM1040, *Roseovarius* sp. 217, *R. nubinhibens* ISM, Rhodobacterales strain Y4I, *S. pontiacus* CB-D, and *E. coli* DH5α. Protein identity searches were done using BLASTP against available genomes at the Joint Genome Institute Integrated Microbial Genomes & Microbiomes System (https://img.jgi.doe.gov/). Query amino acid sequences were selected to cover a diverse range of proteins involved in PAH degradation and obtained from NCBI. Query sequences had their function experimentally proven (**Table A.2.2**) except for PahE sequences from *Novosphingobium pentaromativorans* US6-1 and *Rhodococcus opacus* B4, included to cover the known diversity of PahE proteins as previously described in Liang et al. (52).

Hidden Markov Models were constructed from a PAH biomarker sequence database (64). Sequences for each biomarker were aligned in BioEditv7.2.5 using CLUSTALW (65). KBase (www.kbase.us) and HMMERv3.3.2 were used to search each PAH biomarker model (NarC, NarAa, NahAc, NahE, NidA, and PhdG) against the available genomes above.

Phylogenetic analysis was conducted for putative PahE proteins from over 750 *Roseobacteraceae* strains using BLASTP in JGI IMG (**Table A.2.4**). PahE from *Pseudomonas aeruginosa* PaK1 was used as the search query. Strains that showed at least one protein over 50% amino acid identity and highest amino acid identity results for *Roseobacteraceae* strains in this study were used to construct a maximum likelihood phylogenetic tree. Protein sequences were aligned using BioEditv7.2.5.(65), and the tree was constructed using MEGAXv10.2.2. (66). To further investigate the functionality of these proteins, we aligned putative PahE sequences of

Roseobacteraceae strains listed in this paper with the PahE sequence from *P. aeruginosa* PaK1 (UniProt ACN P0A142). Catalytic residues and putative active sites were predicted based on conserved residues from the NCBI Conserved Domains Database (https://www.ncbi.nlm.nih.gov/cdd) of the CHBPH_aldolase subfamily, containing trans-o-hydroxybenzylidenepyruvate hydratase-aldolase and trans-2'-carboxybenzalpyruvate hydratase-aldolase, both of which are PAH hydratase aldolases.

REFERENCES

1. Gupta G, Kumar V, Pal AK. 2017. Microbial Degradation of High Molecular Weight Polycyclic Aromatic Hydrocarbons with Emphasis on Pyrene. Polycycl Aromat Compd 39:124–138.

2. Sakshi, Haritash AK. 2020. A comprehensive review of metabolic and genomic aspects of PAH-degradation. Arch Microbiol 202:2033–2058.
3. Environmental Protection Agency. 2019. CWA Priority-126 Priority Pollutants.
4. Ghosal D, Ghosh S, Dutta TK, Ahn Y. 2016. Current State of Knowledge in Microbial Degradation of Polycyclic Aromatic Hydrocarbons (PAHs): A Review. Front Microbiol 7:1369.
5. Sieradzki ET, Morando M, Fuhrman JA. 2021. Metagenomics and Quantitative Stable Isotope Probing Offer Insights into Metabolism of Polycyclic Aromatic Hydrocarbon Degraders in Chronically Polluted Seawater. mSystems 6.
6. Ambade B, Sethi SS, Giri B, Biswas JK, Bauddh K. 2021. Characterization, Behavior, and Risk Assessment of Polycyclic Aromatic Hydrocarbons (PAHs) in the Estuary Sediments. Bulletin of Environmental Contamination and Toxicology 1:1–10.
7. Zada S, Zhou H, Xie J, Hu Z, Ali S, Sajjad W, Wang H. 2021. Bacterial degradation of pyrene: Biochemical reactions and mechanisms. Int Biodeterior Biodegradation 162:105233.
8. Head IM, Jones DM, Röling WFM. 2006. Marine microorganisms make a meal of oil. Nat Rev Microbiol 4:173–182.
9. Ahmadun l-R, Pendashteh A, Chuah Abdullah L, Radiah Awang Biak D, Siavash Madaeni S, Zainal Abidin Z. 2009. Review of technologies for oil and gas produced water treatment. J Hazard Mater 170:530–551.
10. Gaurav GK, Mehmood T, Kumar M, Cheng L, Sathishkumar K, Kumar A, Yadav D. 2021. Review on polycyclic aromatic hydrocarbons (PAHs) migration from wastewater. J Contam Hydrol 236:103715.
11. Kim SJ, Kweon O, Jones RC, Edmondson RD, Cerniglia CE. 2008. Genomic analysis of polycyclic aromatic hydrocarbon degradation in *Mycobacterium vanbaalenii* PYR-1. Biodegradation 19:859–881.
12. Kim SJ, Kweon O, Jones RC, Freeman JP, Edmondson RD, Cerniglia CE. 2007. Complete and integrated pyrene degradation pathway in *Mycobacterium vanbaalenii* PYR-1 based on systems biology. J Bacteriol 189:464–472.

13. Kim S-J, Song J, Kweon O, Holland RD, Kim D-W, Kim J, Yu L-R, Cerniglia CE. 2012. Functional Robustness of a Polycyclic Aromatic Hydrocarbon Metabolic Network Examined in a *nidA* Aromatic Ring-Hydroxylating Oxygenase Mutant of *Mycobacterium vanbaalenii* PYR-1. Appl Environ Microbiol 78:3715.
14. Supaka N, Pinphanichakarn P, Pattaragulwanit K, Thaniyavarn S, Omori T, Juntongjin K. 2001. Isolation and Characterization of a Phenanthrene-Degrading *Sphingomonas* sp. Strain P2 and Its Ability to Degrade Fluoranthene and Pyrene via Cometabolism. ScienceAsia 27:21-28.
15. Zhou HW, Luan TG, Zou F, Tam NFY. 2008. Different bacterial groups for biodegradation of three- and four-ring PAHs isolated from a Hong Kong mangrove sediment. J Hazard Mater 152:1179–1185.
16. Zhang X, Zhang Y, Wang X, Zhang L, Ning G, Feng S, Zhang A, Yang Z. 2023. Enhancement of soil high-molecular-weight polycyclic aromatic hydrocarbon degradation by *Fusarium* sp. ZH-H2 using different carbon sources. Ecotoxicol Environ Saf 249:114379.
17. Zhou H, Zhang S, Xie J, Wei H, Hu Z, Wang H. 2020. Pyrene biodegradation and its potential pathway involving Roseobacter clade bacteria. Int Biodeterior Biodegradation 150:104961.
18. Rodríguez A, Zárate SG, Bastida A. 2022. Identification of New Dioxygenases Able to Recognize Polycyclic Aromatic Hydrocarbons with High Aromaticity. Catalysts 12:279.
19. Liang C, Huang Y, Wang H. 2019. *pahE*, a Functional Marker Gene for Polycyclic Aromatic Hydrocarbon-Degrading Bacteria. Appl Environ Microbiol 85.
20. Sunanda S, Varsha V, Prajakti P, Chattopadhyay S, Sachan SG. 2023. Biodegradation of Polycyclic Aromatic Hydrocarbons and the Impact of Various Genes for their Enhanced Degradation. Lett Appl Microbiol 76.
21. Zhang S, Hu Z, Wang H. 2019. Metagenomic analysis exhibited the co-metabolism of polycyclic aromatic hydrocarbons by bacterial community from estuarine sediment. Environ Int 129:308–319.
22. Liang C, Ye Q, Huang Y, Zhang Z, Wang C, Wang Y, Wang H. 2022. Distribution of the new functional marker gene (*pahE*) of aerobic polycyclic aromatic hydrocarbon (PAHs)

degrading bacteria in different ecosystems. Science of The Total Environment 865:161233.

23. Gallego S, Vila J, Tauler M, Nieto JM, Breugelmans P, Springael D, Grifoll M. 2014. Community structure and PAH ring-hydroxylating dioxygenase genes of a marine pyrene-degrading microbial consortium. Biodegradation 25:543–556.
24. Zhang YH, Dong JD, Wang YS, Gu JD, Yin JP, Ahmad M, Ling J. 2022. Comparative genomics reveals the evidence of aromatic hydrocarbons degradation potential in genus *Roseovarius* in marine environment. Int Biodeterior Biodegradation 171:105408.
25. Suenaga H, Koyama Y, Miyakoshi M, Miyazaki R, Yano H, Sota M, Ohtsubo Y, Tsuda M, Miyazaki K. 2009. Novel organization of aromatic degradation pathway genes in a microbial community as revealed by metagenomic analysis. The ISME Journal 3:12 3:1335–1348.
26. Cao J, Lai Q, Yuan J, Shao Z. 2015. Genomic and metabolic analysis of fluoranthene degradation pathway in *Celeribacter indicus* P73 T. Sci Rep 5:1–12.
27. Buchan A, González JM, Chua MJ. 2019. Aerobic Hydrocarbon-Degrading Alphaproteobacteria: *Rhodobacteraceae* (Roseobacter), p. 93–104. *In* McGenity, TJ (ed.), Taxonomy, Genomics and Ecophysiology of Hydrocarbon-Degrading Microbes. Springer International Publishing.
28. Cude WN, Mooney J, Tavanaei AA, Hadden MK, Frank AM, Gulvik CA, May AL, Buchan A. 2012. Production of the antimicrobial secondary metabolite indigoidine contributes to competitive surface colonization by the marine roseobacter *Phaeobacter* sp. strain Y4I. Appl Environ Microbiol 78:4771–4780.
29. Kweon O, Kim SJ, Holland RD, Chen H, Kim DW, Gao Y, Yu LR, Baek S, Baek DH, Ahn H, Cerniglia CE. 2011. Polycyclic aromatic hydrocarbon metabolic network in *Mycobacterium vanbaalenii* PYR-1. J Bacteriol 193:4326–4337.
30. Parales RE, Resnick SM. 2006. Aromatic Ring Hydroxylating Dioxygenases, p. 287–340. *In* Pseudomonas. Springer, Boston, MA.
31. Grant Pearce F, Hudson AO, Loomes K, Dobson RCJ. 2017. Dihydrodipicolinate Synthase: Structure, Dynamics, Function, and Evolution. Subcell Biochem 83:271–289.

32. Buchan A, Neidle EL, Moran MA. 2004. Diverse Organization of Genes of the β-Ketoadipate Pathway in Members of the Marine Roseobacter Lineage. Appl Environ Microbiol 70:1658–1668.
33. Gutierrez T, Whitman WB, Huntemann M, Copeland A, Chen A, Vargese N, Kyrpides NC, Pillay M, Ivanova N, Mikhailova N, Mukherjee S, Stamatis D, Reddy TBK, Ngan CY, Chovatia M, Daum C, Shapiro N, Woyke T. 2017. Genome Sequence of *Oceanicola* sp. Strain MCTG156(1a), Isolated from a Scottish Coastal Phytoplankton Net Sample. Genome Announc 5.
34. Jami M, Lai Q, Ghanbari M Moghadam MS, Kneifel W, Domig KJ. 2016. *Celeribacter persicus* sp. nov., a polycyclic-aromatic-hydrocarbon-degrading bacterium isolated from mangrove soil. Int J Syst Evol Microbiol 66:1875–1880.
35. Jeong HI, Jin HM, Jeon CO. 2015. *Confluentimicrobium naphthalenivorans* sp. Nov., A naphthalene-degrading bacterium isolated from sea-tidal-flat sediment, and amended description of the genus *Confluentimicrobium* Park *et al*. 2015. Int J Syst Evol Microbiol 65:4191–4195.
36. Suarez-Suarez LY, Brunet-Galmes I, Piña-Villalonga JM, Christie-Oleza JA, Peña A, Bennasar A, Armengaud J, Nogales B, Bosch R. 2012. Draft genome sequence of *Citreicella aestuarii* strain 357, a member of the Roseobacter clade isolated without xenobiotic pressure from a petroleum-polluted beach. J Bacteriol 194:5464–5465.
37. Xue J, Yu Y, Bai Y, Wang L, Wu Y. 2015. Marine Oil-Degrading Microorganisms and Biodegradation Process of Petroleum Hydrocarbon in Marine Environments: A Review. Curr Microbiol 71:220–228.
38. Vila J, Nieto JM, Mertens J, Springael D, Grifoll M. 2010. Microbial community structure of a heavy fuel oil-degrading marine consortium: Linking microbial dynamics with polycyclic aromatic hydrocarbon utilization. FEMS Microbiol Ecol 73:349–362.
39. Arora PK. 2020. Bacilli-Mediated Degradation of Xenobiotic Compounds and Heavy Metals. Front Bioeng Biotechnol 8:1100.
40. Kong X, Dong R, King T, Chen F, Li H. 2022. Biodegradation Potential of *Bacillus* sp. PAH-2 on PAHs for Oil-Contaminated Seawater. Molecules 27.

41. Hedlund BP, Staley JT. 2001. *Vibrio cyclotrophicus* sp. nov., a polycyclic aromatic hydrocarbon (PAH)-degrading marine bacterium. Int J Syst Evol Microbiol 51:61–66.
42. Cui Z, Lai Q, Dong C, Shao Z. 2008. Biodiversity of polycyclic aromatic hydrocarbon-degrading bacteria from deep sea sediments of the Middle Atlantic Ridge. Environ Microbiol 10:2138.
43. Viñas M, Sabaté J, Espuny MJ, Solanas AM. 2005. Bacterial community dynamics and polycyclic aromatic hydrocarbon degradation during bioremediation of heavily creosote-contaminated soil. Appl Environ Microbiol 71:7008–7018.
44. Dash HR, Mangwani N, Chakraborty J, Kumari S, Das S. 2013. Marine bacteria: Potential candidates for enhanced bioremediation. Appl Microbiol Biotechnol 97:561–571.
45. Lauro FM, McDougald D, Thomas T, Williams TJ, Egan S, Rice S, DeMaere MZ, Ting L, Ertan H, Johnson J, Ferriera S, Lapidus A, Anderson I, Kyrpides N, Munkf AC, Detterg C, Hang CS, Brown M V., Robb FT, Kjelleberg S, Cavicchioli R. 2009. The genomic basis of trophic strategy in marine bacteria. Proc Natl Acad Sci USA 106:15527–15533.
46. Moran MA, Belas R, Schell MA, González JM, Sun F, Sun S, Binder BJ, Edmonds J, Ye W, Orcutt B, Howard EC, Meile C, Palefsky W, Goesmann A, Ren Q, Paulsen I, Ulrich LE, Thompson LS, Saunders E, Buchan A. 2007. Ecological Genomics of Marine Roseobacters. Appl Environ Microbiol 73:4559–4569.
47. Segura A, Udaondo Z, Azaro Molina L. 2021. PahT regulates carbon fluxes in *Novosphingobium* sp. HR1a and influences its survival in soil and rhizospheres. Environ Microbiol 23:2969–2991.
48. Zafra G, Taylor TD, Absalón AE, Cortés-Espinosa D V. 2016. Comparative metagenomic analysis of PAH degradation in soil by a mixed microbial consortium. J Hazard Mater 318:702–710.
49. Teng Y, Luo Y, Ping L, Zou D, Li Z, Christie P. 2010. Effects of soil amendment with different carbon sources and other factors on the bioremediation of an aged PAH-contaminated soil. Biodegradation 21:167–178.
50. Lozada M, Riva Mercadal JP, Guerrero LD, Di Marzio WD, Ferrero MA, Dionisi HM. 2008. Novel aromatic ring-hydroxylating dioxygenase genes from coastal marine sediments of Patagonia. BMC Microbiol 8.

51. Phale PS, Malhotra H, Shah BA. 2020. Degradation strategies and associated regulatory mechanisms/features for aromatic compound metabolism in bacteria. Adv Appl Microbiol 112:1–65.
52. Liang C, Ye Q, Huang Y, Wang Y, Zhang Z, Wang H. 2022. Shifts of the new functional marker gene (*pahE*) of polycyclic aromatic hydrocarbons (PAHs) degrading bacterial population and its relationship with PAHs biodegradation. J Hazard Mater 437.
53. González JM, Mayer F, Moran MA, Hodson RE, Whitman WB. 1997. *Microbulbifer hydrolyticus* gen. nov., sp. nov., and *Marinobacterium georgiense* gen. nov., sp. nov., two marine bacteria from a lignin-rich pulp mill waste enrichment community. Int J Syst Bacteriol 47:369–376.
54. Buchan A, Neidle EL, Moran MA. 2001. Diversity of the Ring-Cleaving Dioxygenase Gene *pcaH* in a Salt Marsh Bacterial Community. Appl Environ Microbiol 67:5801.
55. Morris JJ, Kirkegaard R, Szul MJ, Johnson ZI, Zinser ER. 2008. Facilitation of robust growth of *Prochlorococcus* colonies and dilute liquid cultures by "helper" heterotrophic bacteria. Appl Environ Microbiol 74:4530–4534.
56. Bang SS, Baumann L, Woolkalis MJ, Baumann P. Evolutionary Relationships in *Vibrio* and *Photobacterium* as Determined by Immunological Studies of Superoxide Dismutase. Arch Microbiol.
57. González JM, Covert JS, Whitman WB, Henriksen JR, Mayer F, Scharf B, Schmitt R, Buchan A, Fuhrman JA, Kiene RP, Moran MA. 2003. *Silicibacter pomeroyi* sp. nov. and *Roseovarius nubinhibens* sp. nov., dimethylsulfoniopropionate-demethylating bacteria from marine environments. Int J Syst Evol Microbiol 53:1261–1269.
58. Gonzalez JM, Mayer F, Moran MA, Hodson RE, Whitman WB. 1997. *Sagittula stellata* gen. nov., sp. nov., a lignin-transforming bacterium from a coastal environment. Int J Syst Bacteriol 47:773–780.
59. Buchan A, Collier LS, Neidle EL, Moran MA. 2000. Key aromatic-ring-cleaving enzyme, protocatechuate 3,4-dioxygenase, in the ecologically important marine Roseobacter lineage. Appl Environ Microbiol 66:4662–4672.
60. Slightom RN, Buchan A. 2009. Surface colonization by marine Roseobacters: Integrating genotype and phenotype. Appl Environ Microbiol 75:6027–6037.

61. Schäfer H, McDonald IR, Nightingale PD, Murrell JC. 2005. Evidence for the presence of a CmuA methyltransferase pathway in novel marine methyl halide-oxidizing bacteria. Environ Microbiol 7:839–852.
62. Tuttle MJ, May FS, Basso JTR, Gann ER, Xu J, Buchan A. 2022. Plasmid-Mediated Stabilization of Prophages. mSphere 7.
63. Bogardt AH, Hemmingsen BB. 1992. Enumeration of phenanthrene-degrading bacteria by an overlayer technique and its use in evaluation of petroleum-contaminated sites. Appl Environ Microbiol 58:2579–2582.
64. Huang Y, Li L, Yin X, Zhang T. 2023. Polycyclic aromatic hydrocarbon (PAH) biodegradation capacity revealed by a genome-function relationship approach. Environ Microbiome 18:1–13.
65. Hall, TA. 1999. BioEdit: A User-Friendly Biological Sequence Alignment Editor and Analysis Program for Windows 95/98/NT. Nucleic Acids Symposium Series 41:95-98.
66. Kumar S, Stecher G, Li M, Knyaz C, Tamura K. 2018. MEGA X: Molecular Evolutionary Genetics Analysis across Computing Platforms. Mol Biol Evol 35:1547–1549.

APPENDIX A

Appendix Table A.2.1: Marine strains used in this study.

Bacteria name	**Taxa**	**Colony Morphology**	**Genome Sequence Available?**	**16S rRNA Gene Accession Number**	**WGS Accession**	**Isolation Site**
Marinobacterium georgiense	Gamma-Proteobacteria	small, circular, translucent, white	Yes	U58339.1	NZ_CP022297.1	Coastal Georgia (USA) seawater by

						enrichment with lignocellulose from a pulp mill (1)
Bacillus-Clostridium strain SE165	Bacillus-Clostridium group	Large, orange colonies	No	AY038905.1	N/A	*Spartina* leaves; Skidaway Island, Georgia (USA) (2)
Bacillus-Clostridium strain SE98	Bacillus-Clostridium group	Large, white flat colonies	No	AY038926.1	N/A	*Spartina* leaves; Skidaway Island, Georgia (USA) (2)
Alteromonas macleodii strain EZ55	Gamma-Proteobacteria	Medium, white, flat colonies	Yes	EU704114	NZ_CABDXN010000001.1	Isolated from a Prochloroccus strain MIT 9215 lab culture (3)

Appendix Table A.2.1 Continued.

Vibrio natriegens ATCC 14048	Gamma-Proteobacteria	Large, beige, flat colonies	Yes	NR_117890.1	ASM145625v1	Salt marsh sediment; Sapelo Island, Georgia (USA) (4)
Rhodospirillaceae strain EZ35	Alpha-proteobacteria	Medium, beige, flat colonies	No	AF493974	N/A	Isolated from a Prochlorococcus strain MED4 lab culture (3)

Flavobacteriaceae strain EZ40	Bacteriodetes	small, flat, yellow colonies	No	EU591706	N/A	Isolated from a Prochlorococcus strain MIT 9312 lab culture (3)
Alcanivorax sp. strain EZ46	Gamma-Proteobacteria	Slow grower, small, white colonies	No	EU591711	N/A	Isolated from a Prochlorococcus strain NATL2A lab culture (3, 5)
Ruegeria pomeroyi DSS-3	Alpha-proteobacteria	Small, beige (turns dark brown), raised colonies	Yes	NR_028727	NC_003911.12	Coastal seawater; Sapelo Island, Georgia (USA), via enrichment on DMSP (6)

Appendix Table A.2.1 Continued.

Citreicella sp. SE45	Alpha-proteobacteria	Medium, mucoid, whiteish-yellow colonies	Yes	AF388308	ACNW00000000.1	*Spartina alterniflora* (smooth cordgrass) detritus; southeastern US salt marshes off Skidaway Island, Georgia (USA) (2)

Sagittula stellata E-37	Alpha-proteobacteria	Small, white, raised colonies	Yes	NR_026016	NZ_AAYA00000000.1	Coastal Georgia (USA) seawater by enrichment with lignocellulose from a pulp mill (7)
Sulfitobacter sp. EE-36	Alpha-proteobacteria	Small, white colonies with orange center	Yes	AF007254	GCA_000152605.1	Salt marsh; Sapelo Island, Georgia (USA) (7)
Sulfitobacter sp. NAS-14.1	Alpha-proteobacteria	Small, white colonies	Yes	642973159 (IMG)	NZ_AALZ00000000.1	Surface waters in North Atlantic Ocean via enrichment on DMSP (8)

Appendix Table A.2.1 Continued.

Ruegeria sp. TM1040	Alpha-proteobacteria	Small, yellow colonies	Yes	640715081 (IMG)	NC_008044.1	Phycosphere of the dinoflagellate *Pfiesteria piscicida* (9)
Roseovarius sp. 217	Alpha-proteobacteria	Tiny, white colonies	Yes	642973074 (IMG)	NZ_AAMV00000000.1	Surface waters near Plymouth, England enriched for growth

						on methyl halide (10)
Roseovarius nubinhibens ISM	Alpha-proteobacteria	Small, orange colonies	Yes	AF098495.1	GCF_000152625.1	Surface waters of the Caribbean Sea (6)
Rhodobacterales strain Y4I	Alpha-proteobacteria	Small, blue/white colonies	Yes	AF388307.1	ABXF00000000.1	Spartina alterniflora (smooth cordgrass) detritus; southeastern salt marshes off Skidaway Island, Georgia (USA) (11)

Appendix Table A.2.1 Continued.

Sulfitobacter pontiacus CB-D	Alpha-proteobacteria	Small, white colonies	Yes	JN121396	IV89_000278	*Emiliania huxleyi* bloom in Raunefjorden, Norway enriched for growth on DMSP (12)
Escherichia coli DH5α	Gamma-Proteobacteria	Medium, mucoid, white colonies	Yes	KC161283	JRYM00000000.1	N/A

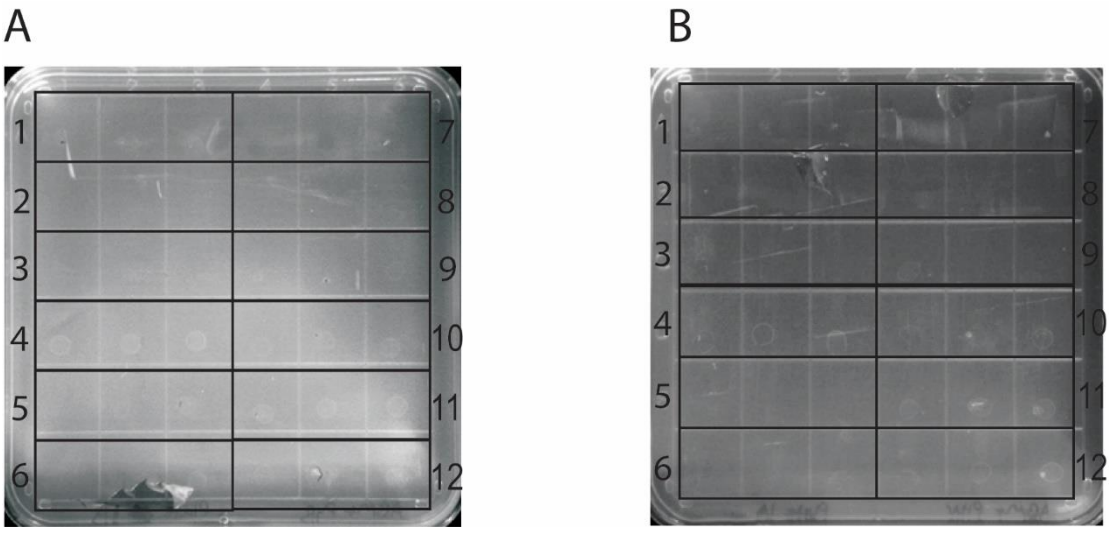

Appendix Figure A.2.1: Minimal medium PAH plate screening for marine strains. (A) Pyrene top agar screening plates after 7 days of incubation. Colonies have been scraped from plates to score for clearing zones. B) Phenanthrene top agar screening plates after 7 days of incubation. Colonies have been scraped from plates to score for clearing zones. 1) *R. pomeroyi* DSS-3, 2) *Citreicella* sp. SE45, 3) *S. stellata* E-37, 4) *Bacillus-Clostridium* strain SE165, 5) *Bacillus-Clostridium* strain SE98, 6) *M. georgiense* DSM 11526, 7) *V. natriegens* ATCC 14048, 8) *Rhodospirillaceae* strain EZ35, 9) *Alcanivorax* sp. strain EZ46, 10) *A. macleodii* strain EZ55, 11) *Flavobacteriaceae* strain EZ40, and 12) *E. coli* DH5α. Clearing zones appear as dark circles on the media.

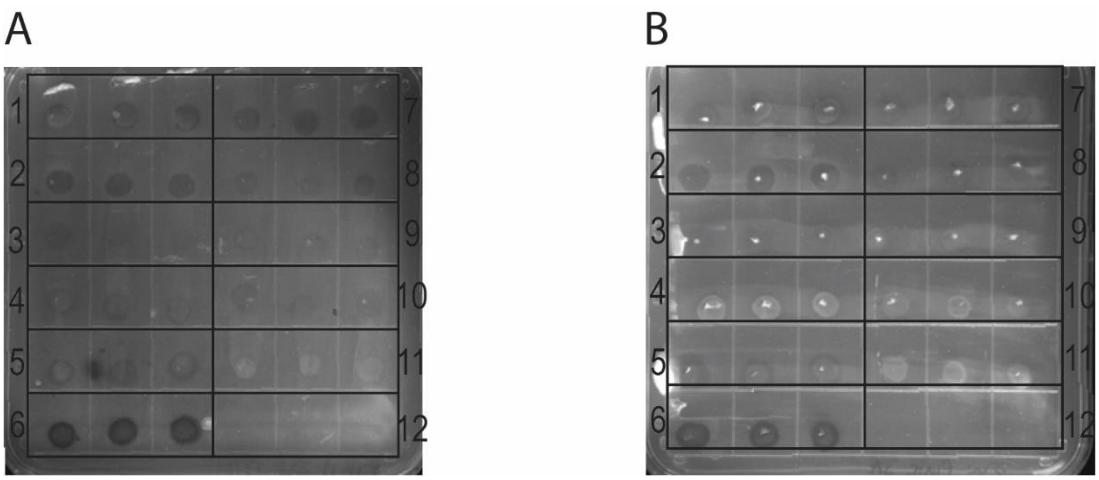

Appendix Figure A.2.2: Complex medium PAH plate screening for *Roseobacteraceae* strains. A) *Roseobacteraceae* strains in pyrene top agar screening plates after 4 days of incubation. Colonies have been scraped from plates to score for clearing zones. B) *Roseobacteraceae* strains on phenanthrene top agar screening plates after 3 days of incubation. Colonies have been scraped from plates to score for clearing zones. 1) *R. pomeroyi* DSS-3, 2) *S. stellata* E-37, 3) *R. nubinhibens* ISM, 4) *Sulfitobacter* sp. EE-36, 5) *Citreicella* sp. SE45, 6) Rhodobacterales strain Y4I, 7) *Ruegeria* sp. TM1040, 8) *Roseovarius* sp. 217, 9) *Sulfitobacter* sp. NAS-14.1, 10) *S. pontiacus* CB-D, 11) *E. coli* DH5α, and 12) None. Clearing zones appear as dark circles on the media.

Appendix Table A.2.2: Query sequences for protein identity searches.

Protein	Group	Query Strain Name	GenBank Accession Number/NCBI Reference Sequence Number	Reference
PahE-NP	PAH Hydratase Aldolase	*Novosphingobium pentaromativorans* US6-1	AIT82654.1	Liang et al., 2019; Liang et al., 2022 (13, 14)
PahE-RO	PAH Hydratase Aldolase	*Rhodococcus opacus* B4	BAH47216	Liang et al., 2019; Liang et al., 2022 (13, 14)
PahE-MV	PAH Hydratase Aldolase	*Mycobacterium vanbaalenii* PYR-1	ABM11319	Liang et al., 2019; Liang et al., 2022 (13, 14)
PahE-PA	PAH Hydratase Aldolase	*Pseudomonas aeruginosa* PaK1	BAA12246.1	Takizawa et al., 1999 (15)
NidA	Gram + PAH/Phthalate	*Mycobacterium vanbaalenii* PYR-1	AF249301.2	Kim et al., 2012 (16)
PobA	I	*Pseudomonas pseudoalcaligenes* POB310	CAA55400.1	Dehmel et al., 1995 (17)
AntA	II	*Pseudomonas resinovorans* CA10	WP_011077861.1	Urata et al., 2004 (18)
PahAc	III	Pseudomonas putida OUS82	BAA20391.1	Kiyohara et al., 1994 (19)
BphA1	IV	*Rhodococcus globerulus* P6	CAA56346.1	McKay et al., 1997 (20)
NagG	Salicylate	*Ralstonia* sp. U2	AAD12607.1	Fuenmayor et al., 1995 (21)

Appendix Table A.2.2 Continued.

PcaH	Protocatechuate 3,4-Dioxygenase	*Pseudomonas* sp. Strain HR199	CAB43484.1	Overhage et al., 1999 (22)
PcaA/LigB	Protocatechuate 4,5-Dioxygenase	*Pseudarthrobacter phenanthrenivorans* Sphe3	ADX75303.1	Tsagogiannis et al., 2021 (23)
CatA	Catechol 1,2-Dioxygenase	*Acinetobacter calcoaceticus*	SUU57696.1	Neidle &Ornston, 1986 (24)
CatE/YfiE	Catechol 2,3-Dioxygenase	*Bacillus subtilis* 168	BAA09109.1	Thi Tam et al., 2006 (25)

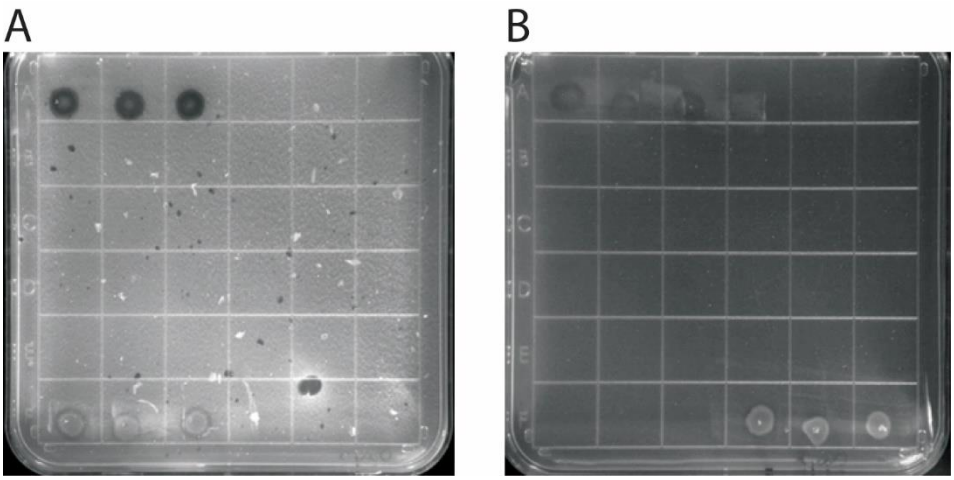

Appendix Figure A.2.3: Rhodobacterales strain Y4I and igiD$^-$ pyrene and phenanthrene screening. Wild type Y4I is shown on the top of the plate and the *igiD*$^-$ mutant strain is shown on the bottom of the plate. A) Pyrene top agar screening plate and B) Phenanthrene top agar screening plate after 5 days of incubation.

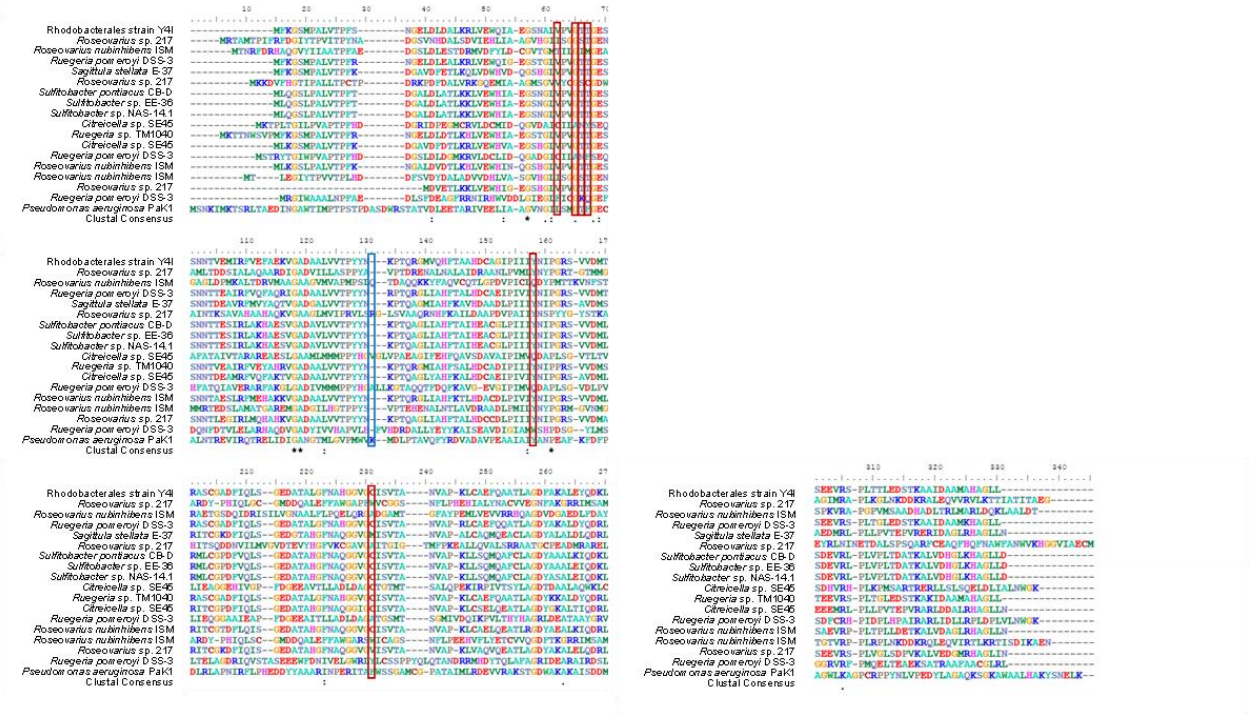

Appendix Figure A.2.4: Alignment of *Roseobacteraceae* strain putative PahE sequences. Putative active site residues are marked in red and the catalytic site is marked in blue. Amino acid consensus is denoted in the last line of the alignment (* indicates Fully Conserved Residue; : indicates Strong Similarity; · Weak Similarity). Active and catalytic sites were derived from the CHBPH_aldolase subfamily using the NCBI Conserved Domains Database (https://www.ncbi.nlm.nih.gov/cdd).

APPENDIX A REFERENCES

1. González JM, Mayer F, Moran MA, Hodson RE, Whitman WB. 1997. *Microbulbifer hydrolyticus* gen. nov., sp. nov., and *Marinobacterium georgiense* gen. nov., sp. nov., two marine bacteria from a lignin-rich pulp mill waste enrichment community. Int J Syst Bacteriol 47:369–376.
2. Buchan A, Neidle EL, Moran MA. 2001. Diversity of the ring-cleaving dioxygenase gene *pcaH* in a salt marsh bacterial community. Appl Environ Microbiol 67:5801.
3. Morris JJ, Kirkegaard R, Szul MJ, Johnson ZI, Zinser ER. 2008. Facilitation of robust growth of *Prochlorococcus* colonies and dilute liquid cultures by "helper" heterotrophic bacteria. Appl Environ Microbiol 74:4530–4534.
4. Austin B, Zachary A, Colwell RR. 1978. Recognition of *Beneckea natriegens* (Payne *et al*.) Baumann *et al*. as a member of the genus *Vibrio*, as previously proposed by Webb and Payne. Int J Syst Bacteriol 28:315–317.
5. Moran MA, Buchan A, González JM, Heidelberg JF, Whitman WB, Klene RP, Henriksen JR, King GM, Belas R, Fuqua C, Brinkac L, Lewis M, Johri S, Weaver B, Pai G, Elsen JA, Rahe E, Sheldon WM, Ye W, Miller TR, Carlton J, Rasko DA, Paulsen IT, Ren Q, Daugherty SC, Deboy RT, Dodson RJ, Durkin AS, Madupu R, Nelson WC, Sullivan SA, Rosovitz MJ, Haft DH, Selengut J, Ward N. 2004. Genome sequence of *Silicibacter pomeroyi* reveals adaptations to the marine environment. Nature 432:910–913.
6. González JM, Covert JS, Whitman WB, Henriksen JR, Mayer F, Scharf B, Schmitt R, Buchan A, Fuhrman JA, Kiene RP, Moran MA. 2003. *Silicibacter pomeroyi* sp. nov. and *Roseovarius nubinhibens* sp. nov., dimethylsulfoniopropionate-demethylating bacteria from marine environments. Int J Syst Evol Microbiol 53:1261–1269.
7. Buchan A, Collier LS, Neidle EL, Moran MA. 2000. Key aromatic-ring-cleaving enzyme, protocatechuate 3,4-dioxygenase, in the ecologically important marine Roseobacter lineage. Appl Environ Microbiol 66:4662–4672.
8. Slightom RN, Buchan A. 2009. Surface colonization by marine Roseobacters: Integrating genotype and phenotype. Appl Environ Microbiol 75:6027–6037.
9. Moran MA, Belas R, Schell MA, González JM, Sun F, Sun S, Binder BJ, Edmonds J, Ye W, Orcutt B, Howard EC, Meile C, Palefsky W, Goesmann A, Ren Q, Paulsen I, Ulrich

LE, Thompson LS, Saunders E, Buchan A. 2007. Ecological genomics of marine Roseobacters. Appl Environ Microbiol 73:4559–4569.

10. Schäfer H, McDonald IR, Nightingale PD, Murrell JC. 2005. Evidence for the presence of a CmuA methyltransferase pathway in novel marine methyl halide-oxidizing bacteria. Environ Microbiol 7:839–852.
11. Buchan A, Neidle EL, Moran MA. 2004. Diverse organization of genes of the β-ketoadipate pathway in members of the marine Roseobacter lineage. Appl Environ Microbiol 70:1658–1668.
12. Ankrah NYD, Lane T, Budinoff CR, Hadden MK, Buchan A. 2014. Draft genome sequence of *Sulfitobacter* sp. CB2047, a member of the Roseobacter clade of marine bacteria, isolated from an *Emiliania huxleyi* bloom. Genome Announc 2.
13. Liang C, Huang Y, Wang H. 2019. *pahE*, a functional marker gene for polycyclic aromatic hydrocarbon-degrading bacteria. Appl Environ Microbiol 85.
14. Liang C, Ye Q, Huang Y, Wang Y, Zhang Z, Wang H. 2022. Shifts of the new functional marker gene (*pahE*) of polycyclic aromatic hydrocarbons (PAHs) degrading bacterial population and its relationship with PAHs biodegradation. J Hazard Mater 437.
15. Takizawa N, Iida T, Sawada T, Yamauchi K, Wang YW, Fukuda M, Kiyohara H. 1999. Nucleotide sequences and characterization of genes encoding naphthalene upper pathway of *Pseudomonas aeruginosa* PaK1 and *Pseudomonas putida* OUS82. J Biosci Bioeng 87:721–731.
16. Kim S-J, Song J, Kweon O, Holland RD, Kim D-W, Kim J, Yu L-R, Cerniglia CE. 2012. Functional robustness of a polycyclic aromatic hydrocarbon metabolic network examined in a *nidA* aromatic ring-hydroxylating oxygenase mutant of *Mycobacterium vanbaalenii* PYR-1. Appl Environ Microbiol 78:3715.
17. Dehmel U, Engesser KH, Timmis KN, Dwyer DF. 1995. Cloning, nucleotide sequence, and expression of the gene encoding a novel dioxygenase involved in metabolism of carboxydiphenyl ethers in *Pseudomonas pseudoalcaligenes* POB310. Archives of Microbiology 1995 163:1 163:35–41.
18. Urata M, Miyakoshi M, Kai S, Maeda K, Habe H, Omori T, Yamane H, Nojiri H. 2004. Transcriptional regulation of the ant operon, encoding two-component anthranilate 1,2-

dioxygenase, on the carbazole-degradative plasmid pCAR1 of *Pseudomonas resinovorans* strain CA10. J Bacteriol 186:6815–6823.

19. Kiyohara H, Torigoe S, Kaida N, Asaki T, Iida T. 1994. Cloning and characterization of a chromosomal gene cluster, *pah*, that encodes the upper pathway for phenanthrene and naphthalene utilization by *Pseudomonas putida* OUS82. J Bacteriol 176:2439–2443.
20. McKay DB, Seeger M, Zielinski M, Hofer B, Timmis KN. 1997. Heterologous expression of biphenyl dioxygenase-encoding genes from a gram-positive broad-spectrum polychlorinated biphenyl degrader and characterization of chlorobiphenyl oxidation by the gene products. J Bacteriol 179:1924–1930.
21. Fuenmayor SL, Wild M, Boyes AL, Williams PA. 1998. A gene cluster encoding steps in conversion of naphthalene to gentisate in *Pseudomonas* sp. strain U2. J Bacteriol 180:2522–2530.
22. Overhage J, Priefert H, Steinbüchel A. 1999. Biochemical and genetic analyses of ferulic acid catabolism in *Pseudomonas* sp. strain HR199. Appl Environ Microbiol 65:4837–4847.
23. Tsagogiannis E, Vandera E, Primikyri A, Asimakoula S, Tzakos AG, Gerothanassis IP, Koukkou AI. 2021. Characterization of protocatechuate 4,5-dioxygenase from *Pseudarthrobacter phenanthrenivorans* Sphe3 and *in situ* reaction monitoring in the NMR tube. Int J Mol Sci 22.
24. Neidle EL, Ornston LN. 1986. Cloning and expression of *Acinetobacter calcoaceticus* catechol 1,2-dioxygenase structural gene *catA* in *Escherichia coli*. J Bacteriol 168:815–820.
25. Le TT, Eymann C, Albrecht D, Sietmann R, Schauer F, Hecker M, Antelmann H. 2006. Differential gene expression in response to phenol and catechol reveals different metabolic activities for the degradation of aromatic compounds in *Bacillus subtilis*. Environ Microbiol 8:1408–1427.

CHAPTER 3

CHARACTERIZATION OF POLYCYCLIC AROMATIC HYDROCARBON CO-METABOLISM BY *RUEGERIA POMEROYI* DSS-3

JW conceived the project, conducted experiments, analyzed results, created figures, and wrote the article; AB supervised the project and provided feedback on the article.

Abstract

Ruegeria pomeroyi DSS-3 is a model *Roseobacteraceae* able to degrade polycyclic aromatic hydrocarbons (PAHs) via co-metabolism. As *R. pomeroyi* DSS-3 lacks described PAH degradation biomarkers, including PahE and characterized PAH ring-hydroxylating dioxygenases, its mechanism of PAH transformation is unknown. To address this knowledge gap, we investigated the growth stage, labile carbon sources, and protein-coding genes involved in the PAH co-metabolism of this organism. Growth dynamics and pyrene concentration (via HPLC) demonstrated the co-metabolism of *R. pomeroyi* DSS-3 is dependent on both labile carbon source and growth phase. Pyrene degradation was evident when either *p*-hydroxybenzoate or a yeast extract and tryptone mixture were provided as labile carbon sources. Conversely, acetate did not support pyrene degradation. To identify genetic loci involved in PAH co-metabolism, a > 6000 member Tn5 random mutant library of *R. pomeroyi* DSS-3 was generated and screened for pyrene degradation using a qualitative PAH top agar assay. Two Tn5 mutants with diminished pyrene degradation mapped to a putative catabolic region, harboring genes with homology to proteins predicted to mediate monocyclic aromatic compound degradation. After constructing additional mutants in this genetic locus, we confirmed the involvement of SPO3678, a predicted Rieske 2Fe-2S domain protein, in co-metabolism and hypothesized its role in the initial hydroxylation of pyrene. Homologs of this protein are found in other *Roseobacteraceae,* including several capable of degrading PAHs via co-metabolism, suggesting a conserved mechanism for PAH transformation in lineage members.

Introduction

Polycyclic aromatic hydrocarbons (PAHs) are toxic, carcinogenic pollutants present in atmospheric, terrestrial, and aquatic environments (1). These pollutants enter environments through various natural (i.e., volcanoes and forest fires) and anthropogenic (i.e., oil spills and industrial waste discharge) sources (2). Coastal marine ecosystems are a common final destination for PAHs, where they can enter via atmospheric deposition, terrestrial run-off, or direct discharge into aquatic environments (1, 3, 4). While these pollutants are found ubiquitously in the environment, their removal poses a challenge. The stability, hydrophobicity,

and low bioavailability of these compounds increase their recalcitrance, thus categorizing them as persistent organic pollutants (5, 6). While physical and chemical removal methods are available, these methods often have low degradation efficiencies and high costs. In contrast, biological removal methods, such as biodegradation by microorganisms, present a potentially more efficient and cost-effective solution to PAH pollution (2).

Significant research has been done to investigate the PAH degradation ability of bacteria, with particular focus on *Mycobacterium* spp., *Pseudomonas* spp., *Rhodococcus* spp. and *Sphingomonadales* representatives. These taxa demonstrate high degradation efficiencies as well as the ability to utilize PAHs as sole carbon substrates (7–10). From studies of these bacteria, a limited number of degradation pathways have been described and degraders are frequently identified by the presence of one or more genetic biomarkers (i.e., PahAc, PahE) from these pathways (5, 11). While prior studies overwhelmingly focused on microbes capable of sole-metabolism (i.e., use of PAH as a sole carbon and energy source), recent studies suggest that alternative pathways, including co-metabolism, exist and warrant further study (12, 13). Here, we define co-metabolism as the ability of a microbe to degrade a recalcitrant compound only in the presence of a more labile carbon source.

One group capable of PAH co-metabolism is the *Roseobacteraceae* family of Alphaproteobacteria. Family members are commonly found in marine systems, most notably coastal regions where they can represent upwards of one-quarter of bacterial communities (14). Collectively, family members display tremendous metabolic and genetic diversity, even among closely related strains (15, 16). Representatives are adept at transforming monocyclic aromatic compounds, principally those derived from lignin, and possess numerous ring-cleaving pathways that facilitate the complete degradation of these compounds (15, 17). Mounting evidence indicates they also degrade polycyclic aromatics, including those of anthropogenic origin, such as PAHs. Yet the pathways utilized by these strains are relatively unknown (15, 18–20). Recently, we suggested that *Roseobacteraceae* family members possess a novel pathway(s) for PAH degradation due to the lack of previously characterized genetic biomarkers (Chapter 2; 12). Furthermore, while some members possess the ability to degrade PAHs via sole-metabolism, co-metabolism appears to be a prevalent degradation strategy in this family (12, 18).

Here, we investigate the PAH degradation pathway and co-metabolism mechanism of *Ruegeria pomeroyi* DSS-3, a model *Roseobacteraceae* family member. Despite previous documentation of PAH co-metabolism in this strain, the function and mechanism of this metabolic strategy is currently unknown (12, 18, 21). To investigate the role of co-metabolism in survival and growth of the strain when exposed to PAHs, we assessed both the labile carbon source and growth requirements for co-metabolism to occur. While co-metabolism in this strain has been shown to occur in the presence of complex carbon substrates (e.g., yeast extract and tryptone) here, we assessed whether a monocyclic aromatic compound and/or central metabolism precursor was sufficient to promote co-metabolism (12). Finally, we identified a genomic region within *R. pomeroyi* DSS-3 that may be involved in PAH catabolism. From this, we propose that a gene within the region, SPO3678, encodes an uncharacterized dioxygenase that is able to act on PAHs and may be a candidate biomarker for PAH degradation.

Results

Evidence of co-metabolism of PAHs with different carbon sources

To assess PAH co-metabolism requirements of *Ruegeria pomeroyi* DSS-3, both growth and pyrene degradation of the strain were monitored with three different carbon sources: a complex carbon mixture containing yeast extract and tryptone (YTSS), a common organic acid and central metabolism precursor (acetate), and a monocyclic aromatic compound commonly derived from lignin (*p*-hydroxybenzoate; POB) (**Figure 3.1**). YTSS was previously shown to support co-metabolism in this strain, while acetate and POB had not yet been investigated (12). Pyrene was utilized in this study as a model PAH due to its abundance and structural similarity to carcinogenic PAHs (5, 22).

Each carbon source supported growth of *R. pomeroyi* DSS-3 in the presence of pyrene, albeit at different rates. YTSS cultures reach stationary by 13 hours, acetate cultures by 25 hours, and POB at around 170 hours (7 days). POB cultures also had an extended exponential period (130 hours; >5 days), compared to ~10 hour exponential period for YTSS and the ~22 hour for acetate. Substantial pyrene degradation was only detected in the YTSS cultures (14%) and the POB cultures (13%), whereas little to no degradation was observed in the acetate cultures (1%). In addition, while pyrene degradation appeared to occur in early exponential phase (5 hours) for the YTSS cultures, degradation started early exponential phase and continued until late

exponential phase in the POB cultures (153 hours; >6 days). Both YTSS and acetate cultures with pyrene reached 10^8 viable cells/mL, whereas POB only reached a magnitude of 10^7 cells/mL. The solvent controls lagged in growth compared to the pyrene containing cultures for YTSS and POB, whereas there is little difference between the control and treatment cultures for acetate.

Identification of R. pomeroyi DSS-3 transposon mutants with altered pyrene degradation phenotype

A 6,060 member Tn5 mutant library was constructed and screened for pyrene degradation using a top agar screening approach (12). Sixty-two pyrene degradation deficient mutants were selected for further study (**Figure 3.2; Table B.3.4**). Mapping of the Tn5 insertions revealed 53 were located on the chromosome of *R. pomeroyi* DSS-3 and nine on a megaplasmid. Disrupted genes included those predicted to be involved in energy production and conversion (9.6%), transcription and translation (9.6%), amino acid metabolism and transport (9.6%), carbohydrate transport and metabolism (6.5%), lipid metabolism and transport (6.5%), inorganic ion metabolism and transport (4.8%), motility (3.2%), coenzyme metabolism and transport (3.2%), signal transduction (3.2%). Nearly 20% of the insertions were mapped to conserved hypothetical genes and 11% to non-coding regions. All mutants were screened for growth anomaly and those showing defects (18-E9; 33-F8; 56-D11) were not analyzed further (**Table B.3.5**).

Ten mutants had disruptions in putative oxidoreductase genes and one in a hydratase gene. These enzymes have the potential to play a role in the upper catabolic pathway required for PAH degradation based on the presence of homologous genes in canonical PAH degradation pathways (7). In addition, three mutants had disruptions within one of the two LuxRI-type quorum sensing systems, which is of interest due to the previously documented role of quorum sensing in PAH degradation in other strains (**Figure B.3.2**) (23, 24).

Identification of a putative PAH catabolic region

Two mutants (8-5F and 41-G7) were mapped to a putative catabolic region and found to disrupt a FAD-binding oxidoreductase (SPO3666) and a Rieske 2Fe-2S domain protein (SPO3678), respectively (Figure 3.3; Table B.3.4). The Rieske 2Fe-2S domain protein was of particular interest because it showed limited amino acid sequence similarity to the characterized PAH ring-hydroxylating dioxygenases, PahAc (35%) and NidA (25%) (12). Within this ~60 kb catabolic

Figure 3.1: Pyrene degradation during *R. pomeroyi* DSS-3 growth on A) 5% YTSS, B) 5mM Acetate, and C) 2.5mM p-hydroxybenzoate (POB). Percent degradation is relative to T0 culture and accounts for deviation from uninoculated controls. Standard error was calculated for three replicate cultures. Viable cell counts were taken from three replicate cultures at discrete timepoints during growth on each carbon source. Acetone control and no carbon added controls were also assessed for viable cells to account for any inhibitory effect of the pyrene and any growth in the medium. The 5% YTSS did not have no carbon added controls since it is a complex medium.

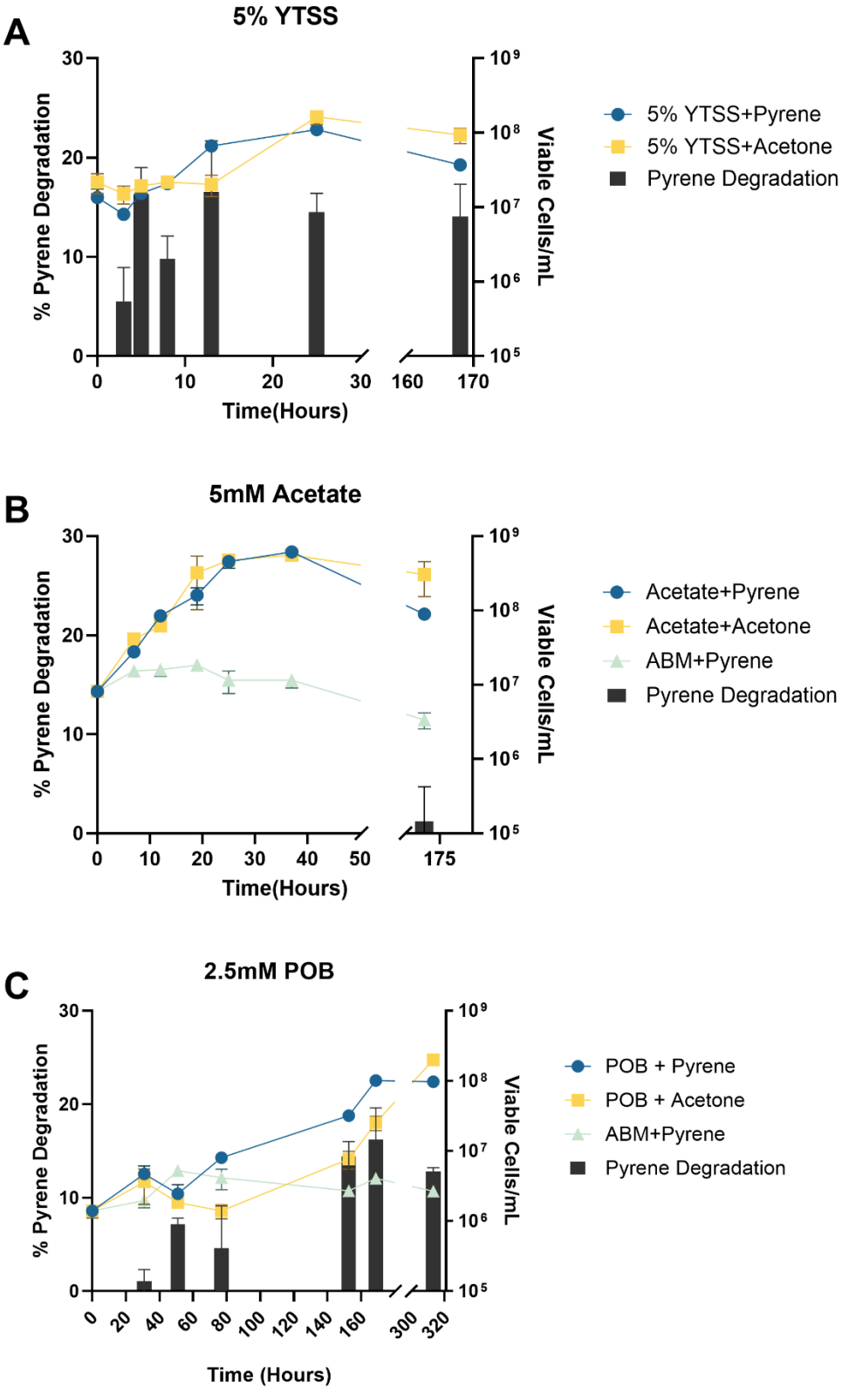
A
5% YTSS
% Pyrene Degradation
Viable Cells/mL
Time(Hours)
5% YTSS+Pyrene
5% YTSS+Acetone
Pyrene Degradation
B
5mM Acetate
% Pyrene Degradation
Viable Cells/mL
Time(Hours)
Acetate+Pyrene
Acetate+Acetone
ABM+Pyrene
Pyrene Degradation
C
2.5mM POB
% Pyrene Degradation
Viable Cells/mL
Time (Hours)
POB + Pyrene
POB + Acetone
ABM+Pyrene
Pyrene Degradation

Figure 3.2: Genome map of 62 Tn5 insertion sites identified using arbitrary PCR from the deficient pyrene degradation *R. pomeroyi* DSS-3 mutants. Locus IDs for insertion locations are found in **Table B.3.4.**

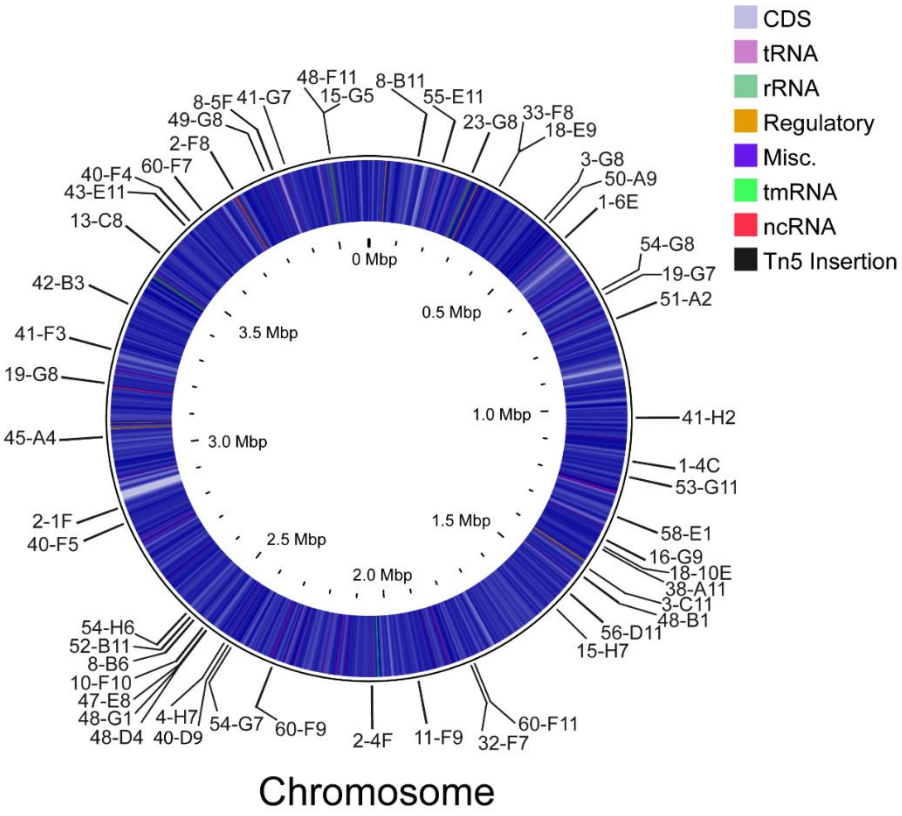

Chromosome

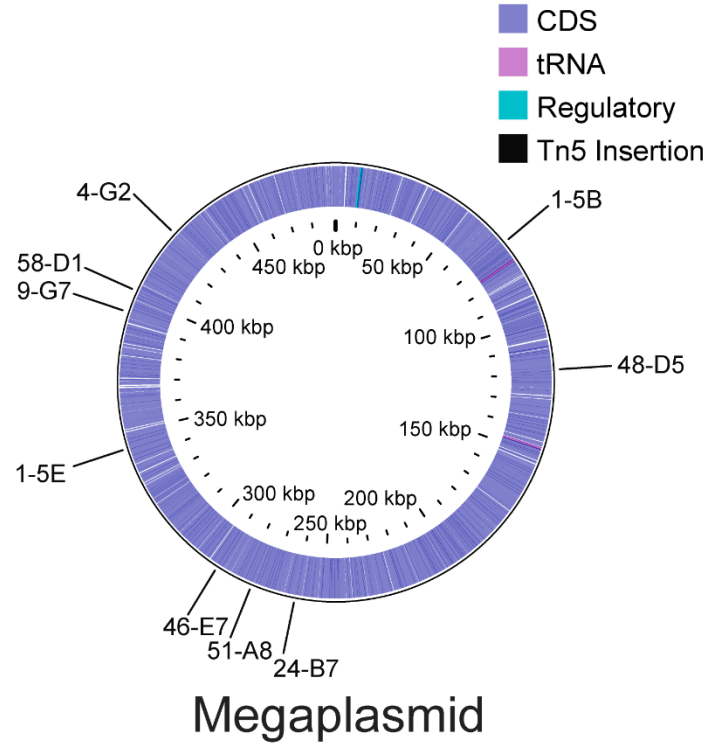

Megaplasmid

region, genes encoding for homologs to characterized aromatic compound catabolism genes are found, including genes for gentisate (SPO3690; SPO3691) and benzoate (SPO3692; SPO3697; SPO3700; SPO3701; SPO3703) degradation (**Figure 3.3**). Another Rieske 2Fe-2S domain protein (SPO3681) was also present, proximal to SPO3678 and within the same putative operon (**Figure 3.3**). To further characterize this region, targeted insertional mutagenesis was conducted on several genes within this region, including SPO3678. The four additional genes selected for mutagenesis were: (i) SPO3690 predicted to encode a gentisate 1,2-dioxygenase (GtdA-1), (ii) SPO3700 predicted to encode a 2,3-dihydro-2,3-dihydroxybenzoyl-CoA ring cleavage enzyme (BoxC), (iii) SPO3688 predicted to encode an extradiol ring-cleavage dioxygenase family protein, and (iv) SPO3681 predicted to encode a Rieske 2Fe-2S domain protein (**Figure 3.3**). Pyrene co-metabolism was quantified for these seven mutants using HPLC. While all mutants retained some ability to transform pyrene, SPO3666::Tn5-KanR, SPO3678::Tn5-KanR, and SPO3678::pKnock-Km showed (58-70%) diminished activity (**Figure 3.4**). Conversely, SPO3688::pKnock-Km and SPO3681::pKnock-Km showed only slight impairment of activity (5-18%). Finally, SPO3690::pKnock-Km and SPO3700::pKnock-Km had increased degradation (130-155%).

After confirming the phenotype of the SPO3678 disruption, we wanted to further investigate this locus and thus obtained additional Tn5 mutants from an existing arrayed library targeting the following genes: SPO3677, SPO3679, SPO3680, and SPO3682 (25). All but one mutant (SPO3682::Tn5) had no pleiotropic deficiency (**Table B.3.5**). Each mutant was subjected to the same HPLC analysis as previously conducted. These mutants only showed slight impairment in degradation compared to WT: SPO3677::Tn5 (2%), SPO3679::Tn5(8%), SPO3680::Tn5(10%), and SPO3682::Tn5(2%) (**Figure 3.4**).

SPO3678 is conserved in some Roseobacteraceae PAH degraders

To determine the distribution SPO3678 homologs and determine the potential for this gene to be involved in PAH co-metabolism in other bacteria, both sequence identity and gene neighborhood investigations were conducted on all whole genome sequences available through JGI IMG (https://img.jgi.doe.gov/mer/) as of October 2023. While a large diversity of queried strains had proteins with >40% amino acid identity (a higher threshold than SPO3678 relative to other PAH

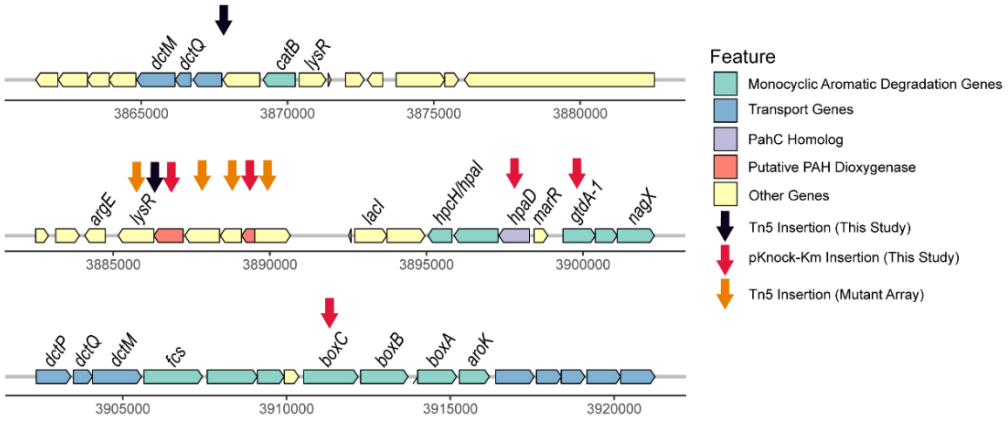

Figure 3.3: Putative PAH catabolic region in *R. pomeroyi* DSS-3. Gene insertions from this study are marked in black for transposon insertions and red for pKnock-Km insertions. Transposon insertions for the array mutants used from Mejia et al., 2022 are marked in orange (25). Genes are colored by predicted category of the annotated protein-coding genes listed in the legend. Numbers under the gene symbols represent chromosomal position from the ASN: GCA_000011965 reference.

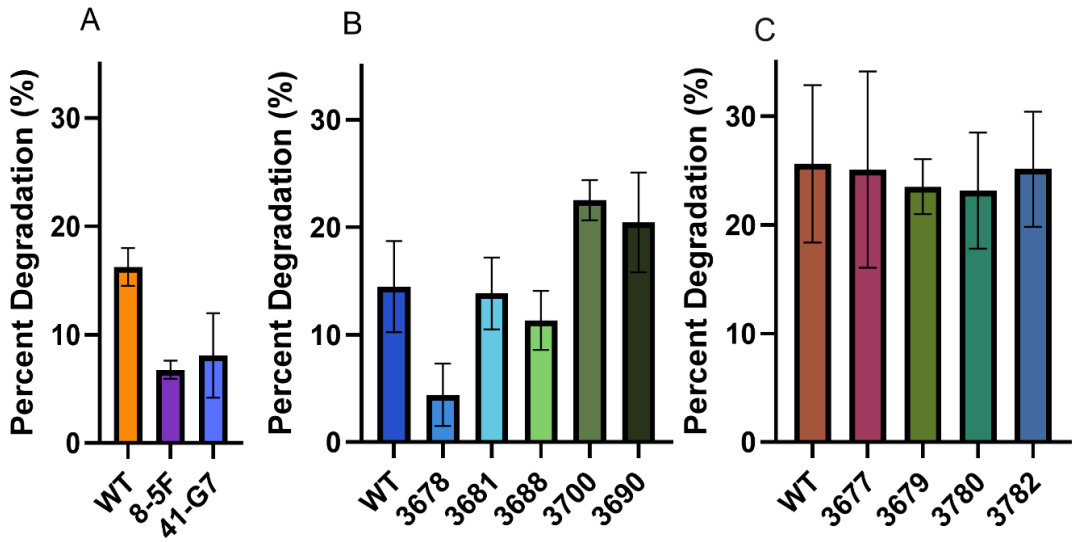

Figure 3.4: Percent degradation of pyrene for A) Tn5 mutants, B) pKnock mutants, and C) Tn5 array mutants. Percent degradation is relative to T0 culture and accounts for deviation from uninoculated controls. Standard error was calculated for three replicate cultures. Tn5 mutant names and gene locus disrupted with pKnock are listed on the x-axis.

ring-hydroxylating dioxygenases) to SPO3678, most were Alphaproteobacteria either closely related to *Roseobacteraceae* or within the family. Within the *Roseobacteraceae* family, 49 strains had above 40% identity to SPO3678. Three *Roseobacteraceae* family members that previously had reports of PAH degradation, *Aliiroseovarius* sp. PrR006, *Roseovarius nubinhibens* ISM, and *Ruegeria* sp. PrR009, had high amino acid identity (62.8-80%) at this locus. In addition, an investigation into the gene neighborhoods revealed that these strains have high gene synteny to *R. pomeroyi* DSS-3 due to the presence of 4 to 6 homologous genes within the putative operon (**Figure 3.5**) (18).

To further explore the possible function of SPO3678 in PAH hydroxylation, a protein model of SPO3678 was constructed using ColabFold and compared against publicly available protein databases using FoldSeek (26, 27). Of the protein models in the AlphaFold database, a predicted biphenyl dioxygenase from *Roseobacteraceae* member *Shimia thalassica* was the top hit with an E-value of $9.02e^{-65}$, a TM-score of 0.9929, and an RMSD of 0.6, which confirmed that it had a highly similar fold to SPO3678. In addition, this protein sequence had an amino acid identity of 74% to SPO3678. Furthermore, the FoldSeek results also revealed that several experimentally proven protein structures were similar to the SPO3678 model. Many of the top hits in the PDB database were for a quaternary ammonium Rieske monooxygenase CntA from *Acinetobacter baumannii*, which is involved in the cleavage of carnitine, a non-cyclic compound (28). Additionally, several biphenyl, terephthalate, and naphthalene dioxygenases as well as dioxygenases for other aromatic compounds showed similar protein structure to the SPO3678 model (**Figure 3.6; Table B.3.7**). Each of these dioxygenases was experimentally found to act on their predicted substrate and the protein structure was obtained via X-ray diffraction (29–31).

Discussion

The objective of this work was to investigate the mechanism of co-metabolic PAH degradation in *Ruegeria pomeroyi* DSS-3. Based on the results of this study, pyrene co- metabolism does not appear to be cell density dependent, but rather dependent on the labile carbon source present. This is supported both by the lack of degradation in the acetate cultures as well as the degradation in early exponential phase for the YTSS cultures. Both YTSS and POB were able to promote pyrene degradation, suggesting that enzymes induced by these carbon sources also act

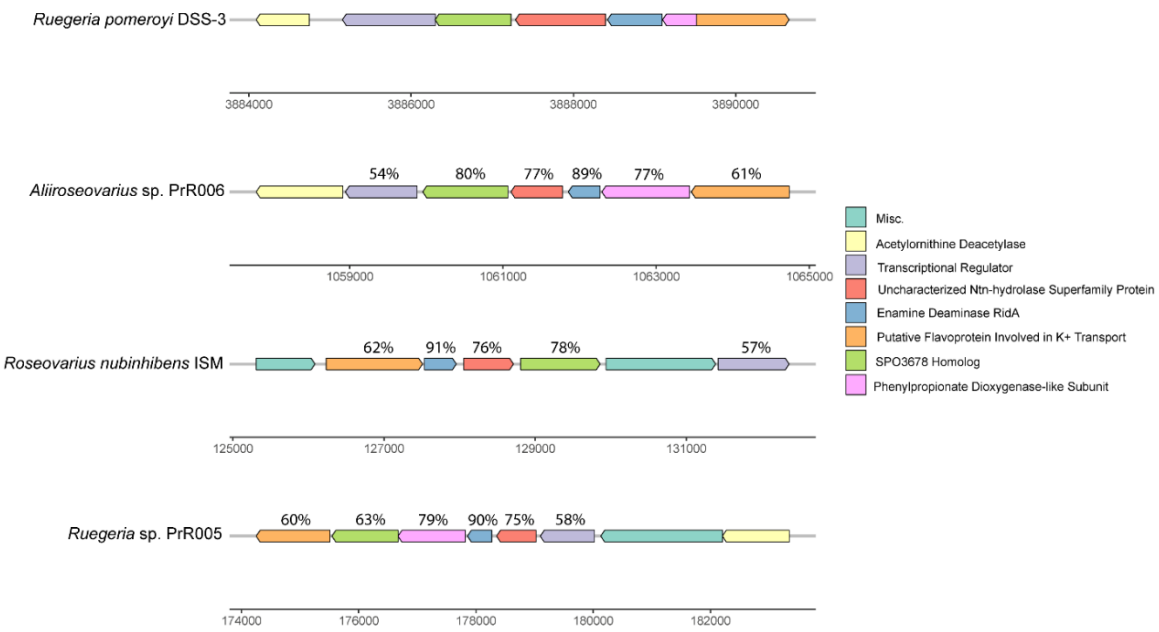

Figure 3.5: SPO3678 putative homologs in other known *Roseobacteraceae* degraders. Putative homologs to *R. pomeroyi* DSS-3 genes are listed for each strain with the color corresponding to the gene and the percent amino acid identity (BLAST) of each compared to *R. pomeroyi* DSS-3 is above each gene. Gene annotations are derived from JGI IMG records.

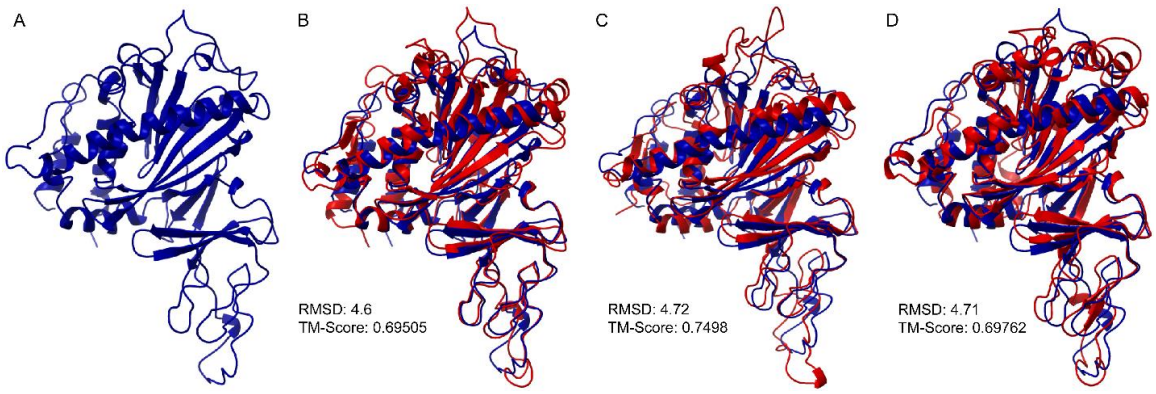

Figure 3.6: SPO3678 structural similarity to other aromatic pollutant dioxygenases. A) *R. pomeroyi* DSS-3 strucuture constructed from ColabFold. B) Crystal structure of naphthalene 1,2-dioxygenase from *Rhodococcus* sp. (red) aligned with SPO3678 from *R. pomeroyi* DSS-3 (blue)(31). C) Crystal Structure of terephthalate dioxygenase from *Comamonas testosteroni* KF1 (red) aligned with SPO3678 from *R. pomeroyi* DSS-3 (blue) (29). D) Biphenyl dioxygenase (BphA1A2) from *Rhodococcus* sp. strain RHA1 (red) aligned with SPO3678 from *R. pomeroyi* DSS-3 (blue) (30).

on PAHs. POB is degraded via the protocatechaute branch of the β-ketoadipate pathway and is also the most recalcitrant of the three labile carbon sources due to its monocyclic aromatic structure (32). The acetate had slightly more carbon available for growth than POB, but the aromatic structure of POB also likely contributed to its extended lag and exponential phases. The different degradation rates during different growth phases also indicate that degradation rate may be related to enzyme induction rate rather than cell growth, further supporting that this co-metabolism mechanism is an enzymatic response, not a growth response.

The random Tn5 library failed to generate a null mutant for pyrene degradation, suggesting that the strain likely possesses functional redundancy, with multiple oxidoreductase-like proteins contributing to PAH co-metabolism. Similar functional redundancy has been reported in *Mycobacterium vanbaalenii* PYR-1 and *Cycloclasticus* sp. P1 (33, 34). This hypothesis is further supported by both POB and YTSS acting as sufficient carbon sources for co-metabolism and the degradation deficiency shown by both 41-G7 and 8-5F Tn5 mutants which had disrupted putative oxidoreductase genes. While these two mutants showed degradation deficiency in the putative PAH catabolic region, disruption to other genes within this region did not show the same deficiency. In addition, the monocyclic aromatic degradation genes that were disrupted, SPO3700 and SPO3690, showed increased degradation despite not having a significant growth rate difference (**Table B.3.5**). As this appears to be a carbon source specific response, this phenomenon could be explained by directing regulation to those dioxygenases able to act on PAHs, rather than a slew of aromatic ring dioxygenases, for a more specific and targeted response to PAHs. While PAH co-metabolism occurs partly in the catabolic region discussed here, only a subset of genes in this locus are involved in degradation, suggesting that *R. pomeroyi* DSS-3 likely does not have dedicated regions for PAH degradation. This suggests that this may be a promiscuous function (35, 36).

Due to the seven degradation deficient mutants with disruptions in transport-related genes, it is possible that *R. pomeroyi* DSS-3 can uptake pyrene by both passive and active transport as is common for diverse PAH degraders (37–39). Few stress response genes showed deficient pyrene degradation, thus *R. pomeroyi* DSS-3 likely has several stress response systems to combat PAH stress or PAH stress may have little to no effect on degradation in this organism. Viable cell count data revealed that pyrene showed no inhibitory effect on growth when compared to solvent

control cultures, which supports the hypothesis that *R. pomeroyi* DSS-3 can mediate pyrene toxicity. Quorum sensing may be an important regulation system for pyrene degradation during surface attached growth in *R. pomeroyi* DSS-3. Several quorum sensing gene disruptions showed decreased degradation on the pyrene top agar assay. This same degradation deficiency disappears when grown in liquid culture, suggesting that biofilm formation during surface attached growth may aid in its pyrene degradation (**Figure B.3.3**). Previous reports of PAH degradation state that biofilm formation and quorum sensing system assist organisms in their ability to degrade PAHs. Specifically, quorum sensing has been implicated in activating PAH degradation genes (23, 24, 40).

One disrupted gene of particular interest was SPO3678, a predicted Rieske 2Fe-2S domain protein. SPO3678 disruptions in both 41-G7 and SPO3678::pKnock-Km had decreased pyrene degradation, thus this protein-coding gene likely encodes for a ring-hydroxylating dioxygenase. Specifically, this gene may encode for the alpha subunit involved in substrate specificity due to its limited homology to other PAH ring-hydroxylating dioxygenase alpha subunits. In addition, another Rieske 2Fe-2S domain protein (SPO3681) is located two genes downstream that may be another ring-hydroxylating dioxygenase subunit, despite the SPO3681::pKnock-Km mutant showing little degradation deficiency. This evidence suggests that SPO3678 likely is a non-specific dioxygenase induced by certain carbon sources that is able to act on PAHs.

Further protein analysis using Colabfold and FoldSeek, revealed that this protein is related to dioxygenases that are involved in the degradation of other aromatic pollutants, such as biphenyl, terephthalate, and naphthalene. All matches to the SPO3678 protein model had RMSD scores above 2Å but TM-scores above 0.5, suggesting that they have a similar fold. This protein model had a similar structure to another *Roseobacteraceae* member previously shown to degrade PAHs via co-metabolism, *Ruegeria* sp. TM1040, with a high RMSD of 4.83 but a TM-score of 0.74802 (12). In addition, this gene appears to be present in a plethora of *Roseobacteraceae* strains, 3 of which are known *Roseobacteraceae* PAH degraders that degrade PAHs via co-metabolism (12, 18). Outside of the *Roseobacteraceae* family, similar proteins appear to be present in other Alphaproteobacteria and Gammaproteobacteria (**Table B.3.6**). Thus, SPO3678 has the potential to act as an additional biomarker for PAH co-metabolism for strains related to the *Roseobacteraceae* family. While further investigation is needed to determine the diversity of this

enzyme in bacteria and the precise function of the protein homologs, initial evidence suggests that this protein is involved in PAH co-metabolism and is found in a diverse array of marine bacteria.

Due to its ability to co-metabolize PAHs, *R. pomeroyi* DSS-3 likely possesses a novel degradation pathway. This pathway is carbon source dependent with only certain labile carbon sources supporting PAH degradation. In addition, the rate of enzyme induction as well as what enzymes are induced likely influence PAH co-metabolism rate. Many diverse genes appear to play a role in its degradation, including quorum sensing genes, transport genes, and several oxidoreductases. The pathway of *R. pomeroyi* DSS-3 does not contain PAH degradation biomarkers, but biomarker-based approaches are important for surveying environmental PAH degraders (12). Thus, SPO3678, a putative ring-hydroxylating dioxygenase able to act on PAHs, may act as an additional genetic biomarker, targeting PAH co-metabolism in *Roseobacteraceae*-related organisms. Since PAH co-metabolism with non-PAH carbon sources has not been readily investigated, more study is needed into these co-metabolic PAH degradation pathways and enzymatic reactions to uncover the true diversity of PAH degraders in marine ecosystems.

Methods

Strains and growth conditions

Ruegeria pomeroyi DSS-3 was originally isolated from coastal GA seawater DMSP enrichment cultures (21). Unless otherwise noted, wild type *R. pomeroyi* DSS-3 and any mutant derivatives were grown at 30°C in Yeast Tryptone Sea Salt (YTSS) medium [per liter: 15 g Instant Ocean (Thermo Fisher Scientific), 4 g tryptone, 2.5 g yeast extract]. *Escherichia coli* strains used for cloning, conjugation, and screening were grown at 37°C in LB broth (per liter, 10 g tryptone, 5 g yeast extract, 10 g NaCl). Pyrene screening plates were constructed as previously described in Walton & Buchan, 2023 (Chapter 2; 12). For the large-scale *R. pomeroyi* DSS-3 Tn5 library screening, 120mm x 15mm plates were used with the same concentration of pyrene as previously reported. *E. coli* EA145, a diaminopimelic acid (DAP) auxotroph, was grown with 1mM DAP unless otherwise noted. The *R. pomeroyi* DSS-3 Tn5 array mutant library was received as a gift from the Moran lab (25).

Pyrene degradation and growth assay

R. pomeroyi DSS-3 pyrene degradation was assessed using High Performance Liquid Chromatography as done in Walton & Buchan, 2023 (Chapter 2; 12, 25). For the 5% YTSS, the strain was grown up in 5% YTSS overnight, then concentrated to ~10^9 and subcultured into 5% YTSS containing 25 µg/mL pyrene + acetone in triplicate cultures for each of the seven timepoints. For the acetate and POB cultures, they were grown in Aromatic Basal Media (ABM) agar (ABM - per liter 8.7 mM KCl, 8.7 mM $CaCl_2$, 43.5 mM $MgSO_4$, and 174 mM NaCl with 225 uM K_2HPO_4, 13.35 mM NH_4Cl, 71 mM Tris-HCl [pH 7.5], 15 g agar (Thermo Fisher Scientific), 68 uM Fe-EDTA, trace metals [7.85 mM nitriloacetic acid, 0.53 mM $MnSO_4{*}H_2O$, 0.42 mM $CoCl_2 {*}6H_2O$, 0.35 mM $ZnSO_4 {*}7H_2O$, 0.038 mM $CuSO_4$, 0.11 mM $NiCl_2 {*}6H_20$, 1.16 mM Na_2SeO_3, 0.41 mM $Na_2MoO_4{*}2H_2O$, 0.33 mM $Na_2WO_4{*}2H_2O$, 0.25 mM $Na_2SiO_3{*}9H_2O$] and trace vitamins [0.0020% vitamin H (Biotin), 0.0020% folic acid, 0.0100% pyridoxine-HCl (B6), 0.0050% riboflavin (B2), 0.0050% thiamine (B1), 0.0050% nicotinic acid, 0.0050% pantothenic acid (B5), 0.0001% cyanocobalamin (B12), 0.0050% *p*-aminobenzoic acid]) with either 5mM acetate or 2.5mM POB until cell density reached ~10^8. Cells were then concentrated to ~10^9 cells and subcultured into ABM containing the carbon source and 25 µg/mL pyrene + acetone in triplicate cultures for each of the seven timepoints. Both acetone control and medium control cultures were included for the acetate and POB experiments and only acetone controls for the 5% YTSS experiment to monitor viable cells. YTSS and acetate cultures were incubated for 7 days, while POB cultures were incubated for 13 days due to slower rates on this substrate. Seven viable cell and pyrene concentration samples were taken at various points in the growth of R. *pomeroyi* DSS-3 with the intention of capturing the growth phase in which pyrene co-metabolism occurred. Throughout the growth of *R. pomeroyi* DSS-3 on each carbon source, both viable cell counts and pyrene disappearance measurements were taken. One volume of ethyl acetate was used to extract pyrene from the culture media at the initial timepoint and each timepoint after. The disappearance of pyrene in the ethyl acetate extracts was detected using a UV detector (254nm). Peak area was compared with that of the initial inoculum and peak area was normalized to account for any abiotic loss in the uninoculated control cultures.

Generation of R. pomeroyi DSS-3 random transposon library

The *R. pomeroyi* DSS-3 random transposon library was constructed using a hyperactive Tn5 transposase as previously described with the following modifications (41, 42). Mating mixtures of *E. coli* EA145 containing the pRL27::mini-Tn5-Kmr-oriR6K vector and *R. pomeroyi* DSS-3 were prepared using 500 µl of early-log-phase cells (~1.7 OD; optical density at 540nm for *R. pomeroyi* DSS-3 and at 600nm for *E. coli* EA145). Cells were pelleted and resuspended in 15 µl fresh YTSS broth. The whole mating mixture was spotted onto YTSS agar plates and incubated overnight. The following day, cells were collected using disposable cell scrapers and re-suspended in 1 mL of YTSS. Spot dilutions on YTSS with and without 50 µg/mL kanamycin were conducted to determine the number of transconjugants. Mutant *R. pomeroyi* DSS-3 colonies were picked from plates using a sterile toothpick and transferred in a 96-grid pattern to square 120mmx15mm plates containing 50 µg/mL kanamycin to maintain selection and 25 µg/mL cycloheximide to prevent fungal contamination. Plates were incubated for 5 days and then transferred to 4°C to preserve colonies for pyrene degradation screening.

Screening of R. pomeroyi DSS-3 Tn5 mutants

Pyrene screening plates were constructed with the addition of 50 µg/mL kanamycin and 25 µg/mL cycloheximide to the YTSS agar base layer. A flame sterilized 96 pin replicator was used to transfer mutants from library plates to pyrene screening plates. Following a 7-day incubation period, mutants were scraped off screening plates using disposable cell scrapers. Clearing zones under the colonies were assessed and any mutants that showed deficient pyrene degradation were selected for a second screening (**Figure B.3.1**). Each mutant was subsequently screened two additional times. At the end of the third screening, any mutants that had a consistent deficient pyrene degradation phenotype were stored as freezer stocks.

Identification of R. pomeroyi DSS-3 transposon insertion site

Mutant genomic DNA was extracted using the DNeasy Blood & Tissue Kit (Qiagen, Valencia, CA). Arbitrarily primed PCR was used as previously described with the following modifications and primers sequences are listed in **Table B.3.2** (42, 43). In brief, TNPR13OUT and ARB6, were used to amplify DNA upstream of the 5’ end of the transposon and TNPR17OUT and ARB6 were used to amplify the DNA downstream of the 5’ end of the transposon. To amplify the transposon insert site during the first round of PCR, the following thermocycler conditions

were used: [95°C for 5 minutes, 94°C for 30 seconds, 30°C for 30 seconds, 72°C for 1 minute] repeated 4 times, [94°C for 30 seconds, 45°C for 30 seconds, 72°C for 1 minute] repeated 29 times, and 72°C for 5 minutes. The PCR reactions of the first step were used for the subsequent amplification step. To enrich amplicons around the insertion site, the ARB2 primer was used in both subsequent PCR reactions with either TNPR13Nest or TNPR17Nest. The following thermocycler conditions were used to enrich for amplicons: 95°C for 5 minutes, [94°C for 30 seconds, 45°C for 30 seconds, 72°C for 1 minute] repeated 29 times, and 72°C for 10 minutes. PCR products were subsequently purified using the QIAquick PCR Purification Kit (Qiagen, Valencia, CA) and sequenced using the corresponding Nest primer.

Generation of R. pomeroyi DSS-3 pyrene catabolism mutants

Antibiotics were added to either YTSS or LB medium to maintain selective pressure on *R. pomeroyi* DSS-3 pKnock-Km transconjugants or transformed *E. coli* cells. Plasmids, strains, and primers used are shown in **Tables B.3.1-3**, respectively. Insert sequences were amplified using primers containing restriction enzyme cut sites, ligated into the pKnock-Km vector, and introduced into *E. coli* EZ180 via heat shock. Constructed plasmids were verified by sequence analysis. Plasmids were mobilized into *R. pomeroyi* DSS-3 by mating with EZ180 strains and DSS-3 mutants were selected on YTSS plates containing 50 µg/mL kanamycin as previously described in Armes & Buchan, 2021 (44). Transconjugants were verified by sequence analysis (**Table B.3.2**).

Pleiotropic assessment of R. pomeroyi DSS-3 mutants

To assess if the transposon insertion in the *R. pomeroyi* DSS-3 mutants had a pleiotropic effect on the mutants, growth curves were conducted and compared to WT *R. pomeroyi* DSS-3. Three biological replicates of mutant and WT strains were grown up in 96-well plates (Falcon™ 96-Well, Cell Culture-Treated, Flat-Bottom Microplate, Fisher Scientific). After 3 days of growth, strains were subcultured into fresh YTSS in 96-well plates and grown at 30°C to mid-to-late exponential (24 hrs). Strains were then subcultured again into fresh YTSS in 96-well plates and biological replicates were split into technical replicates for a total of 9 replicates per strain. Plates were incubated at 30°C with optical density (540 nm) measurements taken every hour for 48 hours using a Cytation™5 Imaging Reader (BioTek, CA, US). After each set of growth curves, optical density measurements were adjusted to blank wells and a linear regression was conducted

to determine the growth rate of each strain. Each mutant strain's growth rate was compared to that of WT using an unpaired t-test and any significantly lower growth rates were recorded (**Table B.3.5**). The same methods were used to assess pleiotropic effects of the pKnock-Km insertion, with the addition of 50 µg/mL kanamycin to mutant wells. SPO3678::pKnock-Km was also assessed for pleiotropic effects with 5% YTSS (used for pyrene disappearance experiments) using the above methods.

Quantification of R. pomeroyi DSS-3 mutant pyrene degradation

Transposon mutants, from this experiment and a previously generated *R. pomeroyi* DSS-3 Tn5 mutant array, and pKnock-Km mutant strains were assessed for pyrene degradation using High Performance Liquid Chromatography as done in Walton & Buchan, 2023 (Chapter 2; 12, 25). In brief, strains grown up in 5% YTSS overnight, then subcultured into 5% YTSS containing 25 µg/mL pyrene in triplicate. For the pKnock-Km mutant strains and the associated uninoculated control cultures, 50 µg/mL kanamycin was added to maintain selective pressure on the insertion. For the wild type strains, 10 µl of sterile MilliQ water was added to keep the same volume. One volume of ethyl acetate was used to extract pyrene from the culture media at the initial timepoint and after 7 days. HPLC methods were conducted as stated above.

Genome analyses

All genomic analyses were conducted using the Joint Genome Institute's Integrate Microbial Genomes & Microbiomes (JGI IMG) (https://img.jgi.doe.gov/). Tn5 insertion locations were identified by using IMG's BLAST function and more in-depth analysis was done by identifying transposon sequence from the arbitrary PCR sequence. Transposon locations were mapped onto the genome of *R. pomeroyi* DSS-3 (**Figure 3.1**) using Prokksee (https://proksee.ca/). Chromosomal region maps were generated using the gggenes package (https://github.com/wilkox/gggenes) in RStudio v2022.07.1. The JGI IMG Top IMG Homolog Hits and Conserved Neighborhood functions were used to determine the conservation of SPO3678 in other *Roseobacteraceae* (**Figure 3.5**).

Statistical analyses

Mutant growth rate differences were analyzed using GraphPad Prism 10.0.0. Exponential growth rates for each strain were compared to wild type via unpaired two-tailed t-test to determine any significant differences in growth rate. Those that had a significantly lower growth rate than wild

type was determined to have a pleiotropic effect that could have given the pyrene degradation deficiency phenotype.

SPO3678 structural similarity

ColabFold v1.5.2 was used with default settings to determine the predicted structure of SPO3678 in *R. pomeroyi* DSS-3 (27). FoldSeek (https://search.foldseek.com/) was used with default settings to determine structural similarity of the SPO3678 model to other protein models previously generated by AlphaFold and experimentally proven structures in RCSB Protein Data Bank (26). The FoldSeek results were evaluated using the Root Mean Square Deviation (RMSD), Template-Modeling score (TM-score), E-value, and amino acid sequence coverage. Resulting protein structures of interest were visualized using ChimeraX v1.6.1 (45).

Acknowledgements

We would like to acknowledge the Howard Hughes Medical Institute Gilliam Fellowship and the University of Tennessee Institute for a Secure and Sustainable Environment Seed Grant to AB and JW. We would also like to thank Taylor Smith for her assistance in constructing the Tn5 mutant library and the UP3-6 Tn5 mutant strain and Dr. Ed Wright and the Bioanalytical Resources Facility for assistance using and optimizing the HPLC for PAH concentration analysis.

REFERENCES

1. Sakshi, Haritash AK. 2020. A comprehensive review of metabolic and genomic aspects of PAH-degradation. Arch Microbiol 202:2033–2058.
2. Ghosal D, Ghosh S, Dutta TK, Ahn Y. 2016. Current State of Knowledge in Microbial Degradation of Polycyclic Aromatic Hydrocarbons (PAHs): A Review. Front Microbiol 7:1369.
3. Sieradzki ET, Morando M, Fuhrman JA. 2021. Metagenomics and Quantitative Stable Isotope Probing Offer Insights into Metabolism of Polycyclic Aromatic Hydrocarbon Degraders in Chronically Polluted Seawater. mSystems 6.
4. Ambade B, Sethi SS, Giri B, Biswas JK, Bauddh K. 2021. Characterization, Behavior, and Risk Assessment of Polycyclic Aromatic Hydrocarbons (PAHs) in the Estuary Sediments. Bulletin of Environmental Contamination and Toxicology 2021 1:1–10.
5. Zada S, Zhou H, Xie J, Hu Z, Ali S, Sajjad W, Wang H. 2021. Bacterial degradation of pyrene: Biochemical reactions and mechanisms. Int Biodeterior Biodegradation 162:105233.
6. Henner P, Schiavon M, Morel J-L, Lichtfouse E,. 1997. Polycyclic aromatic hydrocarbon (PAH) occurrence and remediation methods. Analusis 25:M56–M59.
7. Kweon O, Kim SJ, Holland RD, Chen H, Kim DW, Gao Y, Yu LR, Baek S, Baek DH, Ahn H, Cerniglia CE. 2011. Polycyclic aromatic hydrocarbon metabolic network in *Mycobacterium vanbaalenii* PYR-1. J Bacteriol 193:4326–4337.
8. Jimenez JI, Minambres B, Garcia JL, Diaz E. 2002. Genomic analysis of the aromatic catabolic pathways from *Pseudomonas putida* KT2440. Environ Microbiol 4:824–841.
9. Demanèche S, Meyer C, Micoud J, Louwagie M, Willison JC, Jouanneau Y. 2004. Identification and functional analysis of two aromatic-ring-hydroxylating dioxygenases from a *Sphingomonas* strain that degrades various polycyclic aromatic hydrocarbons. Appl Environ Microbiol 70:6714–6725.
10. Di Gennaro P, Terreni P, Masi G, Botti S, De Ferra F, Bestetti G. 2010. Identification and characterization of genes involved in naphthalene degradation in *Rhodococcus opacus* R7. Appl Microbiol Biotechnol 87:297–308.

11. Liang C, Huang Y, Wang H. 2019. *pahE*, a Functional Marker Gene for Polycyclic Aromatic Hydrocarbon-Degrading Bacteria. Appl Environ Microbiol 85.
12. Walton JL, Buchan A. 2024. Evidence for novel polycyclic aromatic hydrocarbon degradation pathways in culturable marine isolates. Microbiol Spectr 12.
13. Ahmad M, Ling J, Yin J, Chen L, Yang Q, Zhou W, Zhang Y, Huang X, Khan I, Dong J. 2023. Evaluation of the Different Nutritional and Environmental Parameters on Microbial Pyrene Degradation by Mangrove Culturable Bacteria. Int J Mol Sci 24:8282.
14. Wagner-Döbler I, Biebl H. 2006. Environmental biology of the marine Roseobacter lineage. Annu Rev Microbiol 60:255–280.
15. Buchan A, González JM, Chua MJ. 2019. Aerobic Hydrocarbon-Degrading Alphaproteobacteria: *Rhodobacteraceae* (Roseobacter), p. 93–104. *In* McGenity, TJ (ed.), Taxonomy, Genomics and Ecophysiology of Hydrocarbon-Degrading Microbes. Springer International Publishing.
16. Liang HK, Orata FD, Boucher Y, Case RJ. 2021. Roseobacters in a Sea of Poly- and Paraphyly: Whole Genome-Based Taxonomy of the Family *Rhodobacteraceae* and the Proposal for the Split of the "Roseobacter Clade" Into a Novel Family, *Roseobacteraceae* fam. nov. Front Microbiol 12.
17. Parales RE, Resnick SM. 2006. Aromatic Ring Hydroxylating Dioxygenases, p. 287–340. *In* Pseudomonas. Springer, Boston, MA.
18. Zhou H, Zhang S, Xie J, Wei H, Hu Z, Wang H. 2020. Pyrene biodegradation and its potential pathway involving Roseobacter clade bacteria. Int Biodeterior Biodegradation 150:104961.
19. Cao J, Lai Q, Yuan J, Shao Z. 2015. Genomic and metabolic analysis of fluoranthene degradation pathway in *Celeribacter indicus* P73 T. Sci Rep 5:1–12.
20. Zhang YH, Dong JD, Wang YS, Gu JD, Yin JP, Ahmad M, Ling J. 2022. Comparative genomics reveals the evidence of aromatic hydrocarbons degradation potential in genus *Roseovarius* in marine environment. Int Biodeterior Biodegradation 171:105408.
21. Moran MA, Buchan A, González JM, Heidelberg JF, Whitman WB, Klene RP, Henriksen JR, King GM, Belas R, Fuqua C, Brinkac L, Lewis M, Johri S, Weaver B, Pai G, Elsen JA, Rahe E, Sheldon WM, Ye W, Miller TR, Carlton J, Rasko DA, Paulsen IT, Ren Q,

Daugherty SC, Deboy RT, Dodson RJ, Durkin AS, Madupu R, Nelson WC, Sullivan SA, Rosovitz MJ, Haft DH, Selengut J, Ward N. 2004. Genome sequence of *Silicibacter pomeroyi* reveals adaptations to the marine environment. Nature 432:910–913.

22. Gupta G, Kumar V, Pal AK. 2017. Microbial Degradation of High Molecular Weight Polycyclic Aromatic Hydrocarbons with Emphasis on Pyrene. Polycycl Aromat Compd 39:124–138.
23. Yu Z, Hu Z, Xu Q, Zhang M, Yuan N, Liu J, Meng Q, Yin J. 2020. The LuxI/LuxR-Type Quorum Sensing System Regulates Degradation of Polycyclic Aromatic Hydrocarbons via Two Mechanisms. Int J Mol Sci 21:1–15.
24. Mangwani N, Kumari S, Das S. 2015. Involvement of quorum sensing genes in biofilm development and degradation of polycyclic aromatic hydrocarbons by a marine bacterium *Pseudomonas aeruginosa* N6P6. Appl Microbiol Biotechnol 99:10283–10297.
25. Mejia C, Rodriguez LT, Poudel R, Ellington A, Rivers AR, Reisch CR. 2022. An Arrayed Transposon Library of *Ruegeria pomeroyi DSS-3*. bioRxiv 2022.09.11.507510.
26. van Kempen M, Kim SS, Tumescheit C, Mirdita M, Lee J, Gilchrist CLM, Söding J, Steinegger M. 2023. Fast and accurate protein structure search with Foldseek. Nature Biotechnology 2023 1–4.
27. Mirdita M, Schütze K, Moriwaki Y, Heo L, Ovchinnikov S, Steinegger M. 2022. ColabFold: making protein folding accessible to all. Nature Methods 2022 19:6 19:679–682.
28. Massmig M, Reijerse E, Krausze J, Laurich C, Lubitz W, Jahn D, Moser J. 2020. Carnitine metabolism in the human gut: characterization of the two-component carnitine monooxygenase CntAB from *Acinetobacter baumannii*. Journal of Biological Chemistry 295:13065–13079.
29. Mahto JK, Neetu N, Sharma M, Dubey M, Vellanki BP, Kumar P. 2022. Structural Insights into Dihydroxylation of Terephthalate, a Product of Polyethylene Terephthalate Degradation. J Bacteriol 204.
30. Furusawa Y, Nagarajan V, Tanokura M, Masai E, Fukuda M, Senda T. 2004. Crystal Structure of the Terminal Oxygenase Component of Biphenyl Dioxygenase Derived from *Rhodococcus* sp. Strain RHA1. J Mol Biol 342:1041–1052.

31. Gakhar L, Malik ZA, Allen CCR, Lipscomb DA, Larkin MJ, Ramaswamy S. 2005. Structure and increased thermostability of *Rhodococcus* sp. naphthalene 1,2-dioxygenase. J Bacteriol 187:7222–7231.
32. Alejandro-Marín CM, Bosch R, Nogales B. 2014. Comparative genomics of the protocatechuate branch of the β-ketoadipate pathway in the Roseobacter lineage. Mar Genomics 17:25–33.
33. Kim S-J, Song J, Kweon O, Holland RD, Kim DW, Kim J, Yu L-R, Cerniglia CE. 2012. Functional Robustness of a Polycyclic Aromatic Hydrocarbon Metabolic Network Examined in a *nidA* Aromatic Ring-Hydroxylating Oxygenase Mutant of *Mycobacterium vanbaalenii* PYR-1. Appl Environ Microbiol 78:3715.
34. Wang W, Wang L, Shao Z. 2018. Polycyclic aromatic hydrocarbon (PAH) degradation pathways of the obligate marine PAH degrader *Cycloclasticus* sp. strain P1. Appl Environ Microbiol 84.
35. Basta T, Buerger S, Stolz A. 2005. Structural and replicative diversity of large plasmids from sphingomonads that degrade polycyclic aromatic compounds and xenobiotics. Microbiology 151:2025–2037.
36. Segura A, Udaondo Z, Azaro Molina L. 2021. PahT regulates carbon fluxes in *Novosphingobium* sp. HR1a and influences its survival in soil and rhizospheres. Environ Microbiol 23:2969–2991.
37. Bugg T, Foght JM, Pickard MA, Gray MR. 2000. Uptake and active efflux of polycyclic aromatic hydrocarbons by *Pseudomonas fluorescens* LP6a. Appl Environ Microbiol 66:5387–5392.
38. Kallimanis A, Frillingos S, Drainas C, Koukkou AI. 2007. Taxonomic identification, phenanthrene uptake activity, and membrane lipid alterations of the PAH degrading Arthrobacter sp. strain Sphe3. Appl Microbiol Biotechnol 76:709–717.
39. Liang J, Xu J, Zhao W, Wang J, Chen K, Li Y, Tian Y. 2021. Benzo[a]pyrene might be transported by a TonB-dependent transporter in *Novosphingobium pentaromativorans* US6-1. J Hazard Mater 404:124037.
40. Meng Q, Xu Q, Xu Y, Ren H, Ge X, Yu J, Cao X, Yin J, Yu Z. 2023. A FadR-Type Regulator Activates the Biodegradation of Polycyclic Aromatic Hydrocarbons by

Mediating Quorum Sensing in *Croceicoccus naphthovorans* Strain PQ-2. Appl Environ Microbiol https://doi.org/10.1128/AEM.00433-23.

41. Larsen RA, Wilson MM, Guss AM, Metcalf WW. 2002. Genetic analysis of pigment biosynthesis in *Xanthobacter autotrophicus* Py2 using a new, highly efficient transposon mutagenesis system that is functional in a wide variety of bacteria. Archives of Microbiology 2002 178:3 178:193–201.
42. Cude WN, Mooney J, Tavanaei AA, Hadden MK, Frank AM, Gulvik CA, May AL, Buchan A. 2012. Production of the antimicrobial secondary metabolite indigoidine contributes to competitive surface colonization by the marine roseobacter *Phaeobacter* sp. strain Y4I. Appl Environ Microbiol 78:4771–4780.
43. O'Toole GA, Pratt LA, Watnick PI, Newman DK, Weaver VB, Kolter R. 1999. Genetic approaches to study of biofilms. Methods Enzymol 310:91–109.
44. Armes AC, Buchan A. 2021. Cyclic di-GMP Is Integrated Into a Hierarchal Quorum Sensing Network Regulating Antimicrobial Production and Biofilm Formation in Roseobacter Clade Member Rhodobacterales Strain Y4I. Front Mar Sci 8:681551.
45. Meng EC, Goddard TD, Pettersen EF, Couch GS, Pearson ZJ, Morris JH, Ferrin TE. 2023. UCSF ChimeraX: Tools for structure building and analysis. Protein Science 32:e4792.

APPENDIX B

Appendix Table B.3.1: Strains used in this study.

Strains	Description	Reference
Ruegeria pomeroyi DSS-3	Wild type strain	Gonzalez et al., 2003 (1)
***E. coli* EZ180**	DAP auxotroph mating strain	Dashiff &Kadouri, 2009 (2)
***E. coli* EA145**	DAP auxotroph mating strain containing pRL27	Larsen et al., 2002 (3)
DSS-3 SPO3678::pKnock-Km	Contains pKnock-Km insertion in SPO3678	This study
DSS-3 SPO3681::pKnock-Km	Contains pKnock-Km insertion in SPO3681	This study
DSS-3 SPO3688::pKnock-Km	Contains pKnock-Km insertion in SPO3688	This study
DSS-3 SPO3690::pKnock-Km	Contains pKnock-Km insertion in SPO3690	This study
DSS-3 SPO3700::pKnock-Km	Contains pKnock-Km insertion in SPO3700	This study

Appendix Table B.3.2: Primers used in this study

Primer Name	Sequence	Function
SPO3678_300F	NNNNNNGGATCCACCAAACGGTTTGTGTGTTCC	Insert amplification
SPO3678_803R	NNNNNNCTCGAGGCTGGCCACCTGAGTTGG	Insert amplification
SPO3678_17F	CGAAGCTTCAAGACCTGGC	pKnock-Km insertion confirmation
SPO3678_979R	CGAGCTTTTCCCGATCCTCT	pKnock-Km insertion confirmation
SPO3681_283F	NNNNNNGGATCCATGTCGACCCTCTTGCATGG	Insert amplification
SPO3681_776R	NNNNNNCTCGAGCGGTCATTGCTGGGATGC	Insert amplification
SPO3681_185F	GAGATTATGTGGCGTGCGAA	pKnock-Km insertion confirmation
SPO3681_949R	CATCCGGATCAGCTGCAAAA	pKnock-Km insertion confirmation
SPO3688_182F	NNNNNNGGATCCACTGCATCGTCCTGGTTGAG	Insert amplification
SPO3688_671R	NNNNNNCTCGAGTCGATGATGTTGAGCGGAGT	Insert amplification
SPO3688_133F	CATCCGGATCAGCTGCAAAA	pKnock-Km insertion confirmation
SPO3688_915R	TCCCTCTTCGAACCAGCTTT	pKnock-Km insertion confirmation
SPO3690_518F	NNNNNNGGATCCAGCTCGAAGGGTCCTATGC	Insert amplification
SPO3690_989R	NNNNNNCTCGAGCGGTCGTGGATTCGGACC	Insert amplification
SPO3690_1022R	TCCTCGTAGTAACCAAGTTTCTC	pKnock-Km insertion confirmation
SPO3690_42F	CTATCGCGAACAGATGGCT	pKnock-Km insertion confirmation
SPO3700_166F	NNNNNNGGATCCCATGCGCACAAGGTCAACT	Insert amplification
SPO3700_636R	NNNNNNCTCGAGCTCGGCAAAGCGTCGGTC	Insert amplification
SPO3700_14F	TCGACTTTCAGACCGACCC	pKnock-Km insertion confirmation

Appendix Table B.3.2 Continued.

SPO3700_807R	GCGCTCCACAACGACTTC	pKnock-Km insertion confirmation
pKnock-Km_746F	CACTTAACGGCTGACATGG	pKnock-Km multiple cloning site primer
pKnock-Km_895R	TTAATTCGACGCGTCCTC	pKnock-Km multiple cloning site primer
ARB6	GGCCACGCGTCGACTAGTACNNNNNNNNNACGCC	Arbitrary PCR Primer (4)
TNPR13Out	CAGCAACACCTTCTTCACGA	Arbitrary PCR Primer (4)
TNPR17Out	AACAAGCCAGGGATGTAACG	Arbitrary PCR Primer (4)
ARB2	GGCCACGCGTCGACTAGTAC	Arbitrary PCR Primer (4)
TNPR13Nest	CTAGAGTCGACCTGCAGGCAT	Arbitrary PCR Primer and Sequencing Primer (4)
TNPR17Nest	CTGACATGGGGGGGTACC	Arbitrary PCR Primer and Sequencing Primer (4)

Appendix Table B.3.3: Plasmids used in this study.

Plasmids	Description	Reference
pKNOCK-Km	Vector with kanamycin resistance marker used to disrupt *R. pomeroyi* DSS-3 genes	Alexeyev, M., 2018 (5)
pKNOCK-Km_SPO3678	Vector with partial SPO3678 gene insertion	This Study
pKNOCK-Km_SPO3681	Vector with partial SPO3681 gene insertion	This Study
pKNOCK-Km_SPO3688	Vector with partial SPO3688 gene insertion	This Study
pKNOCK-Km_SPO3690	Vector with partial SPO3690 gene insertion	This Study
pKNOCK-Km_SPO3700	Vector with partial SPO3700 gene insertion	This Study
pRL27	Vector containing hyperactive Tn5 transposon and kanamycin resistance marker	Larsen et al., 2002 (3)

Appendix Table B.3.4: Mutant pleiotropy growth rates.

Mutant	Growth Rate	Significantly Different (P<0.05) from WT?	P-Value
10-F10	0.01338	n.d.	0.648
11-F9	0.01415	+	0.0029
13-C8	0.01387	n.d.	0.0502
1-4C	0.0145	+	0.0003
1-5B	0.01388	+	0.0261
1-5E	0.01385	n.d.	0.3159
15-G5	0.01453	n.d.	0.0547
15-H7	0.0128	+	<0.0001
1-6E	0.01346	n.d.	0.4164
16-G9	0.01368	n.d.	0.6645
18-10E	0.01297	+	<0.0001
18-E9	0.01343	-	0.0042
19-G8	0.01322	n.d.	0.3317
19-G7	0.01084	n.d.	0.2891
2-1F	0.01467	n.d.	0.1987
23-G8	0.009482	n.d.	0.8
24-B7	0.01431	n.d.	0.6578
2-4F	0.01337	n.d.	0.6826
2-F8	0.01333	n.d.	0.4111
32-F7	0.01444	n.d.	0.4559
33-F8	0.01301	-	0.0057
38-A11	0.01156	+	<0.0001
3-C11	0.01058	+	0.0041
3-G8	0.01377	+	0.0041
40-D9	0.01282	+	<0.0001
40-F4	0.1234	n.d.	0.214
40-F5	0.01331	+	0.0014
41-F3	0.01338	+	0.0002
41-G7	0.01436	n.d.	0.3219
41-H2	0.01337	+	<0.0001
42-B3	0.01294	+	0.0266
43-E11	0.0119	n.d.	0.1294
45-A4	0.01385	+	<0.0001
46-E7	0.01226	n.d.	0.9499
47-E8	0.01431	+	<0.0001
48-B1	0.01352	+	0.004
48-D4	0.01346	+	0.0008

Appendix Table B.3.5 Continued.

48-D5	0.013	+	0.0138
48-F11	0.0132	+	0.0018
48-G1	0.01376	+	<0.0001
49-G8	0.01119	n.d.	0.5818
4-G2	0.0135	n.d.	0.2832
4-H7	0.01343	+	<0.0001
50-A9	0.01388	+	<0.0001
51-A2	0.01372	+	<0.0001
51-A8	0.01377	+	<0.0001
52-B11	0.01374	+	<0.0001
53-G11	0.01299	+	<0.0001
54-G7	0.01162	n.d.	0.1255
54-G8	0.01323	+	<0.0001
54-H6	0.01256	+	<0.0001
55-E11	0.01145	+	0.0096
56-D11	0.007677	-	<0.0001
58-D1	0.01349	+	<0.0001
58-E1	0.01318	+	<0.0001
60-F11	0.01218	+	<0.0001
60-F7	0.01329	+	<0.0001
60-F9	0.01386	+	<0.0001
8-5F	0.01454	+	<0.0001
8-B11	0.01368	n.d.	0.6958
8-B6	0.01303	+	<0.0001
9-G7	0.01403	+	<0.0001
SPO3700::pKnock-Km	0.01456	n.d.	0.6757
SPO3688::pKnock-Km	0.01499	+	0.0468
SPO3690::pKnock-Km	0.01498	n.d.	0.0755
SPO3678::pKnock-Km	0.01343	-	0.0007
SPO3681::pKnock-Km	0.0147	n.d.	0.7043
SPO3677::Tn5-Km	0.01446	n.d.	0.2173
SPO3679::Tn5-Km	0.01473	n.d.	0.6585
SPO3680::Tn5-Km	0.01540	+	0.0001
SPO3682::Tn5-Km	0.01243	-	0.0018

n.d. No difference

+ Significantly greater

- Significantly less

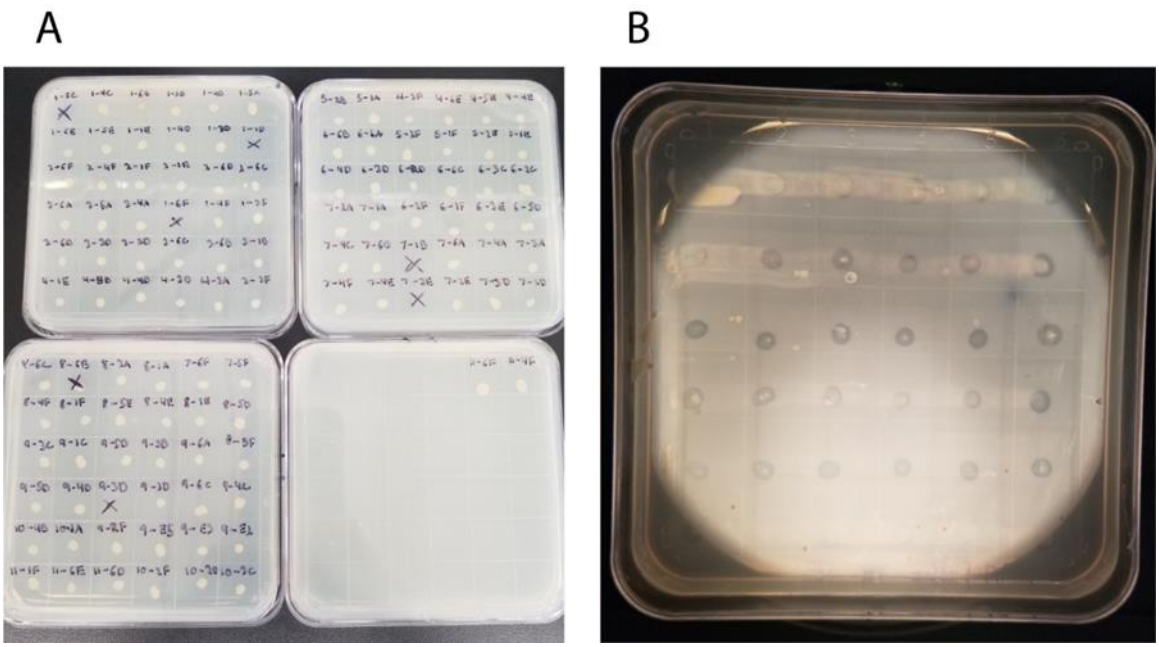

Appendix Figure B.3.1: Sample library screening plates. A) Third screening library plates before colonies were scraped. B) Third screening library plate after colonies were scraped.

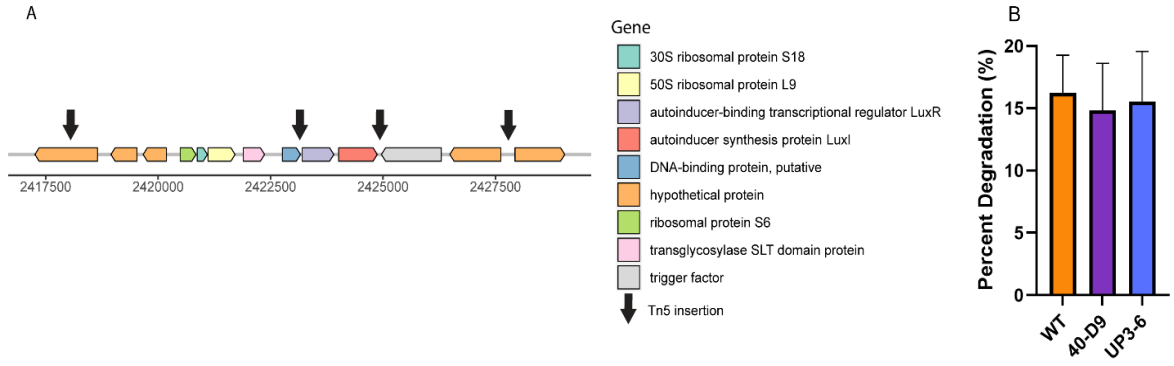

Appendix Figure B.3.2: Quorum sensing transposon mutants and pyrene degradation. A) Transposon insertion locations in one of the quorum sensing regions in *R. pomeroyi* DSS-3. Gene names were assigned via annotations on JGI IMG. Numbers under the gene symbols represent chromosomal position from the ASN: GCA_000011965 reference. B) Percent degradation of pyrene for quorum sensing Tn5 mutants. Percent degradation is relative to T0 culture and accounts for deviation from uninoculated controls. Standard error was calculated for three replicate cultures. Tn5 mutant names are listed on the x-axis.

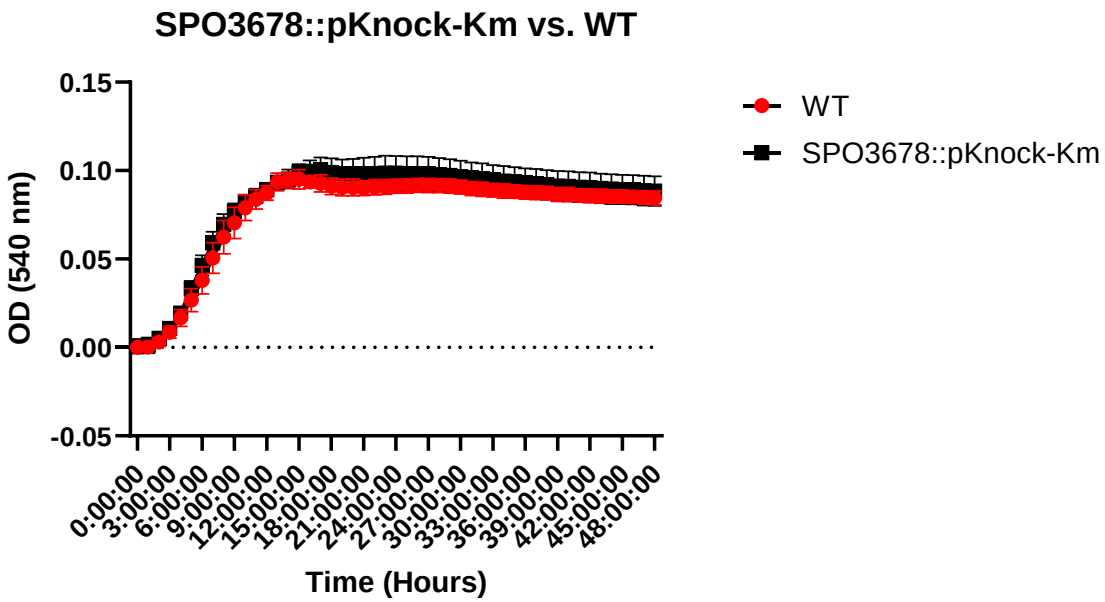

Appendix Figure B.3.3: SPO3678::pKnock-Km pleiotropy assay in 5% YTSS compared to WT *R. pomeroyi* DSS-3. OD measurements at 540nm were taken over 48 hours in biological and technical triplicate. The growth rate between the two strains was not significantly different when analyzed with an unpaired t-test.

APPENDIX B REFERENCES

1. González JM, Covert JS, Whitman WB, Henriksen JR, Mayer F, Scharf B, Schmitt R, Buchan A, Fuhrman JA, Kiene RP, Moran MA. 2003. *Silicibacter pomeroyi* sp. nov. and *Roseovarius nubinhibens* sp. nov., dimethylsulfoniopropionate-demethylating bacteria from marine environments. Int J Syst Evol Microbiol 53:1261–1269.
2. Dashiff A, Kadouri DE. 2009. A New Method for Isolating Host-Independent Variants of *Bdellovibrio bacteriovorus* Using *E. coli* Auxotrophs. Open Microbiol J 3:87.
3. Larsen RA, Wilson MM, Guss AM, Metcalf WW. 2002. Genetic analysis of pigment biosynthesis in *Xanthobacter autotrophicus* Py2 using a new, highly efficient transposon mutagenesis system that is functional in a wide variety of bacteria. Archives of Microbiology 2002 178:3 178:193–201.
4. Cude WN, Prevatte CW, Hadden MK, May AL, Smith RT, Swain CL, Campagna SR, Buchan A. 2015. *Phaeobacter* sp. strain Y4I utilizes two separate cell-to-cell communication systems to regulate production of the antimicrobial indigoidine. Appl Environ Microbiol 81:1417–1425.
5. Alexeyev MF. 1999. The pKNOCK Series of Broad-Host-Range Mobilizable Suicide Vectors for Gene Knockout and Targeted DNA Insertion into the Chromosome of Gram-Negative Bacteria. BioTechniques 26:824–828.

CHAPTER 4 COASTAL MARINE BACTERIAL COMMUNITY RESPONSE TO POLYCYCLIC AROMATIC HYDROCARBON ENRICHMENT

JW collected samples, conceived experiments, conducted experiments, analyzed data, and wrote manuscript; EB assisted with isolate screening and identification; ZB conducted 16S rDNA amplicon analysis and assisted in writing manuscript; AB advised project and assisted in writing manuscript.

Abstract

Polycyclic aromatic hydrocarbons (PAHs) are common pollutants in coastal marine ecosystems that affect both macro- and microfauna. While microbial response to and degradation of PAHs has been well-studied, the taxonomic diversity of marine microbial degraders and the prevalence of PAH co-metabolism have not received as much attention. To address these knowledge gaps, we established PAH seawater enrichment cultures, with and without the addition of labile carbon sources, using inoculants from two coastal Florida sites, a public beach and a public boat ramp. 16S rDNA amplicon sequencing results showed that seawater inoculation site, addition of a labile carbon source, and PAH type affected the resulting microbial community. Alphaproteobacteria was the most abundant class in most of the public beach enrichment communities while most of the boat ramp enrichment communities had high relative abundances of both Alphaproteobacteria and Gammaproteobacteria. Furthermore, the Alphaproteobacterial proportion of the communities was primarily made up of *Rhodobacteraceae*/*Roseobacteraceae*, families with known PAH degraders. In addition, 98% of the bacterial isolates (52/53) from the enrichment cultures were only capable of PAH co-metabolism and were unable to use PAHs as a sole carbon source. Draft genome sequences were generated for 32 representative isolates to investigate the presence of characterized genetic biomarkers for PAH degradation. These biomarkers were absent from these genomes suggesting the presence of uncharacterized genes/pathways. Overall, this study supports the hypothesis that bacterial PAH co-metabolizers may be the first line of defense against PAH pollution in non-chronically polluted areas, whereas chronically polluted areas may have prior selection for sole-metabolizers.

Introduction

Marine ecosystems are reservoirs of persistent organic pollutants (POPs) (1). These POPs are problematic due to their varying recalcitrance and harmful health affects for aquatic and human life (2). One group of POPs, polycyclic aromatic hydrocarbons (PAHs), owe their recalcitrance to both their hydrophobicity and linked benzene ring structure (3). PAHs are principally formed

by the incomplete combustion of carbon or naturally underground as a component of crude oil. These compounds can be released into the environment through volcanic eruptions, forest fires, industrial wastewater, and oil drilling, among other sources (4). Following their release, PAHs enter marine environments through atmospheric deposition, terrestrial runoff, and direct inputs (i.e., oil spills) (3, 5, 6). In addition to their stability in the environment, these compounds have a variety of toxic and carcinogenic effects (3). While these pollutants are hazardous to aquatic life, the potential for bioaccumulation, especially in concert with microplastics, poses a significant threat to marine ecosystems (7). To combat PAH pollution, some marine bacteria have evolved the ability to utilize these compounds as a growth substrate and/or as a mechanism to detoxify their environment (8, 9).

A variety of marine bacteria have been described to degrade PAHs or increase in abundance when exposed to them, most in the context of crude oil bioremediation (10, 11). For instance, *Cycloclasticus* spp. and *Marinobacter* spp. have been shown to degrade the PAH fraction of crude oils and are commonly found in oil contaminated marine waters and sediment (11, 12). Initial studies focused on bacterial response to oil spills led to further investigation of marine bacteria able to degrade non-petroleum derived PAHs (13). To date, bacteria able to degrade PAHs have been isolated in both coastal and open ocean environments as well as throughout the water column (14, 15). A disproportionate number of bacteria have been found to degrade low-molecular weight (LMW) PAHs versus high-molecular weight (HMW) PAHs, the latter having increased stability and toxicity (4). While bacterial degradation of this compound class in marine environments is prevalent, the range of metabolic strategies these bacteria use to degrade both HMW and LMW variants and the true diversity of bacterial PAH degraders has not been well-studied (16–19).

Overwhelmingly, studies investigate microbial PAH degradation with these compounds acting as the sole carbon and energy source (i.e., requiring no additional supplemental carbon substrate). However, recent evidence suggests that numerous marine bacteria can co-metabolize PAHs with the addition of an external carbon source (i.e., yeast extract and tryptone) (16, 17). Here, we define co-metabolism as the degradation or transformation of PAHs only with the addition of a more labile carbon source. These co-metabolic degraders are suspected to have novel enzymatic pathways as they are missing characterized PAH degradation biomarkers in the genomes (i.e.,

pahAc, *pahE*) (16, 20, 21). The lack of characterization of PAH co-metabolizing strains as well as their absence of genetic biomarkers, has highlighted the need for further study of the ecology and response of bacterial PAH co-metabolizers.

Here, we studied the response of coastal marine microbial communities to these compounds. With a specific focus on bacteria capable of PAH co-metabolism, we seek to expand the known diversity of marine microbial degraders, investigate bacterial metabolic strategies, and begin to unravel the function of co-metabolism in marine environments. To study the microbial communities under the presence of PAHs, we established seawater enrichment cultures with these pollutants to isolate marine microbial PAH degraders. In addition, we determined the community composition of the enrichment cultures with and without an added labile carbon source. Finally, we analyzed the microbial PAH co-metabolism in these enrichment cultures in detail by searching for PAH degradation biomarkers within selected isolates and estimating the relative abundance of these co-metabolism degraders within the enrichment culture communities.

Results

To study the response of coastal marine microbial communities to PAHs in the presence and absence of labile carbon substrates, enrichment cultures were established. Complex carbon medium (CM) containing yeast extract and tryptone or minimal medium (MM) containing no additional carbon source were used for enrichments. PAH amendment was achieved via the addition of either phenanthrene (PHE), a LMW PAH, or pyrene (PYR), a HMW PAH, to the enrichment cultures. Finally, the enrichment cultures were inoculated with coastal surface seawater from a public beach (PB) or a boat ramp (BR) in the Tampa Bay. Viable cell counts for each biological and technical replicate were conducted over four weeks. The minimal medium enrichment cultures had a lower average cell density between 7 and 14 days than the complex medium, but minimal medium ended with a similar cell density at 28 days (~10^7 cells/mL) (**Figure C.4.1**). Minimal medium with PHE turned orange after only one week of incubation and the complex medium had a similar color change after two weeks of incubation. Previous studies have shown that the orange color is a product of 1-hydroxy-2-naphthoic acid accumulation from enzymatic degradation, suggestive of phenanthrene degradation in these enrichments (22, 23). After four weeks of incubation, the resulting microbial communities from biological replicate enrichments were characterized via 16S rDNA amplicon sequencing and 61 representative

strains were isolated. These strains were assessed for PAH degradation using a PAH top agar screening assay.

Enrichment community composition

To investigate the community composition of the enrichment cultures, DNA was extracted from cultures after four weeks of incubation and V3/V4 16S rDNA amplicon sequencing was conducted obtaining 0.85-2.20 million unpaired reads (132 ± 0.36 million). The resulting bacterial community composition in all treatment cultures showed a site and medium-based trend. The PB cultures had the highest relative abundance of Alphaproteobacteria (76.0±29.6%), while the BR cultures had high relative abundances of both Alphaproteobacteria (42.4±26.2%) and Gammaproteobacteria (40.1±32.3%) (**Figure 4.1**). Of the Alphaproteobacteria, most (66.9±28.9%) were *Rhodobacteraceae* family members and overwhelmingly represented by one unclassified *Rhodobacteraceae* ASV. The Gammaproteobacteria were made up of several families, *Marinomonadaceae* (31.2±28.8%), *Vibrionaceae* (18.0±23.0%), and *Halomonadaceae* (8.9±21.5%). Outside of Pseudomonadota, Bacteroidia (4.8±7.9%), Planctomycetes (2.0±4.7%), and Bdellovibrionia (1.2±2.3%) make up most of the resulting community composition. The boat ramp, minimal medium, and pyrene (BR_MM_PYR) treatment had the lowest relative abundance of Pseudomonadota and the highest relative abundance of Bacteroidia and Planctomycetes. The enrichment culture community composition was affected by seawater sampling site, PAH molecular weight, and the addition of a labile carbon source. Beta diversity of the communities showed that the communities were signficantly affected by site ($Pr<0.003$), PAH ($Pr<0.037$), and medium type ($Pr<0.001$) after 28 days of incubation (**Figure 4.2B; Table C.4.1**). Medium ($R^2=0.168974$) had the largest impact on community composition (**Figure 4.2B**; **Table C.4.1**). Gammaproteobacteria (47.2±27.1%) was the most abundant class in the complex medium cultures, while Alphaproteobacteria (74.4±29.8%) was in the minimal medium cultures (**Figure 4.1**). The complex medium had a greater alpha diversity than the minimal medium as indicated by the Shannon's diversity index ($q<0.05$) **(Figure 4.2A; Table C.4.2)**. While the Generalized UniFrac distances showed that molecular weight of the PAH ($Pr<0.037$) and site ($Pr<0.003$) had a significant effect on the microbial communities, their alpha diversity was not significantly different ($q<0.115$; $q<0.074$) (**Figure 4.2B; Table C.4.1**).

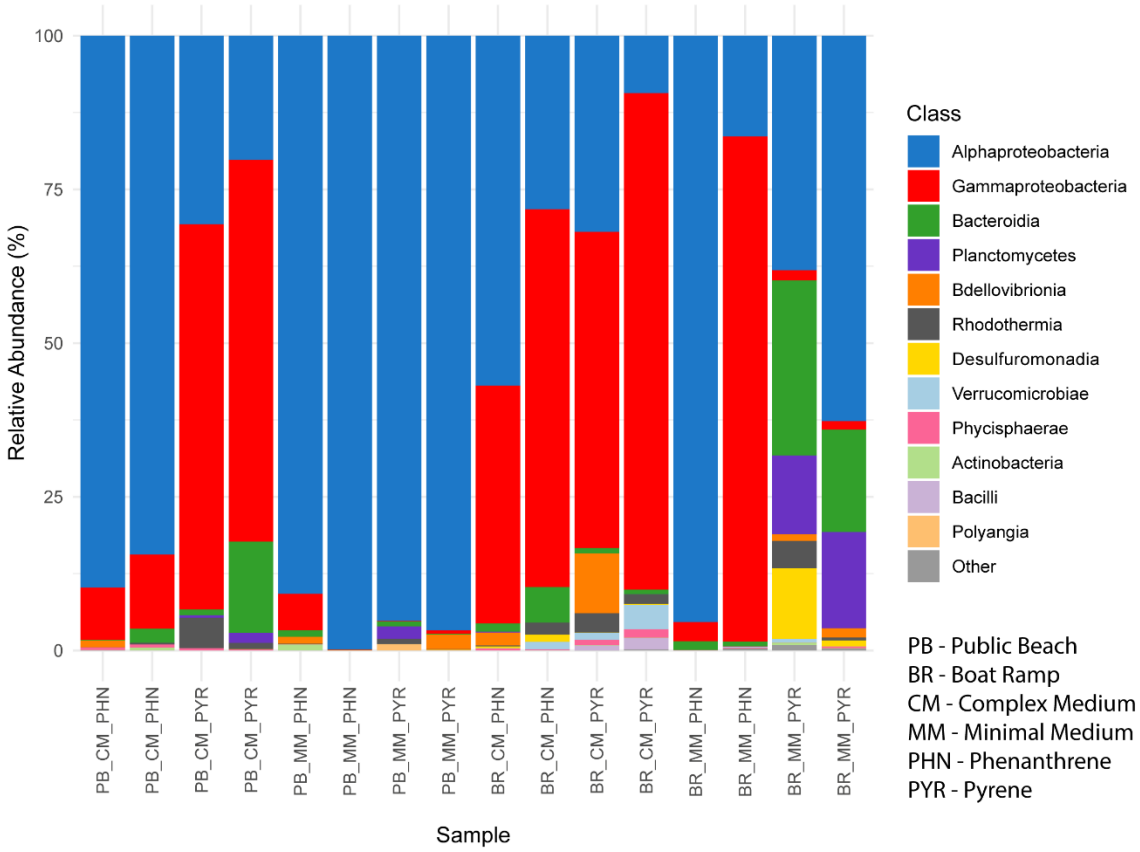

Figure 4.1: Enrichment culture community bacterial relative abundance. Relative abundance of bacterial classes representing >0.07% relative abundance of enrichment cultures after 28 days. “Other” refers to ASVs that contributed <0.07% relative abundance in the entire enrichment culture dataset. Culture names are as follows: Site (PB or BR), medium (CM or MM), and PAH (PHN or PYR). Biological replicate cultures are beside each other.

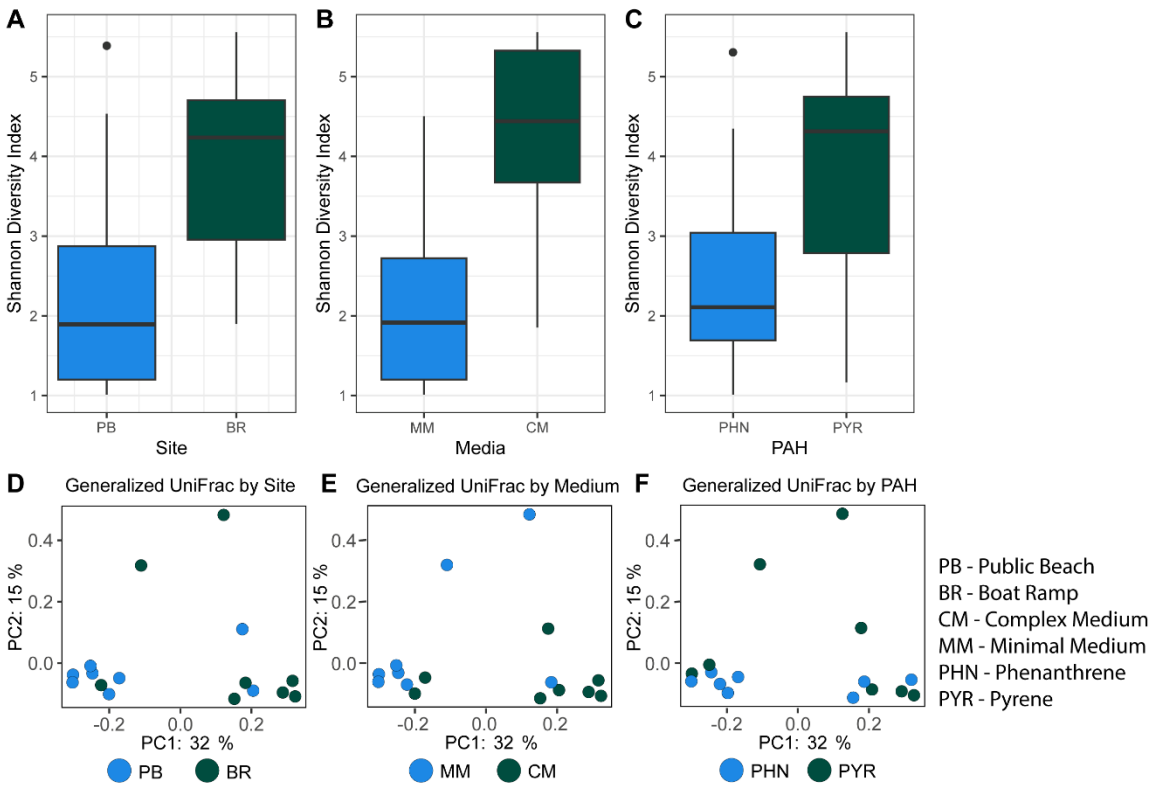

Figure 4.2: Alpha and beta diversity of enrichment culture communities. A), B) & C) Shannon diversity index for all samples based on site, medium, and PAH. D), E), & F) Generalized UniFrac for all samples based on site, medium, and PAH. Significance tests can be found in **Table C.4.1 & C.4.2.**

Bacterial isolate degradation ability and identities

From the minimal medium enrichments, we isolated 61 bacteria to assess their PAH degradative ability. All isolates were then screened on PAH-containing complex medium or minimal medium screening plates to assess PAH degradative ability (i.e., co-metabolism or sole-metabolism). The majority (81%) of the isolates showed the ability to degrade the PAH in which they were enriched (**Table C.4.3**). Thirty-one were isolated from the PYR minimal medium cultures and 22 were isolated from the PHE minimal medium cultures. Despite being isolated from minimal medium, only one isolate, originating from a PHE minimal medium culture, showed evidence of sole-metabolism. The remaining isolates with evidence of PAH degradation only degraded PAHs in the presence of complex medium. Of those able to degrade PAHs via co-metabolism, 56% came from the PYR enrichment cultures and 44% came from the PHE enrichment cultures (**Table C.4.3**).

The 43 PAH degraders were identified via partial 16S rRNA gene sequencing yielding 35 with non-duplicate identities. The majority of these strains were Alphaproteobacteria (23), with the remaining identified as Gammaproteobacteria (8), Flavobacteria (2), Actinobacteria (1), and Cytophagia (1) (**Figure 4.3**; **Table C.4.4**). Of the Alphaproteobacteria, the largest proportion of these isolates were *Roseobacteraceae* with 9 non-duplicate strains. The majority of the Gammaproteobacteria was made up of *Idiomarinaceae* with 5 non-duplicate strains. The isolate found to degrade PAHs via sole-metabolism was putatively identified as *Alteromonas oceani*.

Representative isolate genome sequencing and biomarker HMM searches

Thirty-two isolates were chosen for Illumina whole genome sequencing to investigate genetic biomarkers for PAH degradation (**Table C.4.5**). All genomes had a completeness score of >95% (with the exception of a putative *Marinovum* sp. isolate, which was 92%) and a contamination score of <2% as assessed by CheckM (24). Hidden Markov Models (HMMs) were constructed for PAH ring-hydroxylating dioxygenases and PAH hydratase aldolases amino acid sequences of various taxonomic distribution from a PAH biomarker database assembled by Huang et al., 2023 (25). One PAH RHD associated with gram negative bacteria (NahAc) and two PAH RHDs from gram positive bacteria (NidA and NarAa) were selected for HMMs. The associated PAH hydratase-aldolases for the PAH RHDs were selected for HMMs as well (NahE, PhdJ, and

Figure 4.3: Maximum likelihood phylogenetic tree of bacterial isolate partial 16S rDNA sequences with closest relative from NCBI. Bootstrap values (100 iterations) are shown at branch nodes with circle size corresponding to the value as indicated in the key. Tree scale represents evolutionary distance calculated via the Kimura 2-parameter model.

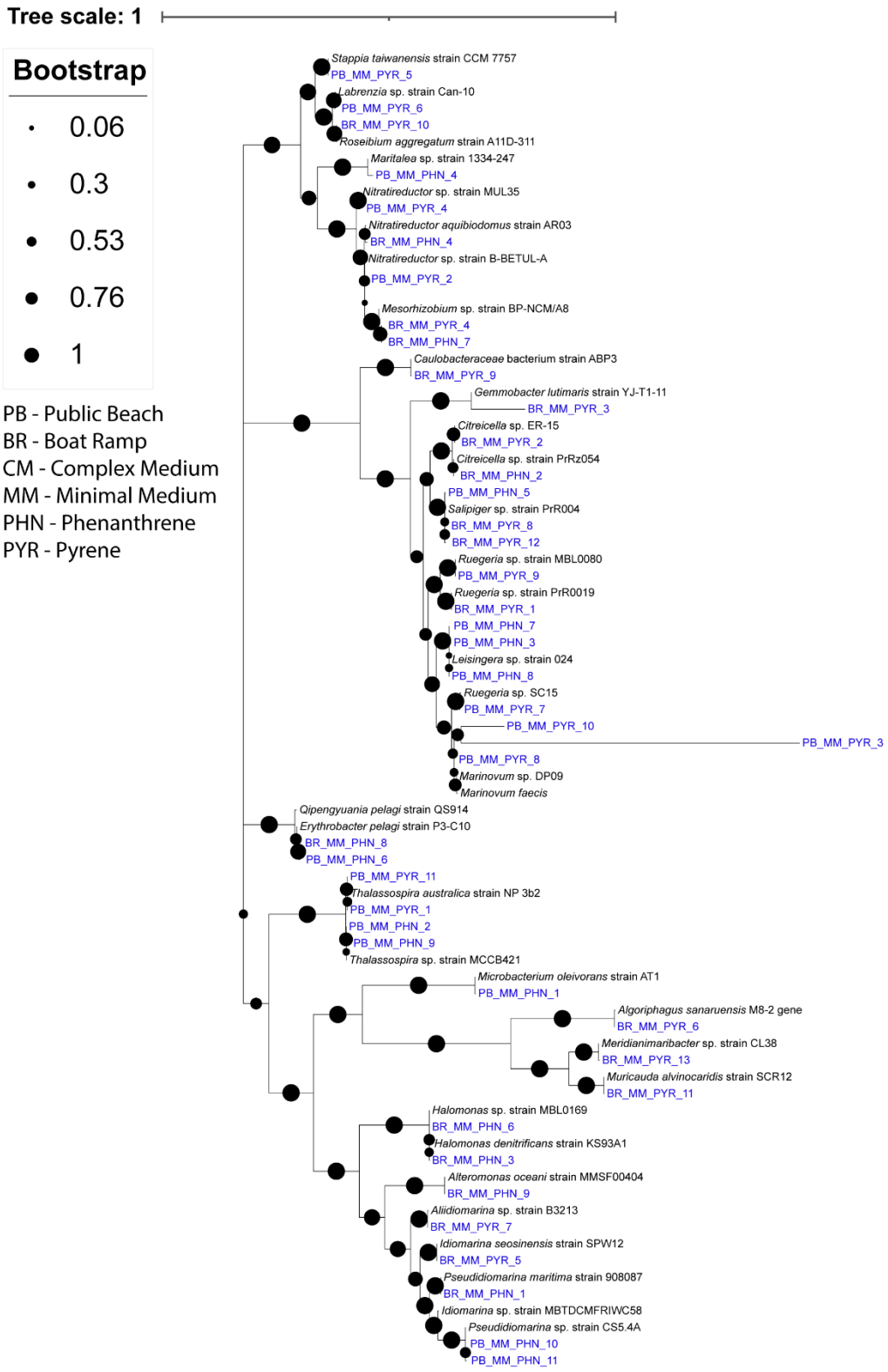
Tree scale: 1
Bootstrap
0.06
0.3
0.53
0.76
1
PB - Public Beach
BR - Boat Ramp
CM - Complex Medium
MM - Minimal Medium
PHN - Phenanthrene
PYR - Pyrene
Stappia taiwanensis strain CCM 7757
PB_MM_PYR_5
Labrenzia sp. strain Can-10
PB_MM_PYR_6
BR_MM_PYR_10
Roseibium aggregatum strain A11D-311
Maritalea sp. strain 1334-247
PB_MM_PHN_4
Nitratireductor sp. strain MUL35
PB_MM_PYR_4
Nitratireductor aquibiodomus strain AR03
BR_MM_PHN_4
Nitratireductor sp. strain B-BETUL-A
PB_MM_PYR_2
Mesorhizobium sp. strain BP-NCM/A8
BR_MM_PYR_4
BR_MM_PHN_7
Caulobacteraceae bacterium strain ABP3
BR_MM_PYR_9
Gemmobacter lutimaris strain YJ-T1-11
BR_MM_PYR_3
Citreicella sp. ER-15
BR_MM_PYR_2
Citreicella sp. strain PrRz054
BR_MM_PHN_2
PB_MM_PHN_5
Salipiger sp. strain PrR004
BR_MM_PYR_8
BR_MM_PYR_12
Ruegeria sp. strain MBL0080
PB_MM_PYR_9
Ruegeria sp. strain PrR0019
BR_MM_PYR_1
PB_MM_PHN_7
PB_MM_PHN_3
Leisingera sp. strain 024
PB_MM_PHN_8
Ruegeria sp. SC15
PB_MM_PYR_7
PB_MM_PYR_10
PB_MM_PYR_3
PB_MM_PYR_8
Marinovum sp. DP09
Marinovum faecis
Qipengyuania pelagi strain QS914
Erythrobacter pelagi strain P3-C10
BR_MM_PHN_8
PB_MM_PHN_6
PB_MM_PYR_11
Thalassospira australica strain NP 3b2
PB_MM_PYR_1
PB_MM_PHN_2
PB_MM_PHN_9
Thalassospira sp. strain MCCB421
Microbacterium oleivorans strain AT1
PB_MM_PHN_1
Algoriphagus sanaruensis M8-2 gene
BR_MM_PYR_6
Meridianimaribacter sp. strain CL38
BR_MM_PYR_13
Muricauda alvinocaridis strain SCR12
BR_MM_PYR_11
Halomonas sp. strain MBL0169
BR_MM_PHN_6
Halomonas denitrificans strain KS93A1
BR_MM_PHN_3
Alteromonas oceani strain MMSF00404
BR_MM_PHN_9
Aliidiomarina sp. strain B3213
BR_MM_PYR_7
Idiomarina seosinensis strain SPW12
BR_MM_PYR_5
Pseudidiomarina maritima strain 908087
BR_MM_PHN_1
Idiomarina sp. strain MBTDCMFRIWC58
Pseudidiomarina sp. strain CS5.4A
PB_MM_PHN_10
PB_MM_PHN_11

NarC). Each biomarker HMM was searched against the genome of each isolate using HMMER and all bit scores with an E-value below $1e^{-10}$ were selected for further analysis (26). Bit scores were used to determine the overall quality of the protein sequence hit to the HMM where a low bit score represents low similarity. *Escherichia coli* DH5α was also assessed for PAH degradation biomarkers to provide a comparison in bit score between a non-degrading organism and the isolates.

Despite isolation from PAH containing minimal medium, the isolates had lower bit scores (<202) than the highest *E. coli* bit score (≤422.9) (**Figure 4.4**). For the PAH ring-hydroxylating dioxygenases, *E. coli* had a higher bit score than all the isolate protein sequences, with most of the isolate protein bit scores below 200. Conversely for the PAH hydratase-aldolases, some isolates had higher bit scores than *E. coli* but they were lower than for the RHD protein hits with all hits below 110. PhdJ had no hits for any isolate nor *E. coli* with an e-value below $1e^{-10}$. Another PAH hydratase-aldolase, PhdG, further up in the Nid/PhD pathway was also chosen to assess the presence of this pathway (27). PhdG showed the same trend as NahE and NarC HMMs.

16S rRNA search in amplicon data

Near complete 16S rRNA gene (either from full genome sequencing or knitting forward and reverse PCR amplified fragments) were aligned against the 16S rRNA V3V4 amplicon representative sequences to pair isolates to the best-matching ASVs (**Table C.4.4**). Nearly all of the 32 isolates were successfully paired with an ASV (30/32), and 24 of those were paired to a unique ASV. After removing the isolate showing PAH sole-metabolism from the results, 14 of the isolates came from PB enrichment cultures and 15 isolates came from BR enrichment cultures. The PAH co-metabolism isolates had a higher relative abundance in the PB samples (57.3±32.2%) than the BR samples (6.8±4.0%) **(Figure 4.5**). In addition, those isolates that were originally isolated from BR cultures (1.2±3.0%) had a much lower relative abundance than those originally isolated from the PB cultures (30.0±35.0%). The isolate paired-ASVs had a lower relative abundance in the complex medium cultures than the minimal medium cultures. The complex medium and PYR treatment had the lowest relative abundance for both sites.

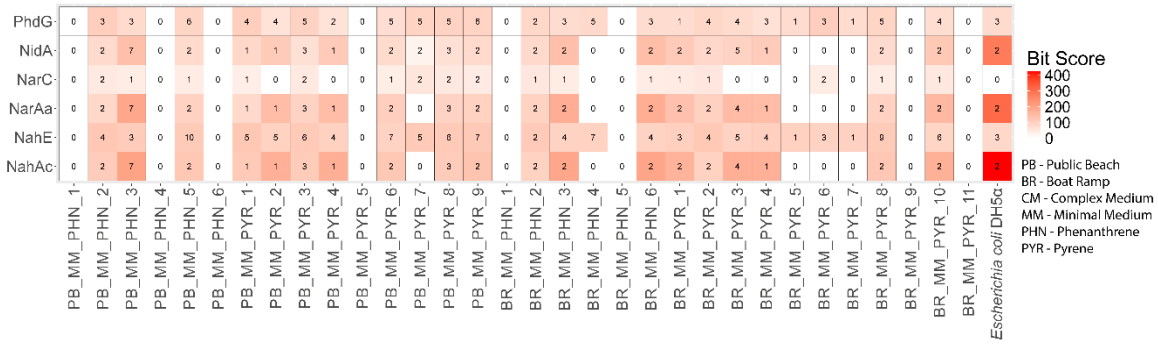

Figure 4.4: Summary of HMM searches for isolate genomes. Boxes are color-coded by the highest bit score of the protein hits for each strain. The numbers in the boxes indicate protein hits for each query sequence below an E-value of 1e-10. White boxes with a 0 indicate no hits with an E-value below 1e-10. Each HMM on the x-axis is named after the proteins that the model was constructed from. *E. coli* DH5α was included as a negative control. Detailed results from the protein identity searches are available from the KBase narrative (https://narrative.kbase.us/narrative/168034).

Discussion

PAHs are common pollutants within marine environments, thus understanding how microbial communities respond to these pollutants is essential to our understanding of natural bio-attenuation (1). Two sites were chosen to investigate the impact of PAHs: a public beach (PB) and a boat ramp (BR). Both sites had evidence of anthropogenic influence. The BR, in particular, is exposed to PAH-containing petroleum fuels and PAH-containing combustion products from boating activity. Chronic PAH pollution has been reported at a variety of boat ramps and marinas (28, 29). In addition, historical evidence indicates that chronic PAH pollution exists in Middle Tampa Bay where the BR samples were taken, while the PB site, at the interface of the Gulf of Mexico and Tampa Bay had much lower concentrations of PAHs (30).

The location of the initial inoculum signficantly affected the community composition when exposed to PAHs. One main difference was the relative abundance of Alphaproteobacteria and Gammaproteobacteria. In general, Gammaproteobacteria have been previously attributed to degradation of the HMW PAH proportion and Alphaproteobacteria to the LMW PAH proportion in marine systems (11, 12). In this study, *Marinomonas* spp. and *Vibrio* spp. ASVs had a higher relative abundance in complex medium regardless of site or the molecular weight of the PAH. While little study has been done on *Marinomonas* spp., evidence suggests that this genus is able to degrade both HMW and LMW PAHs (31). Similarly, little evidence exists for *Vibrio* spp. but studies suggest that this genus cannot utilize PAHs as a sole carbon source but can degrade them through co-metabolism (16, 32). In addition, studies investigating the effect of oil spills on microbial communities found that Gammaproteobacteria are often strongly selected for, but in this study Alphaproteobacteria appear to be selected for in the PB and BR samples (5, 33). This difference may be attributed to the absence of *Cycloclasticus* spp. in all but one enrichment culture as Gammaproteobacterial dominance in PAH contaminated sites is strongly linked to *Cycloclasticus* spp. abundance (34, 35). Evidence from this study suggests that Gammaproteobacteria may have a more dynamic role in PAH degradation than previously established.

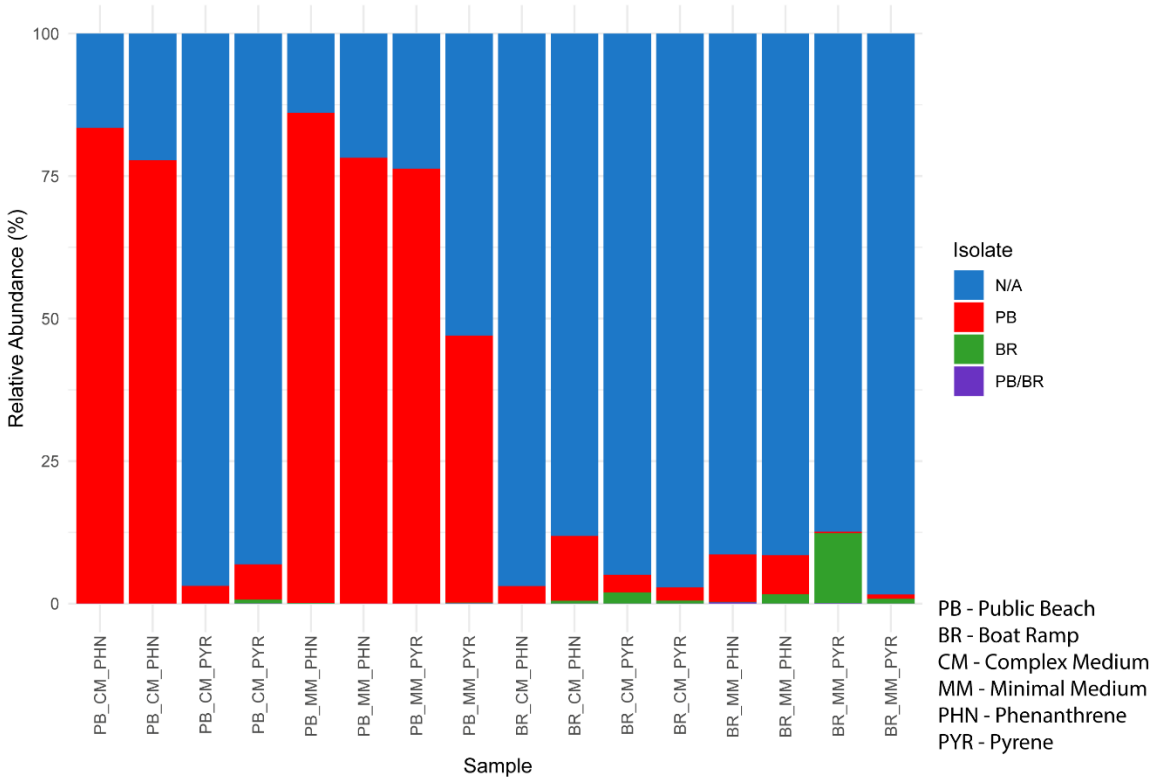

Figure 4.5: Relative abundance of isolates in enrichment culture amplicon sequences. Each isolate was paired to an amplicon sequence variant (ASV) based on its 16S rDNA sequence. The relative abundances of the ASVs that were paired with the isolates are shown above. Each ASV that was paired to an isolate is color-coded based on the site where the isolate originated (PB or BR). One isolate matched two ASVs and is noted as a PB/BR isolate. N/A refers to ASVs that did not correspond to an isolate.

Compared to Gammaproteobacteria the response of Alphaproteobacteria is less well-characterized with studies reporting both decreases and increases in abundance when exposed to PAHs and oil (36, 37). In this study, *Rhodobacteraceae* was the most abundant family in the Alpahproteobacteria proportion of the microbial communities. While this family has been split up into the *Roseobacteraceae* and the *Rhodobacteraceae* families, the taxonomic classification database, SILVA v138.2, has not yet updated to reflect this change, thus only the *Rhodobacteraceae* classification appears in this analysis (38, 39). Almost all marine bacteria in the *Rhodobacteraceae* family were re-classified as part of the *Roseobacteraceae* family, thus it is likely that these ASVs belong to this family (38). *Roseobacteraceae* members are known to degrade PAHs, both with and without a more labile carbon source (16–19). Several *Roseobacteraceae* members in this study displayed co-metabolism on pyrene and phenanthrene. In addition, *Roseobacteraceae* members are highly abundant in coastal regions, making up to 25% of the microbial communities (40). Their PAH degradation ability, along with their high abundance in marine ecosystems could allow them to play a large role in marine microbial community response to these pollutants. Previous studies have hinted at this role as *Roseobacteraceae* strains are commonly found in PAH and crude oil enrichment studies (12, 41–43). Other studies have documented an increase in *Roseobacteraceae* when exposed to oil, but PAH degradation by this family was not assessed (44, 45). As Alphaproteobacteria relative abundance was higher in PB cultures than the BR cultures, *Roseobacteraceae* relative abundance follows this same trend.

The presence of additional carbon sources significantly affected the community composition. Few reports of PAH co-metabolism exist, but evidence suggests that this mechanism of degradation could be widespread among marine bacteria (16). Interestingly, PAH co-metabolizing isolates were found from minimal medium cultures without an added carbon source other than PAHs. Thus, since these bacteria were unable to use PAHs as a sole carbon and energy source, they would require another more labile carbon source to be able to grow and transform PAHs. While some amount of DOC was likely present in the initial seawater inoculum, microbial necromass, from microbial cell death in the enrichments, likely provided a source of labile carbon to facilitate co-metabolism. Thus, bacterial turnover and bacterial death from PAH stress could have fueled the co-metabolism of other cells. Studies found that medium

containing yeast extract was a sufficient carbon source for PAH co-metabolism, which supports the use of microbial necromass, or other forms of DOC, for PAH co-metabolism in coastal communities (16, 17, 46).

The characterized enrichment isolates were also missing known genetic biomarkers for PAH degradation. Previous evidence suggested that bacteria able to co-metabolize PAHs likely had novel pathways for their degradation (16). This is further supported by *Ruegeria pomeroyi* DSS-3, a PAH co-metabolizer, that has been shown to lack these biomarkers and contains a putative PAH ring-hydroxylating dioxygenase involved in this co-metabolism (Chapter 3). Thus, this study highlights the need to further study PAH co-metabolizers as we cannot rely solely on bioinformatic approaches to study PAH degradation in marine environments. While some of the enrichment isolates' genera had reports of PAH degradation, most of these organisms are missing from previous reports of PAH degradation at the strain and/or species level. The absence of genetic biomarkers for PAH degradation and the ability to co-metabolize PAHs may have led to their exclusion.

This study provides insight into how microbial communities respond to PAH pollution. While several other studies have investigated such a response, they do not consider the contribution of co-metabolism. The starting relative abundance of the bacterial communities in this study are unknown, but initial community composition likely influenced the response of these communities due to historical contingency (36). Thus, from the data presented in this study, preexposure to PAHs appears to impact the abundance of co-metabolism degraders in favor of sole-metabolism degraders which have been selected for by prior PAH exposure. In environments where sudden PAH pollution occurs, co-metabolism degraders may be the initial responders to this pollution as sole-metabolism degraders have not been previously selected for. Bacteria that are at high abundances from their ability to thrive with the carbon sources available, such as *Roseobacteraceae* members, may increase in relative abundance due to their ability to degrade PAHs as they utilize other carbon sources. Preexposure to PAHs and available DOC are likely important factors influencing PAH co-metabolism in marine ecosystems.

Methods

Seawater sampling

Seawater samples were taken from two sites near/in Tampa Bay, FL with anthropogenic influence as a product of their recreational use. Public beach site was at Sunset Beach in Treasure Island, FL (27.7480216, -82.7621535) and the boat ramp site was at the public boat ramp at Demens Landing Park in St. Petersburg, FL (27.7714434, -82.6280303). Sterile 50mL conical tubes were used to collect 150mL water at each site. Within 24 hours water was used to inoculate enrichment cultures. Seawater was kept at room temperature until inoculation.

PAH enrichment cultures

Seawater was used to inoculate 10% Yeast Tryptone Sea Salt (YTSS) medium [per liter: 15 g Instant Ocean (Thermo Fisher Scientific), 0.4 g tryptone, 0.25 g yeast extract] or aromatic basal medium (ABM) [per liter 8.7 mM KCl, 8.7 mM $CaCl_2$, 43.5 mM $MgSO_4$, and 174 mM NaCl with 225 uM K_2HPO_4, 13.35 mM NH_4Cl, 71 mM Tris-HCl [pH 7.5], 15 g agar (Thermo Fisher Scientific), 68 uM Fe-EDTA, trace metals [7.85 mM nitriloacetic acid, 0.53 mM $MnSO_4{*}H_2O$, 0.42 mM $CoCl_2 {*}6H_2O$, 0.35 mM $ZnSO_4 {*}7H_2O$, 0.038 mM $CuSO_4$, 0.11 mM $NiCl_2 {*}6H_20$, 1.16 mM Na_2SeO_3, 0.41 mM $Na_2MoO_4{*}2H_2O$, 0.33 mM $Na_2WO_4{*}2H_2O$, 0.25 mM $Na_2SiO_3{*}9H_2O$] and trace vitamins [0.0020% vitamin H (Biotin), 0.0020% folic acid, 0.0100% pyridoxine-HCl (B6), 0.0050% riboflavin (B2), 0.0050% thiamine (B1), 0.0050% nicotinic acid, 0.0050% pantothenic acid (B5), 0.0001% cyanocobalamin (B12), 0.0050% *p*-aminobenzoic acid]]. To each medium, either 100 μg/mL pyrene or phenanthrene dissolved in acetone was added. In 250mL ashed and sterilized flasks, 45mL of the medium + PAH solution was added. Two control cultures with medium only were included to monitor any contamination during sampling and incubation. Before inoculation, cultures were allowed to incubate overnight at 30°C to remove residual acetone. The next day, 5mL of seawater was used to inoculate each enrichment culture with biological and technical duplicates for each treatment. Initial viable cell counts were conducted for each treatment and cultures were incubated at 30°C for 28 days.

After each week, enrichment culture sample was diluted and plated on YTSS agar to assess microbial growth and to isolate marine bacteria. Cultures were also observed for evidence of PAH degradation (i.e., color change). In addition, freezer stocks were made from each enrichment culture (2mL culture + 2mL 50% sterile glycerol).

Isolate screening and identification

Cultivated strains were grown in YTSS, mixed 1:1 with 50% glycerol, and stored at -70°C. All 53 isolates originated from ABM cultures with either pyrene or phenanthrene. To screen isolates for PAH degradation ability, a PAH top-agar screening assay was used, previously used in Walton & Buchan, 2023(16). In brief, base plates of either YTSS or ABM were topped with ~5mL of either pyrene or phenanthrene containing top agar, forming a cloudy film with which to assess degradation. All strains were inoculated into YTSS broth and grown overnight at 30°C. Strains to be plated on complex carbon plates were immediately spotted on PAH top agar plates. Those on minimal media were first washed twice with ABM before plated on PAH top agar plates to remove residual carbon. YTSS plates were incubated for a week at 30°C with plates being scraped after 3, 5, and 7 days. ABM plates were incubated for 2 weeks at 30°C with plates being scraped after 7 and 14 days. *Escherichia coli* DH5α was plated alongside strains as a negative control. Clearing zones under the colonies indicated degradation of the PAH and were recorded as positive for degradation. After confirming degradative ability, strains were identified by extracting the DNA with the DNeasy Blood & Tissue Kit (Qiagen, Germantown, MD) and amplifying the 16S rRNA gene. Resulting amplicons were sent for sequencing and used to determine the closet relative of the isolate via blastn (47). Strains that were not able to be successfully identified were not included in further study.

Phylogenetic analysis

To determine the relatedness and the diversity of the isolated colonies, a maximum likelihood phylogenetic tree was constructed. 16S rDNA sequences from isolates and closest-related relatives were aligned in BioEdit v7.2.5 (48). A maximum likelihood tree was constructed using MEGAX v10.2.2 and the Kimura 2-parameter model (49). The tree was visualized using iTOL v6 (50).

Enrichment culture community analysis

To determine the composition of the final enrichment cultures, 16S rDNA amplicon sequencing was conducted. DNA was extracted from the biological replicate week 4 freezer stocks using the QIAmp Micro DNA Kit (QIAGEN, USA). The following modified procedure was used. Buffer ATL was added to frozen enrichment culture stocks to a volume of 100µl and then 10µl of proteinase K, 100µl of Buffer AL, and 1µl of carrier RNA was added. To lyse cells, tubes were

incubated at 56°C for 10 minutes. 50µl of absolute ethanol was added and tubes were pulse-vortexed for 15 seconds before incubating at room temperature for 3 minutes. The lysate was then transferred to a QIAamp MinElute column and centrifuged at 6000xg for 1 minute. Flow through was discarded and then buffers AW1 and AW2 were added with the same spin and flow through steps after each buffer. Columns were then centrifuged at 16,000xg for 3 minutes before eluting DNA with 30µl of Buffer AE. Once buffer was added, the columns were incubated at room temperature for 1 minute before centrifuging at 16,000xg for 1 minute.

Sample DNA was quantified using a Qubit 4 Fluorometer (Thermo Fisher Scientific, Waltham, MA, USA) and shipped for sequencing at SeqCenter, LLC (https://www.seqcenter.com/). In brief, samples were prepared using the Quick-16S Kit (Zymo Research, Irvine, CA, USA) targeting the V3/V4 regions of the 16S rRNA gene. After cleanup and normalization, samples were sequenced on a P1 600cyc NextSeq2000 (Illumina, San Diego, CA, USA) to generate 2x301bp paired end reads.

Raw paired-end FASTQ reads were imported into the QIIME2 amplicon conda environment (v.2024.5) and demultiplexed. The 16S rRNA V3-V4 primers were trimmed with the cutadapt plugin. Paired-end reads were denoised with the DADA2 plugin to infer exact amplicon sequence variants (ASVs) with the following parameters: --p-trunc-len-f 280, --p-trunc-len-r 275, --p-trim-left-f 0, --p-trim-left-r 0.

The RESCRIPt plugin was used to pull the SILVA SSU r138.1 NR99 RNA sequence database and taxonomy for taxonomic classification. The RNA sequences were reverse transcribed to DNA sequences and low-quality reference sequences were culled with the RESCRIPt command ‘cull-seqs’ with default parameters. Sequences were filtered by minimum length based on taxonomy so that the minimum length for Archaea, Bacteria, and Eukaryota sequences are 900 nt, 1200 nt, and 1400 nt, respectively. The RESCRIPt command ‘dereplicate’ was used to dereplicate sequences and taxonomies when sequences and taxonomies match but retain all sequences that have unique taxonomic annotations even if the sequences are duplicates with ‘--p-mode uniq’. Using the 16S rRNA V3-V4 primer sequences, the 16S rRNA V3-V4 region of the unique SILVA reference sequences were extracted in the forward read orientation using the feature-classifier plugin ‘extract-reads’ command. The extracted 16S rRNA V3-V4 reads were dereplicated as before and subsequently used to train a Naïve Bayes taxonomic classifier with the

feature-classifier plugin ‘fit-classifier-naive-bayes’ command with default parameters. This classifier was used to predict the taxonomic classification of the DADA2 inferred representative ASV (i.e., feature) sequences with the feature-classifier plugin ‘classify-sklearn’ command with default parameters.

The SILVA 128 database was utilized for phylogenetic tree creation with SEPP (SATé-Enabled Phylogenetic Placement) fragment insertion. SEPP fragment insertion performs a phylogenetic placement technique explicitly designed for 16S rRNA data to obtain improved phylogeny trees. Samples with less than 1,000 ASV abundance were considered failed microbiome samples and removed from the analysis. Microbial features were filtered out if they were assigned to mitochondria or chloroplast. Further, features were filtered to reduce noise based on frequency to retain features with at least 1% abundance in 10% of samples. After filtering, the data set included 17 samples and 738 features totaling a frequency of 6,800,574 feature counts. The median frequency per sample was 396,293 (minimum = 287,586; maximum =514,322).

A rarefaction curve analysis was performed by generating alpha diversity metrics at a minimal sampling depth of 1 sequence to a maximum sampling depth of the median feature frequency. This revealed that rarefying to a depth of 285,000 feature counts per sample captures the majority of the alpha diversity signal within the dataset; therefore, this sampling depth was used for calculating diversity metrics. The QIIME2 ‘core-metrics-phylogenetic’ plugin was used to calculate alpha diversity metrics: Faith’s phylogenetic diversity, Peilou’s evenness, Shannon’s diversity, and ASV richness. The beta diversity metrics: unweighted, weighted, and generalized (alpha = 0.5) UniFrac distances were calculated using the generated SEPP fragmentation phylogenetic tree and visualized with principal coordinates analysis (PCoA).

Differences of alpha diversity metrics were statistically tested using Kruskal-Wallis H tests. Unweighted, weighted, and generalized UniFrac distances were statistically compared between collection site, media type, and PAH carbon source using the adonis package permutational multivariate analyses of variance (formula = “Site * Media * PAH”; permutations = 999). The non-rarified ASV feature table was used to test where the abundances of ASVs differed between collection site, media type, and PAH carbon source using the QIIME2 ‘composition’ plugin with the analysis of compositions of microbiomes with bias correction (ANCOM-BC) command using the ‘--p-conserve’ flag as recommended for small sample sizes. The ANCOM-BC

reference levels for the collection site, media type, and PAH carbon source were site 1, YTSS, and pyrene, respectively.

Isolate genome sequence and analysis

DNA was extracted from bacterial isolates using the DNeasy Blood & Tissue Kit (QIAGEN, USA) and then quantified using a Qubit 4 Fluorometer (Thermo Fisher Scientific, Waltham, MA, USA). Samples were shipped to SeqCenter, LLC (https://www.seqcenter.com/) for full genome sequencing. In brief, the libraries were prepared using the Illumina DNA Prep kit (Illumina, San Diego, CA, USA) and custom IDT 10bp unique dual indices. Sequencing was conducted using an Illumina NovaSeq X Plus sequencer (Illumina, San Diego, CA, USA) to produce 2x151bp paired-end reads. Downstream demultiplexing, quality control, and adapter trimming was performed using bcl-convert v4.2.4. Assembly was performed with Unicycler v0.5.0 and the resulting assembly was assessed with QUAST v5.2.0 (51, 52). Bakta v1.8.1 was used to annotate assembled genomes (53). Default parameters were used for all tools. Genome completeness and contamination was assessed using CheckMv1.8.10 and KBase (www.kbase.us) (24, 54). CheckM scores are available through KBase (https://narrative.kbase.us/narrative/168034).

Polycyclic aromatic hydrocarbon degradation biomarker Hidden Markov Model construction and searches

Hidden Markov Models were constructed from a PAH biomarker sequence database (25). Sequences for each biomarker were aligned in BioEditv7.2.5 using CLUSTALW (48). KBase (www.kbase.us) and HMMERv3.3.2 were used to search each PAH biomarker model (NarC, NarAa, NahAc, NahE, NidA, PhdJ, and PhdG) against the isolate genomes (26, 54). HMM results are available through KBase (https://narrative.kbase.us/narrative/168034).

Isolate relative abundance

16S rDNA sequences either partial or full were extracted from the full genome sequences or knit together from forward and reverse sanger sequencing of 16S rDNA PCR amplified fragments. Forward and reverse PCR products were trimmed and then knit together using QIAGEN CLC Genomics Workbench v24.0.1. The full-length 16S rRNA FASTA sequences from the isolates were imported into the QIIME2 amplicon conda environment (v.2024.5). Using the QIIME2 ‘feature-classifier’ plugin ‘vsearch-global’ command, the full-length 16S rRNA sequences were treated as reference reads and the 16S rRNA V3V4 DADA2 representative sequences were

treated as query reads. The query reads were aligned to the reference reads using conservative limits parameters: '--p-perc-identity 0.4', '--p-query-cov 0.1', '--p-maxhits all', '--p-maxrejects all', and '--p-no-search-exact'. To determine the best hit, the alignment results were manually curated initially by removing hits with less than 95% identity and query coverage. From this list, the alignment with the highest percent identity was assigned the 'best hit'. Two isolated samples failed to reliably align and were removed from the analysis: BR_MM_PHN_8 (50.5% highest query coverage) and BR_MM_PYR_8 (48.4% highest percent identity). One isolate, BR_MM_PYR_7, had two equal 'best hits' with 99.1% identity and 100% coverage. For this isolate, the 'best hit' was determined by selecting the query ASV sequence with the highest abundance and prevalence within the 16S rRNA V3V4 dataset. There were some query ASV sequences that were 'best hits' for multiple isolates; therefore, the final total of unique ASV sequences that may correspond to the isolates was 24. The relative abundance of these features was investigated to determine their composition among each treatment group.

Acknowledgements

We would like to acknowledge the Howard Hughes Medical Institute Gilliam Fellowship and the University of Tennessee Institute for a Secure and Sustainable Environment Seed Grant to AB and JW.

REFERENCES

1. Catania V, Cascio Diliberto C, Cigna V, Quatrini P. 2020. Microbes and Persistent Organic Pollutants in the Marine Environment. Water Air Soil Pollut 231:1–10.
2. El-Shahawi MS, Hamza A, Bashammakh AS, Al-Saggaf WT. 2010. An overview on the accumulation, distribution, transformations, toxicity and analytical methods for the monitoring of persistent organic pollutants. Talanta 80:1587–1597.
3. Sakshi, Haritash AK. 2020. A comprehensive review of metabolic and genomic aspects of PAH-degradation. Arch Microbiol 202:2033–2058.
4. Gupta G, Kumar V, Pal AK. 2017. Microbial Degradation of High Molecular Weight Polycyclic Aromatic Hydrocarbons with Emphasis on Pyrene. Polycycl Aromat Compd 39:124–138.
5. Sieradzki ET, Morando M, Fuhrman JA. 2021. Metagenomics and Quantitative Stable Isotope Probing Offer Insights into Metabolism of Polycyclic Aromatic Hydrocarbon Degraders in Chronically Polluted Seawater. mSystems 6.
6. Ambade B, Sethi SS, Giri B, Biswas JK, Bauddh K. 2021. Characterization, Behavior, and Risk Assessment of Polycyclic Aromatic Hydrocarbons (PAHs) in the Estuary Sediments. Bulletin of Environmental Contamination and Toxicology 2021 1:1–10.
7. Honda M, Suzuki N. 2020. Toxicities of Polycyclic Aromatic Hydrocarbons for Aquatic Animals. Int J Environ Res Public Health 17.
8. Dash HR, Mangwani N, Chakraborty J, Kumari S, Das S. 2013. Marine bacteria: Potential candidates for enhanced bioremediation. Appl Microbiol Biotechnol 97:561–571.
9. Kim YH, Moody JD, Freeman JP, Brezna B, Engesser KH, Cerniglia CE. 2004. Evidence for the existence of PAH-quinone reductase and catechol-O-methyltransferase in *Mycobacterium vanbaalenii* PYR-1. J Ind Microbiol Biotechnol 31:507–516.
10. Vila J, Tauler M, Grifoll M. 2015. Bacterial PAH degradation in marine and terrestrial habitats. Curr Opin Biotechnol 33:95–102.
11. Head IM, Jones DM, Röling WFM. 2006. Marine microorganisms make a meal of oil. Nat Rev Microbiol 4:173–182.

12. Vila J, Nieto JM, Mertens J, Springael D, Grifoll M. 2010. Microbial community structure of a heavy fuel oil-degrading marine consortium: Linking microbial dynamics with polycyclic aromatic hydrocarbon utilization. FEMS Microbiol Ecol 73:349–362.
13. Xia M, Chen B, Fan G, Weng S, Qiu R, Hong Z, Yan Z. 2023. The shifting research landscape for PAH bioremediation in water environment: a bibliometric analysis on three decades of development. Environmental Science and Pollution Research 1:1–16.
14. Yuan J, Lai Q, Sun F, Zheng T, Shao Z. 2015. The diversity of PAH-degrading bacteria in a deep-sea water column above the Southwest Indian Ridge. Front Microbiol 6.
15. Duran R, Cravo-Laureau C. 2016. Role of environmental factors and microorganisms in determining the fate of polycyclic aromatic hydrocarbons in the marine environment. FEMS Microbiol Rev 40:814–830.
16. Walton JL, Buchan A. 2024. Evidence for novel polycyclic aromatic hydrocarbon degradation pathways in culturable marine isolates. Microbiol Spectr 12.
17. Zhou H, Zhang S, Xie J, Wei H, Hu Z, Wang H. 2020. Pyrene biodegradation and its potential pathway involving Roseobacter clade bacteria. Int Biodeterior Biodegradation 150:104961.
18. Zhang YH, Dong JD, Wang YS, Gu JD, Yin JP, Ahmad M, Ling J. 2022. Comparative genomics reveals the evidence of aromatic hydrocarbons degradation potential in genus *Roseovarius* in marine environment. Int Biodeterior Biodegradation 171:105408.
19. Cao J, Lai Q, Yuan J, Shao Z. 2015. Genomic and metabolic analysis of fluoranthene degradation pathway in *Celeribacter indicus* P73 T. Sci Rep 5:1–12.
20. Liang C, Huang Y, Wang H. 2019. *pahE*, a Functional Marker Gene for Polycyclic Aromatic Hydrocarbon-Degrading Bacteria. Appl Environ Microbiol 85.
21. Gallego S, Vila J, Tauler M, Nieto M, Breugelmans P, Springael D, Grifoll M. 2014. Community structure and PAH ring-hydroxylating dioxygenase genes of a marine pyrene-degrading microbial consortium. Biodegradation 25:543–556.
22. Kiyohara H, Nagao K, Kouno K, Yano K. 1982. Phenanthrene-degrading phenotype of Alcaligenes faecalis AFK2. Appl Environ Microbiol 43:458.

23. Tao XQ, Lu GN, Dang Z, Yi XY, Yang C. 2007. Isolation of phenanthrene-degrading bacteria and characterization of phenanthrene metabolites. World J Microbiol Biotechnol 23:647–654.
24. Parks DH, Imelfort M, Skennerton CT, Hugenholtz P, Tyson GW. 2015. CheckM: assessing the quality of microbial genomes recovered from isolates, single cells, and metagenomes. Genome Res 25:1043.
25. Huang Y, Li L, Yin X, Zhang T. 2023. Polycyclic aromatic hydrocarbon (PAH) biodegradation capacity revealed by a genome-function relationship approach. Environ Microbiome 18:1–13.
26. Finn RD, Clements J, Eddy SR. 2011. HMMER web server: Interactive sequence similarity searching. Nucleic Acids Res 39:W29–W37.
27. LeVieux JA, Johnson WH, Erwin K, Li W, Jessie Zhang Y, Whitman CP. 2016. The bacterial catabolism of polycyclic aromatic hydrocarbons: Characterization of three hydratase-aldolase-catalyzed reactions. Perspect Sci (Neth) 9:33–41.
28. Neira C, Cossaboon J, Mendoza G, Hoh E, Levin LA. 2017. Occurrence and distribution of polycyclic aromatic hydrocarbons in surface sediments of San Diego Bay marinas. Mar Pollut Bull 114:466–479.
29. Mali M, Dell'Anna MM, Mastrorilli P, Damiani L, Piccinni AF. 2017. Assessment and source identification of pollution risk for touristic ports: Heavy metals and polycyclic aromatic hydrocarbons in sediments of 4 marinas of the Apulia region (Italy). Mar Pollut Bull 114:768–777.
30. Long, Edward R.; Greening HS. 1999. Chemical Contamination in Tampa Bay: Extent, toxicity, potential sources and possible sediment quality management plans.
31. Dong C, Bai X, Lai Q, Xie Y, Chen X, Shao Z. 2014. Draft Genome Sequence of *Marinomonas* sp. Strain D104, a Polycyclic Aromatic Hydrocarbon-Degrading Bacterium from the Deep-Sea Sediment of the Arctic Ocean. Genome Announc 2:1211–1224.
32. Hedlund BP, Staley JT. 2001. *Vibrio cyclotrophicus* sp. nov., a polycyclic aromatic hydrocarbon (PAH)-degrading marine bacterium. Int J Syst Evol Microbiol 51:61–66.

33. Coulon F, McKew BA, Osborn AM, McGenity TJ, Timmis KN. 2007. Effects of temperature and biostimulation on oil-degrading microbial communities in temperate estuarine waters. Environ Microbiol 9:177–186.
34. Teira E, Lekunberri I, Gasol JM, Nieto-Cid M, Álvarez-Salgado XA, Figueiras FG. 2007. Dynamics of the hydrocarbon-degrading *Cycloclasticus* bacteria during mesocosm-simulated oil spills. Environ Microbiol 9:2551–2562.
35. Kasai Y, Kishira H, Harayama S. 2002. Bacteria Belonging to the Genus *Cycloclasticus* Play a Primary Role in the Degradation of Aromatic Hydrocarbons Released in a Marine Environment. Appl Environ Microbiol 68:5625–5633.
36. Gosai HB, Panseriya HZ, Patel PG, Patel AC, Shankar A, Varjani S, Dave BP. 2022. Exploring bacterial communities through metagenomics during bioremediation of polycyclic aromatic hydrocarbons from contaminated sediments. Science of The Total Environment 842.
37. Lekunberri I, Calvo-Díaz A, Teira E, Morán XAG, Peters F, Nieto-Cid M, Espinoza-González O, Teixeira IG, Gasol JM. 2010. Changes in bacterial activity and community composition caused by exposure to a simulated oil spill in microcosm and mesocosm experiments. Aquatic Microbial Ecology 59:169–183.
38. Liang HK ,Orata FD, Boucher Y, Case RJ. 2021. Roseobacters in a Sea of Poly- and Paraphyly: Whole Genome-Based Taxonomy of the Family *Rhodobacteraceae* and the Proposal for the Split of the "Roseobacter Clade" Into a Novel Family, *Roseobacteraceae* fam. nov. Front Microbiol 12.
39. Pruesse E, Quast C, Knittel K, Fuchs BM, Ludwig W, Peplies J, Glöckner FO. 2007. SILVA: a comprehensive online resource for quality checked and aligned ribosomal RNA sequence data compatible with ARB. Nucleic Acids Res 35:7188–7196.
40. Wagner-Döbler I, Biebl H. 2006. Environmental biology of the marine Roseobacter lineage. Annu Rev Microbiol 60:255–280.
41. Pinyakong O, Tiangda K, Iwata K, Omori T. 2012. Isolation of novel phenanthrene-degrading bacteria from seawater and the influence of its physical factors on the degradation of phenanthrene. ScienceAsia 38:36–43.

42. Wang W, Zhong R, Shan D, Shao Z. 2014. Indigenous oil-degrading bacteria in crude oil-contaminated seawater of the Yellow sea, China. Appl Microbiol Biotechnol 98:7253–7269.
43. Shahriari Moghadam M, Ebrahimipour G, Abtahi B, Ghassempour A, Seyed Hashtroudi M. 2014. Biodegradation of polycyclic aromatic hydrocarbons by a bacterial consortium enriched from mangrove sediments. J Environ Health Sci Eng 12:1–9.
44. Liu J, Bacosa HP, Liu Z. 2017. Potential environmental factors affecting oil-degrading bacterial populations in deep and surface waters of the Northern Gulf of Mexico. Front Microbiol 7:220535.
45. Zhou Y, Wang Y, Yang L, Kong Q, Zhang H. 2023. Microbial degradation mechanisms of surface petroleum contaminated seawater in a typical oil trading port. Environmental Pollution 324:121420.
46. Ahmad M, Ling J, Yin J, Chen L, Yang Q, Zhou W, Zhang Y, Huang X, Khan I, Dong J. 2023. Evaluation of the Different Nutritional and Environmental Parameters on Microbial Pyrene Degradation by Mangrove Culturable Bacteria. Int J Mol Sci 24:8282.
47. Camacho C, Coulouris G, Avagyan V, Ma N, Papadopoulos J, Bealer K, Madden TL. 2009. BLAST+: Architecture and applications. BMC Bioinformatics 10:1–9.
48. Hall, TA. 1999. BioEdit: A User-Friendly Biological Sequence Alignment Editor and Analysis Program for Windows 95/98/NT. Nucleic Acids Symposium Series 41:95-98.
49. Kumar S, Stecher G, Li M, Knyaz C, Tamura K. 2018. MEGA X: Molecular Evolutionary Genetics Analysis across Computing Platforms. Mol Biol Evol 35:1547–1549.
50. Letunic I, Bork P. 2024. Interactive Tree of Life (iTOL) v6: recent updates to the phylogenetic tree display and annotation tool. Nucleic Acids Res 52:W78–W82.
51. Wick RR, Judd LM, Gorrie CL, Holt KE. 2017. Unicycler: Resolving bacterial genome assemblies from short and long sequencing reads. PLoS Comput Biol 13:e1005595.
52. Gurevich A, Saveliev V, Vyahhi N, Tesler G. 2013. QUAST: quality assessment tool for genome assemblies. Bioinformatics 29:1072–1075.
53. Schwengers O, Jelonek L, Dieckmann MA, Beyvers S, Blom J, Goesmann A. 2021. Bakta: rapid and standardized annotation of bacterial genomes via alignment-free sequence identification. Microb Genom 7.

54. Arkin AP, Cottingham RW, Henry CS, Harris NL, Stevens RL, Maslov S, Dehal P, Ware D, Perez F, Canon S, Sneddon MW, Henderson ML, Riehl WJ, Murphy-Olson D, Chan SY, Kamimura RT, Kumari S, Drake MM, Brettin TS, Glass EM, Chivian D, Gunter D, Weston DJ, Allen BH, Baumohl J, Best AA, Bowen B, Brenner SE, Bun CC, Chandonia JM, Chia JM, Colasanti R, Conrad N, Davis JJ, Davison BH, Dejongh M, Devoid S, Dietrich E, Dubchak I, Edirisinghe JN, Fang G, Faria JP, Frybarger PM, Gerlach W, Gerstein M, Greiner A, Gurtowski J, Haun HL, He F, Jain R, Joachimiak MP, Keegan KP, Kondo S, Kumar V, Land ML, Meyer F, Mills M, Novichkov PS, Oh T, Olsen GJ, Olson R, Parrello B, Pasternak S, Pearson E, Poon SS, Price GA, Ramakrishnan S, Ranjan P, Ronald PC, Schatz MC, Seaver SMD, Shukla M, Sutormin RA, Syed MH, Thomason J, Tintle NL, Wang D, Xia F, Yoo H, Yoo S, Yu D. 2018. KBase: The United States Department of Energy Systems Biology Knowledgebase. Nature Biotechnology 2018 36:7 36:566–569.

APPENDIX C

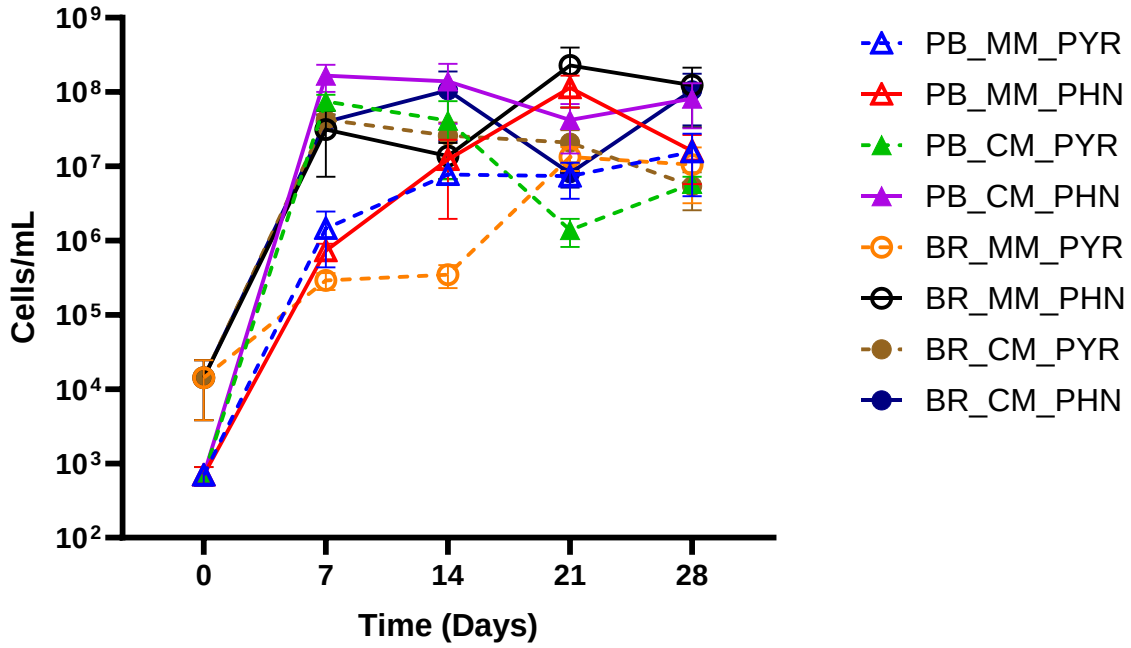

Appendix Figure C.4.1: Enrichment culture viable cell counts over 28 days. Biological duplicate and technical duplicate cultures were plated at 0, 7, 14, 21, and 28 days. The average and standard error of the mean was calculated from the combined biological and technical replicates. Four replicate plate counts were obtained for all but the following: Day 14 PB_MM_PYR, Day 21 PB_MM_PYR, Day 14 PB_MM_PHN, Day 14 BR_MM_PYR, and Day 21 BR_MM_PHN.

Appendix Table C.4.1: Generalized UniFrac adonis results.

	Df	SumsOfSqs	MeanSqs	F.Model	R^2	Pr(>F)
Site	1	0.439535	0.439535	3.935233	0.15924	0.003
Media	1	0.466401	0.466401	4.175771	0.168974	0.001
PAH	1	0.244715	0.244715	2.190972	0.088658	0.037
Site:Media	1	0.18945	0.18945	1.696176	0.068636	0.082
Site:PAH	1	0.172744	0.172744	1.546605	0.062584	0.104
Media:PAH	1	0.168109	0.168109	1.505109	0.060905	0.129
Site:Media:PAH	1	0.185707	0.185707	1.662671	0.06728	0.09
Residuals	8	0.893538	0.111692	NA	0.323722	NA
Total	15	2.760199	NA	NA	1	NA

Appendix Table C.4.2: Shannon diversity index Kruskal-Wallis results.

	H	p-value	q-value
Site	3.1875	0.074203	0.074203
Media	5.338235	0.020863	0.020863
PAH	2.481618	0.115184	0.115184

Appendix Table C.4.3: Summary of screened bacterial isolates.

Isolation Culture	Total Isolates	CM + PAH	MM +PAH	Neither
MM+PYR	31	24	0	7
MM +PHN	22	19	1	3

CHAPTER 5 CONCLUSION

Despite decades of research on polycyclic aromatic hydrocarbon (PAH) degradation, initial investigation into co-metabolism has only occurred over the past few years (1). Numerous studies have investigated the ability of low molecular weight (LMW) PAHs to increase degradation efficiency and rate of high molecular weight (HMW) PAHs as a form of co-metabolism, but even the LMW PAHs are incredibly recalcitrant and present a metabolic hurdle for many bacteria (2, 3). While several studies have shown that PAH degradation may increase in the presence of a more labile carbon source, the mechanism, role, diversity, and conservation of this function is currently unknown (4–6). Bacteria only able to degrade PAHs via co-metabolism (i.e., degradation of PAHs in the presence of another carbon source) has received even less attention. This knowledge gap stems from the vast number of studies that only assess bacteria for sole-metabolism (i.e., degradation of PAHs as a sole carbon and energy source) and from bioinformatic studies that utilize PAH degradation genetic biomarkers to predict microbial functions. While studies focusing on sole-metabolism propelled the field of PAH bioremediation forward, relying on these studies has narrowed our understanding of other metabolic strategies. In addition, several studies show that some PAH sole-metabolism pathways are under regulation by catabolite repression (7, 8). These bacteria may utilize PAHs as a sole carbon and energy source, but environmental carbon sources may trigger catabolite repression, preventing them from acting on PAHs. Co-metabolism degraders do not face the same challenges as they are able to degrade PAHs in the presence of other carbon sources. Furthermore, biomarker-based approaches do not capture PAH co-metabolism degraders and fail to link functions to specific microbes (9). PAH bioremediation research has shifted toward bioinformatic approaches, but until we have sufficient studies on PAH co-metabolism, these studies will not capture the true diversity of PAH degraders in the environment.

Filling this gap in research is difficult as the field has progressed rapidly, leaving co-metabolism far behind in knowledge. With both culture-based and bioinformatic-based studies focused on sole-metabolism, methods to study co-metabolism similarly are underdeveloped. In Chapter 1, I established two methods to assess PAH co-metabolism with a specific emphasis on marine bacteria. First, I adapted a PAH top-agar screening assay to qualitatively assess co-metabolism (10). For this assay I determined what carbon source should be supplemented, PAH

concentration (for both pyrene and phenanthrene), and how to assess degradation using these plates. Initially it took weeks for clearing zones to appear around colonies, indicating degradation, and some bacteria grew faster than the clearing zone could develop. To circumvent this, I attempted to scrape cells from the plate to see whether any clearing zones appeared under the colonies. This allowed me to screen bacteria for PAH co-metabolism using a high-throughput approach. To quantify degradation, I modified a High-Performance Liquid Chromatography assay that extracted PAHs from culture media to determine remaining PAH concentration (6, 11). From this assay I learned that not only is carbon source important, but also the concentration of that source. Although these two assays are disappearance based, disappearance-based assays are widely accepted in the field as measures of PAH degradation. These two assays assisted me in further proving the existence of PAH co-metabolism and the prevalence of this metabolic strategy within marine bacteria.

An unexpected result of this work was how many bacteria were only capable of PAH co-metabolism. Even when selecting for PAH degraders in Chapter 4, most bacteria were only capable of co-metabolism. Many *Roseobacteraceae* family members also co-metabolize PAHs, which is a driving theme throughout all three research chapters (6, 9). As *Roseobacteraceae* members have high genetic diversity, the number of members with evidence of PAH co-metabolism is significant and points toward the conservation of this function within the family (6, 9, 12). This function is likely mediated by promiscuous enzymes able to act on PAHs in addition to their intended substrate. In Chapter 3, I demonstrate that several promiscuous enzymes are involved in co-metabolism by *Ruegeria pomeroyi* DSS-3. Since this function appears conserved within family members and functionally redundant in *R. pomeroyi* DSS-3, PAH co-metabolism likely plays an important role in *Roseobacteraceae* survival since these bacteria are likely not gaining any metabolic benefit from these enzymatic reactions.

PAH co-metabolism as a survival mechanism in polluted marine environments would not only benefit bacteria able to co-metabolize these compounds by reducing their toxicity, but also reduce the metabolic hurdle for PAH sole-metabolizers by overcoming the stability of these compounds and hydroxylating them. In Chapter 4, I hypothesize that these PAH co-metabolizers may act as a first line of defense against PAH pollution in non-chronically polluted areas due to their enzymes acting on PAHs. Overcoming that first metabolic hurdle would allow for sole-

metabolizers to more efficiently degrade PAHs, establishing a synergistic degradation relationship between co- and sole-metabolizers. In addition, the detoxification of the environment increases the survival of other genera more susceptible to PAH pollution. Overall, evidence suggests that these PAH co-metabolizers may play a significant role in the natural attenuation of PAH pollution.

The work in this dissertation only covers a small fraction of the research needed to understand the mechanism of co-metabolism and the role this metabolic strategy plays in the environment. The goal of this dissertation was not to fill in all the knowledge gaps surrounding PAH co-metabolism but present a starting point for future research into this topic. While initial hydroxylation of these compounds appears to occur during co-metabolism, further investigation is needed to confirm this hydroxylation and determine downstream reactions and products occur after this initial hydroxylation. This could provide evidence for synergistic relationships between co-metabolism degraders and sole-metabolism degraders in the environment. While Chapter 4 made efforts to investigate marine bacterial community response to PAHs, *in situ* studies are required to determine if this activity occurs in marine systems and if this activity can occur using marine DOC. While such studies would enhance our understanding of PAH co-metabolism, environmental pollution is a risk when working with pollutants, thus our work focused on *ex situ* investigations. Knowledge from this dissertation as well as future work in PAH co-metabolism has the potential to develop new bioremediation strategies and technologies. The most obvious application of this work would be the formation of a biostimulant that provided the necessary carbon sources to stimulate bacterial co-metabolism in polluted environments to increase degradation efficiency. As co-metabolism appears to be a prevalent function in marine bacteria, this biostimulant could be applied to diverse marine systems as well as oil spill sites.

This research has broad implications in the bioeconomy sector. Bioeconomy is the portion of the economy that relates products, processes, and services derived from biological organisms (13). The global bioeconomy is estimated to be worth anywhere from $4-30 trillion by 2023 (14). Specifically, the bioremediation market is estimated to grow from $15 billion in 2023 to $34 billion by 2032 (15). This growth underscores the need for continued bioremediation research and development of new technologies to continue the growth in this field. Outside of the bioremediation market, *Roseobacteraceae* family members are valuable industrial assets due to

their ability to degrade lignin and lignin-derived compounds into high-value products via bioengineering (16). Such bio-based products offer a sustainable solution to production, but further research is needed for the optimization and scalability of these technologies (17). While PAH co-metabolism research is just beginning to gain traction, the budding bioremediation market and industrial interest in *Roseobacteraceae* members could lead to innovative technologies based off this foundational research.

REFERENCES

1. Xia M, Chen B, Fan G, Weng S, Qiu R, Hong Z, Yan Z. 2023. The shifting research landscape for PAH bioremediation in water environment: a bibliometric analysis on three decades of development. Environmental Science and Pollution Research 1:1–16.
2. Ho Y, Jackson M, Yang Y, Mueller JG, Pritchard PH. 2000. Characterization of fluoranthene-and pyrene-degrading bacteria isolated from PAH-contaminated soils and sediments. Journal of Industrial Microbiology & Biotechnology.
3. Jiang J, Tian W, Lu Z, Chu M, Cao H, Zhang D. Cometabolic degradation of pyrene with phenanthrene as substrate: assisted by halophilic *Pseudomonas stutzeri* DJP1. Biodegradation 2023 1–14.
4. Rao L, Gu D, Xiang X, Zeng J, Wu Y, Lin X, Christie P. 2023. Impact of lignin constituents on the bacterial community and polycyclic aromatic hydrocarbon co-metabolism in an agricultural soil. Environmental Pollution 333:122105.
5. Ahmad M, Ling J, Yin J, Chen L, Yang Q, Zhou W, Zhang Y, Huang X, Khan I, Dong J. 2023. Evaluation of the Different Nutritional and Environmental Parameters on Microbial Pyrene Degradation by Mangrove Culturable Bacteria. Int J Mol Sci 24:8282.
6. Zhou H, Zhang S, Xie J, Wei H, Hu Z, Wang H. 2020. Pyrene biodegradation and its potential pathway involving Roseobacter clade bacteria. Int Biodeterior Biodegradation 150:104961.
7. Shrestha S, Awasthi D, Chen Y, Gin J, Petzold CJ, Adams PD, Simmons BA, Singer SW, Nikel PI. 2023. Simultaneous carbon catabolite repression governs sugar and aromatic co-utilization in *Pseudomonas putida* M2. Appl Environ Microbiol https://doi.org/10.1128/AEM.00852-23.
8. Vandera E, Samiotaki M, Parapouli M, Panayotou G, Koukkou AI. 2015. Comparative proteomic analysis of *Arthrobacter phenanthrenivorans* Sphe3 on phenanthrene, phthalate and glucose. J Proteomics 113:73–89.
9. Walton JL, Buchan A. 2024. Evidence for novel polycyclic aromatic hydrocarbon degradation pathways in culturable marine isolates. Microbiol Spectr 12.

10. Bogardt AH, Hemmingsen BB. 1992. Enumeration of phenanthrene-degrading bacteria by an overlayer technique and its use in evaluation of petroleum-contaminated sites. Appl Environ Microbiol 58:2579–2582.
11. Zhang Y-H, Dong J-D, Wang Y-S, Gu J-D, Yin J-P, Ahmad M, Ling J. 2022. Comparative genomics reveals the evidence of aromatic hydrocarbons degradation potential in genus *Roseovarius* in marine environment. Int Biodeterior Biodegradation 171:105408.
12. Liang HK, Orata FD, Boucher Y, Case RJ, . 2021. Roseobacters in a Sea of Poly- and Paraphyly: Whole Genome-Based Taxonomy of the Family *Rhodobacteraceae* and the Proposal for the Split of the "Roseobacter Clade" Into a Novel Family, *Roseobacteraceae* fam. nov. Front Microbiol 12.
13. Gallo ME. 2022. The Bioeconomy: A Primer (R46881). Congressional Research Service.
14. Hodgson A, Maxon M, Alper J. 2022. The U.S. Bioeconomy: Charting a Course for a Resilient and Competitive Future. Schmidt Futures https://doi.org/10.55879/D2HRS7ZWC.
15. SNS Insider. 2024.Bioremediation Market Reach USD 34.27 Billion By 2032, Driven By Industrial Growth, Environmental Degradation, Technological Advancements, And Government Support. https://www.globenewswire.com/news-release/2024/07/26/2919665/0/en/Bioremediation-Market-Reach-USD-34-27-Billion-By-2032-Driven-By-Industrial-Growth-Environmental-Degradation-Technological-Advancements-And-Government-Support-Report-by-SNS-Insider.html. Retrieved 30 September 2024.
16. Wei Y, Wang S-G, Xia P-F, Nikel PI. 2024. Blue valorization of lignin-derived monomers via reprogramming marine bacterium *Roseovarius nubinhibens*. Appl Environ Microbiol https://doi.org/10.1128/AEM.00890-24.
17. Nielsen J, Tillegreen CB, Petranovic D. 2022. Innovation trends in industrial biotechnology. Trends Biotechnol 40:1160–1172.

APPENDIX D QUORUM SENSING AND ANTIMICROBIAL PRODUCTION ORCHESTRATE BIOFILM DYNAMICS IN MULTISPECIES BACTERIAL COMMUNITIES

A version of this chapter was originally published by April Armes, Jillian Walton, and Alison Buchan:
Armes, AC, Walton, JL. & Buchan, A. 2022. Quorum Sensing and Antimicrobial Production Orchestrate Biofilm Dynamics in Multispecies Bacterial Communities. *Microbiol Spectr* 10:e02615-22.

A.C.A. and A.B. conceived and designed the experiments for surface attachment and biofilm formation assays. A.C.A. designed and conducted the experiments for AHL extraction and growth inhibition. A.C.A. and J.L.W. conducted the experiments for surface attachment and biofilm formation assays, carried out data analysis, generated figures, and drafted the manuscript. The manuscript was edited by A.C.A., J.L.W., and A.B.

Abstract

Microbial interactions are often mediated by diffusible small molecules, including secondary metabolites, that play roles in cell-to-cell signaling and inhibition of competitors. Biofilms are often "hot spots" for high concentrations of bacteria and their secondary metabolites, which make them ideal systems for the study of small-molecule contributions to microbial interactions. Here, we use a five-member synthetic community consisting of *Roseobacteraceae* representatives to investigate the role of secondary metabolites on microbial biofilm dynamics. One synthetic community member, *Rhodobacterales* strain Y4I, possesses two acylated homoserine lactone (AHL)-based cell-to-cell signaling systems (*pgaRI* and *phaRI*) as well as a nonribosomal peptide synthase gene (*igi*) cluster that encodes the antimicrobial indigoidine. Through serial substitution of Y4I with mutants deficient in single signaling molecule pathways, the contribution of these small-molecule systems could be assessed. As secondary metabolite production is dependent upon central metabolites, the influence of growth substrate (i.e., complex medium versus defined medium with a single carbon substrate) on these dynamics was also considered. Depending on the Y4I mutant genotype included, community dynamics ranged from competitive to cooperative. The observed interactions were mostly competitive in nature. However, the community harboring a Y4I variant that was both impaired in quorum sensing (QS) pathways and unable to produce indigoidine (*pgaR* variant) shifted toward more cooperative interactions over time. These cooperative interactions were enhanced in the defined

growth medium. The results presented provide a framework for deciphering complex, small-molecule-mediated interactions that have broad application to microbial biology.

Importance

Microbial biofilms play critical roles in marine ecosystems and are hot spots for microbial interactions that play a role in the development and function of these communities. *Roseobacteraceae* is an abundant and active family of marine heterotrophic bacteria forming close associations with phytoplankton and carrying out key transformations in biogeochemical cycles. Group members are aggressive primary colonizers of surfaces, where they set the stage for the development of multispecies biofilm communities. Few studies have examined the impact of secondary metabolites, such as cell-to-cell signaling and antimicrobial production, on marine microbial biofilm community structure. Here, we assessed the impact of secondary metabolites on microbial interactions using a synthetic, five-member *Roseobacteraceae* community by measuring species composition and biomass production during biofilm growth. We present evidence that secondary metabolites influence social behaviors within these multispecies microbial biofilms, thereby improving understanding of bacterial secondary metabolite production influence on social behaviors within marine microbial biofilm communities.

Introduction

Microbial interactions play critical roles in defining microbial community structure and function. These microbial interactions span from cooperative interactions, such as resistance to antimicrobials and cometabolism (1–3), to more competitive interactions, including the production of inhibitory compounds and resource acquisition (4–6). Many types of microbial interactions are mediated by small molecules. While not essential to primary metabolism, these small molecules (i.e., secondary metabolites) facilitate interactions between microbes and their biotic and abiotic environments (7). Two common classes of secondary metabolites produced by microbes are signaling molecules and antimicrobial compounds. A well-known group of small, diffusible signaling molecules, the acylated homoserine lactones (AHLs), are common to many *Proteobacteria* where they are used to coordinate gene expression, often in a population-density-dependent manner (i.e., quorum sensing [QS]) (8). Canonical AHL-mediated QS consists of a two-component system consisting of a transcriptional regulator (LuxR-type protein) and an

AHL synthase (LuxI-type protein) that produces a diffusible ligand. When bound, these protein-ligand complexes can elicit global changes in gene expression (9). Common bacterial traits that are QS regulated include, but are not limited to, bioluminescence, motility, biofilm formation, and antimicrobial production (10–13). Antimicrobials are thought to contribute to microbial interactions principally through growth inhibition of competitors. However, for some microbes, these compounds may themselves function as intermicrobial signals at low concentrations (14). In addition, antimicrobials have been demonstrated to influence biofilm formation in some bacterial species (15, 16). Thus, these two classes of molecules can have overlapping roles and are crucial to competitive and cooperative microbial interactions.

In many environments, diverse microorganisms are enclosed in biofilms where they are in close physical association with one another and encased in a self-produced polymeric matrix (17, 18). The biological and physicochemical properties of biofilms make them ideal systems to study microbial interactions, especially those that are mediated by diffusible small molecules. In addition, biofilms play critical roles in ecosystem functioning, where they mediate transformations key to biogeochemical cycling (19), bioremediation (20), and biofouling (21). In turn, biofilm-associated microorganisms are afforded some degree of protection by the biofilm matrix from external environmental stressors, predators, toxins, and antibiotics (22).

The current understanding of QS-mediated microbial interactions within biofilms is based principally on coculture and natural assemblages (23, 24). While valuable, coculture studies can be limited by the oversimplification of microbial interactions. On the other hand, mesocosm experiments using complex natural communities introduce a wide range of variables to consider when trying to tease apart microbial interactions (25–27). Synthetic intentional communities provide an opportunity to limit community complexity while still allowing for a higher order level of interactions beyond pairwise interactions. In addition, synthetic communities have been used recently in surface colonization and biofilm studies to mimic interactions found in natural ecosystems (28–30). Despite the recent emergence of synthetic multispecies-based biofilm studies, our knowledge of microbial interactions within natural biofilm communities is still relatively incomplete, specifically those cooperative and competitive interactions influenced by small molecules, such as secondary metabolites. A critical aspect to understanding these small-molecule-linked interactions within multispecies biofilm communities is to evaluate the fitness,

physiological, and ecological aspects between individual species and a multispecies biofilm consortium.

Due to their predilection to form biofilms on a variety of surfaces and robust secondary metabolite production, members of the heterotrophic *Roseobacteraceae* family of bacteria are ideal model organisms for examining the molecular mechanisms that mediate the cooperative and competitive microbial interactions within biofilm communities (31). These bacteria comprise upward of 20% of microbial communities in coastal marine ecosystems, possess a large genetic repertoire, and demonstrate high metabolic diversity (32, 33). Diverse family members have been found to be primary and aggressive colonizers of a variety of surfaces in coastal oceans (32, 33). The production of secondary metabolites likely contributes to the competitive fitness of *Roseobacteraceae* strains in marine biofilms. For example, genomic evidence suggests the majority of sequenced strains possess at least one QS gene (34). Furthermore, nonribosomal peptide synthases and polyketide synthases (PKSs) are pervasive in marine strains (35).

To evaluate the impact of secondary metabolite production, specifically AHLs and antimicrobials, on microbial interactions in biofilms, we conducted synthetic community experiments using a five-member *Roseobacteraceae* community. The selected strains (*Sagittula stellata* sp. E-37, *Rhodobacterales* strain Y4I, *Roseovarius nubinhibens* ISM, *Sulfitobacter* sp. EE-36, and *Citreicella* sp. SE45) are representatives of those found in high abundance in marine environments, where they have been reported to be metabolically active (36, 37). These strains have been studied extensively in their ability to degrade plant-derived aromatic compounds, and each possess genes encoding the protocatechuate pathway, which is responsible for the catabolism of a variety of aromatic compounds, including *p*-coumaric acid (33, 38–40). Additionally, these strains have been used previously in a synthetic community study to evaluate the interactive effects that combinations of labile and recalcitrant substrates have on microbial growth and metabolism (31). One of these strains, *Rhodobacterales* strain Y4I, has been the focus of studies examining the contribution of both quorum sensing and antimicrobials to competitiveness fitness (5, 41, 42). We have access to previously generated Y4I mutants impaired in various aspects of secondary metabolite production and detection (**Table D.1**). Using this synthetic community and substituting different Y4I mutants, we assessed the contribution of secondary metabolites to community dynamics (i.e., community composition and biofilm

formation as well as cooperation and competition over time). To achieve this goal, we expanded upon the previous definition of biofilm community cooperation and competition presented by Ren et al. (28). Here, community cooperation is assessed as an increase in biofilm formation compared with the best biofilm producer in monoculture without the loss of total cell viability in the community. Community competition is defined as a decrease in biofilm formation compared with the worst biofilm producer in monoculture or a decrease in viability in the community (28). As secondary metabolite production is linked intrinsically with central metabolism, we also considered the influence of growth medium (i.e., complex versus defined).

Results

Genomic analysis of QS and secondary metabolites in synthetic community members.

Previous studies have reported that both QS systems and biosynthetic pathways for antimicrobial production (e.g., PKS and nonribosomal polypeptide synthase [NRPS]) are prevalent in *Roseobacteraceae* genomes (5, 39, 43). All five strains used in this study possess at least one QS component. Three of the five strains (E-37, SE45, and Y4I) contain one or more canonical *luxRI* paired QS system(s). Additionally, these strains each harbor an unpaired (i.e., orphan or solo) LuxR homolog. In contrast, two members (ISM and EE-36) possess only orphan LuxR and LuxI homologs (**Table D.2**). It has been demonstrated previously that Y4I possesses two QS systems (*pgaRI* and *phaRI*) which coordinately regulate the production of the blue pigmented antimicrobial indigoidine, encoded by a nonribosomal polypeptide synthase (NRPS) termed *igiD* (41). NRPS-like genes encode secondary metabolites, such as toxins, antimicrobials, and pigments (reviewed in reference 44). Two other community members have been reported to possess NRPS-like genes, namely, E-37 and ISM (38), but neither these genes nor their products have been characterized. Both SSE37_17955 and ISM_16730 share more than 90% sequence identity to luciferase-like monooxygenase (LLM) class flavin-dependent oxidoreductases in more closely related organisms (i.e., organisms in their respective genera) and are distinct from *igiD* in Y4I. ISM produces a dark brown-orange pigment, while E-37 does not produce pigmentation (45, 46). The gene(s) responsible for pigmentation in ISM have yet to be identified. Whether the NRPS genes found in E-37 and ISM confer antimicrobial properties is currently unknown.

Appendix Table D.5.1: Rhodobacterales strain Y4I mutant variant secondary metabolite gene expression and indigoidine phenotypes.

	QS2		QS1		Indigoidine biosynthesis[i]	
	pgaR[i]	***pgaI***[2]	***phaR***[2]	***phaI***[2]	***igiD***[2]	**Pigmentation**[2,ii]
***pgaR*::TN5-Km^R**	-	-	-	-	-	-
***phaR*::TN5-Km^R**	+	+	-	-	-	+/-
***phaI*::pKNOCK**	+	++	+	-	-	-
***igiD*::TN5-Km^R**	+	++	-	-	-	-

[1] For indigoidine biosynthesis expression of the biosynthetic igiD gene was assessed as well as degree of pigmentation when grown on an agar surface, which correlates with indigoidine concentration.
[2] Armes and Buchan 2021
[3] Cude et al 2015

Appendix Table D.5.2: Table of community members, their *luxRI* homologous genetic loci, and putative AHLs produced by community members.

Species	LuxR gene locus	LuxI gene locus
Sagittula stellata E-37	SSE37_11169[ac]	SSE37_11164[ac]
	SSE37_06082[bc]	
Sulfitobacter sp. EE-36		EE36_01635[bc]
	EE36_03628[bc]	
Roseovarius nubinhibens ISM		ISM_03755[bc]
	ISM_09921[bc]	
	ISM_15650[bc]	
Citreicella sp. SE45	CSE45_4055[ac]	CSE45_4054[ac]
	CSE45_1818[bc]	
Rhodobacterales strain Y4I	RBY4I_1689[ac]	RBY4I_3631[ac]
	RBY4I_1027[ac]	RBY4I_3464[ac]
	RBY4I_896[bc]	

[a] Paired QS system, [b] Solo *luxR/luxI* (grey), [c]Cude et al., 2013, [d]Cude et. al 2015

Pairwise comparisons between synthetic community member LuxI homologs to PgaI and PhaI in Y4I revealed that E-37 and SE45 possess more than 50% amino acid identity to PgaI. Both EE-36 and ISM shared more than 25% amino acid identity with PhaI in Y4I (data not shown). The high protein similarity in AHL synthases between community members suggests the synthesis of AHLs with similar structures. Here, we present preliminary evidence that community members likely produce AHLs with overlapping masses corresponding to C5-HSL, C10-HSL, and C12-HSL (see **Figure S.D.1** in the supplemental material).

Secondary metabolites may underlie interactions between synthetic biofilm members.

In order to determine whether secondary metabolite production among individual community members could inhibit the growth of community residents, we performed a pairwise assessment of interactions between the five synthetic community members using a fully factorial growth inhibition assay. Only one strain, *Rhodobacterales* strain Y4I, was able to inhibit the growth of any of the other strains (2 of 4) (**Table D.3**). Using mutants that are either abolished in indigoidine pigment production (*igiD*::Tn5-Km^r) or hyper-pigmented (*clpA*::Tn5-Km^r), the inhibition of strains EE-36 and E-37 was strictly correlated with indigoidine production capability as determined previously (5, 42) (**Table D.3**), indicating this compound could be an important community determinant in this synthetic community. Previous studies demonstrate the competitive nature of Y4I in community members in both coculture and synthetic community studies, likely resulting from indigoidine production (31, 42). Given that competition and surface attachment have been linked to both QS systems and indigoidine, we used Y4I strains harboring disruptions in these pathways to independently assess the impact of secondary metabolites on biofilm community composition and dynamics.

Y4I is an aggressive surface colonizer compared with other community members.

We assessed the surface colonization of the five individual synthetic community members as well as the Y4I QS and indigoidine variants in monoculture (**Figure D.1**) at 12, 24, and 48 h postinoculation. Twelve hours after inoculation, the number of viable Y4I cells colonizing the glass beads was at least an order of magnitude higher than that of all other strains and remained significantly greater than all community members at 24 h and 48 h ($P < 0.05$), with the exception of EE-36 at the final time point (**Figure D.1**). Attachment rate and viable cell abundance among Y4I variants were comparable (see **Figure S.D.2** in the supplemental material).

Appendix Table D.5.3: Factorial growth inhibition of synthetic community members.

	Inhibitor Organism						
Lawn	Y4I	†*clpA*::Tn5 -Km^R	‡*igiD*::Tn5-Km^R	E-37	EE-36	ISM	SE45
Y4I	X	X	X	-	-	-	-
E-37	+	+	-	X	-	-	-
EE-36	+	+	-	-	X	-	-
ISM	+/-	-	-	-	-	X	-
SE45	-	-	-	-	-	-	X

(+) growth inhibition, (+/-) inconsistent growth inhibition, (-) no growth inhibition, (X) not tested; †hyperpigmented Y4I variant, ‡indigoidine null Y4I variant

Secondary metabolites influence biofilm composition.

We next assessed whether QS or antimicrobial production influenced microbial biofilm community structure (composition) and dynamics (cooperation or competition) in the five-member synthetic *Roseobacteraceae* community. Each synthetic community contained one of the following Y4I variants: wild type (WT), *pgaR*::Tn5-Km^r, *phaR*::Tn5-Km^r, *phaI*::pKNOCK, and *igiD*::Tn5-Km^r (**Table D.1**). Both the *pgaR* and *phaR* variants are unable to sense their cognate AHLs, C8-HSL and 3OHC12:1-HSL, respectively. Additionally, the *pgaR* mutant is unable to produce the indigoidine, while the *phaR* variant expresses delayed and reduced amounts of indigoidine (41). To eliminate this leaky phenotype, we previously generated a mutant in the corresponding AHL synthase gene, *phaI*. This mutant is unable to produce 3OHC12:1-HSL, but transcriptional regulators PhaR and PgaR remain functional. Upon exogenous addition of AHLs, a partial restoration of indigoidine production was restored only in the PhaR/I system with the addition of C8-HSL, alone or in combination with 3OHC12:1-HSL. Thus, the *phaI* variant is able to sense AHLs corresponding to the *phaRI* and *pgaRI* QS systems (42). The indigoidine biosynthesis mutant, *igiD*::Tn5-Km^r, is unable to produce indigoidine but expresses WT levels of both QS systems (42). These indigoidine phenotypes were evident even within synthetic communities Thus, we could quantitatively assess the discrete and compounded impact of QS systems and antimicrobial production.

Viable cellular abundances for each synthetic community were assessed, and the relative abundance of each community member over time (days) was determined. Across all communities, the relative abundance of each strain remained moderately stable. However, composite community viable cell abundance varied over time according to the presence of specific Y4I variants within synthetic communities. For example, synthetic communities harboring either wild-type Y4I or the *phaR* variant stabilized after day 1, whereas total viable cells in synthetic communities containing an indigoidine null mutant decreased in viability on day 2. In contrast, communities possessing the *pgaR* mutant increased continually in viability over time. Synthetic communities harboring the *phaI* variant decreased initially in viability but rebounded on day 3. Despite the modality of community dynamics within each synthetic community, biofilm communities within the complex medium were characterized by an

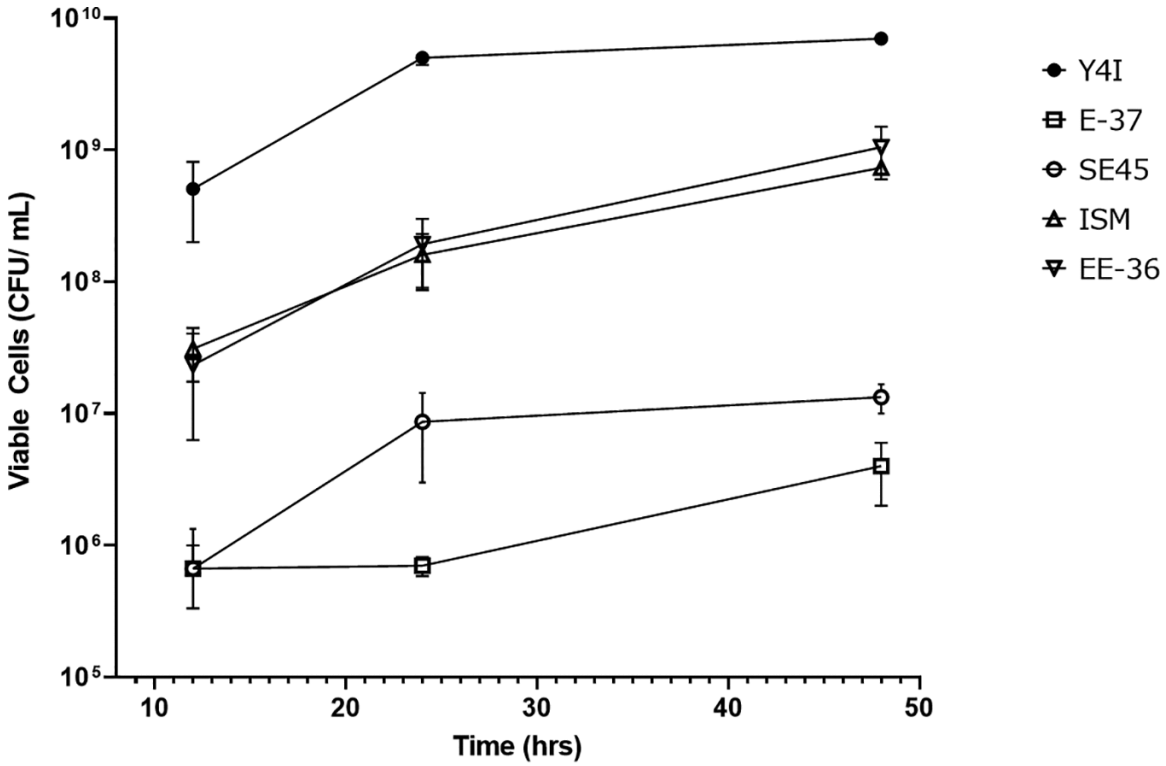

Appendix Figure D.1: Surface colonization of Roseobacter strains to glass beads in a complex medium over 48 hrs. Viable cell abundance of five Roseobacter strains: Y4I (closed circles), E-37 (open squares), SE45 (open circles), ISM (open upward triangles), and EE-36 (open downward triangles). Initial seeding density from liquid culture tubes was ~ 10^8 cells mL^{-1}. Each data point represents the average of three biological replicates. Error bars represent the standard error of the mean. Some error bars are not visible due to low variance between replicates. All cultures were statistically significant from Y4I at 24 hrs and 48 hrs, except EE36 which was only significantly different at 24 hrs (p <0.05). Y4I variants (not shown) were not significantly different from WT Y4I (Figure S.D.2). Two-way ANOVA for all strains used in this assay can be found in **Table S.D.3.**

overwhelming dominance of Y4I regardless of the variant, comprising 57% to 89% of the community (**Figure D.2A**).

We used a defined medium containing *p*-coumaric acid as the sole carbon source to (i) decrease the competitive advantage of Y4I and (ii) determine if the carbon source affected community interactions. When providing a growth disadvantage using this lignin-related phenolic compound, all Y4I variants displayed an initial decrease in viability in synthetic communities (**Figure D.2B**). This result is consistent with previous findings and is posited to be a result of toxicity due to *p*-coumaric acid, a weak acid (31). In fact, Y4I variants demonstrated a loss of viability compared with no carbon controls in liquid monocultures when grown on *p*-coumaric acid (see **Figure S.D.3** in the supplemental material). However, when grown in the synthetic communities, the number of viable cells of each Y4I variant increased in the presence of *p*-coumaric acid, which is suggestive of a detoxification provided by other community members. This increase in viable cells was comparable to no-carbon controls (see **Figure S.D.4** in the supplemental material). Despite an initial lag relative to complex medium experiments, all Y4I variants dominated their synthetic communities by the end of the experiment under the defined medium condition (**Figure D.2**). All synthetic communities grew on *p*-coumaric acid and displayed similar growth dynamics to those observed in complex medium (**Figure D.2**). Communities harboring wild-type Y4I and the *phaR* variant stabilized on day 9, while the synthetic community possessing the *pgaR* mutant continued to increase in viability. At day 14, communities containing the *phaI* variant appeared to stabilize. From day 1 to day 14, the dominant community member in defined medium biofilms switched from SE45 (75% to 87% on day 1) to Y4I (61% to 87% on day 14), regardless of the Y4I variant included (**Figure D.2B**). To investigate the diversity and treatment effects on community structure, we performed alpha and beta diversity analyses using the Shannon index and Bray-Curtis dissimilarity index, respectively. In addition, we used permutational multivariate analysis of variance (PERMANOVA) to measure species richness, species diversity, and significant differences between various communities and growth substrates in each time point (**Figure D.3**; see **Figure S.D.5** and **Table S.D.6** to **S.D.10** in the supplemental material). Within each growth substrate experiment, synthetic communities were not significantly different at day 0 (**Figure D.3**)

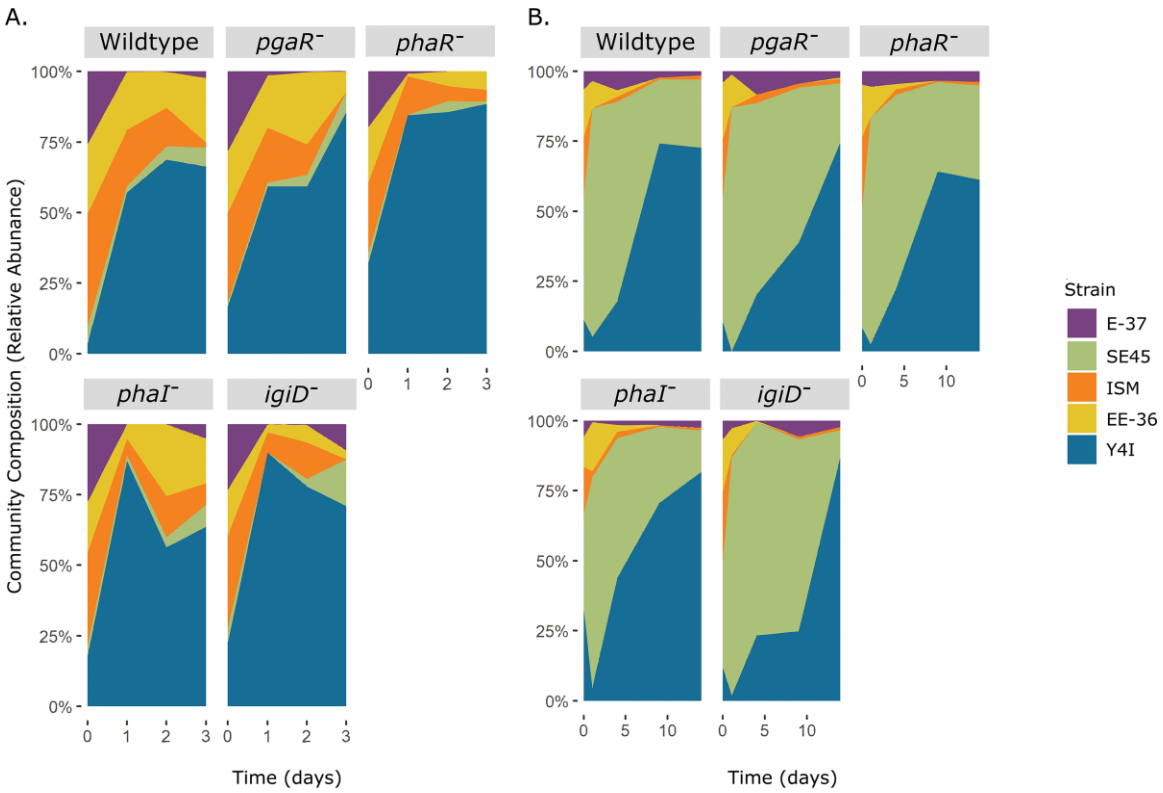

Appendix Figure D.2: Relative abundance of biofilm community members over time in a complex (A) and defined (B) medium. Each synthetic community is designated by the Y4I variant included (gray boxes): Wild type Y4I, *pgaR*::Tn5-Km^{R} (*pgaR*$^{-}$), *phaR*::Tn5-Km^{R} (*phaR*$^{-}$), *phaI*::pKNOCK (*phaI*$^{-}$), *igiD*::Tn5-Km^{R} (*igiD*$^{-}$). Relative abundance was calculated from the mean CFU mL^{-1} count of at least six replicates for each strain within each mix and the total CFU mL^{-1} for each mix. Individual strains are color-coded according to the key.

($P < 0.05$). From day 0 to day 1 community structures of each synthetic community were dissimilar between growth substrates (i.e., complex versus defined media) but became more similar at later time points (**Figure D.3**). Across all time points, the structures of each community were significantly different based on growth substrate ($P < 0.05$) (**Table S.D.6** to **S.D.10**). Additionally, the structures of synthetic communities on day 1 were significantly different based on not only growth substrate but also which Y4I variant was included in the synthetic community ($P < 0.05$) (**Table S.D.8**). Each time point also was significantly different from other time points between medium types ($P < 0.05$) (**Table S.D.6** to **S.D.10**). The alpha diversity of each synthetic community dropped from day 0 to day 1, corresponding to a drop in evenness of the community structure (**Figure S.D.5**).

Secondary metabolites influence biofilm interactions.

Viable cell abundance alone cannot fully explain the interactions within mixed species communities. Thus, we assessed the total biofilm production of our five-member synthetic communities across both growth substrates. To determine interactions within mixed communities, biofilm production was measured in both monocultures and synthetic communities using a crystal violet assay where synthetic communities were compared to the "best" and "worst" biofilm producers in monoculture grown on glass beads (**Figure D.4** and **D.5**).

When cultures were grown on a complex medium, biofilm production was initially similar among mono- and mixed cultures (optical density at 600 nm [OD_{600}], ~0.5), except for EE-36. In this medium, EE-36 produced the most biofilm during each sampling effort (OD_{600} of 0.6, 0.79, and 1.00 on days 1, 2, and 3, respectively). The worst biofilm producer in monoculture switched from ISM (OD_{600}, 0.41) on day 1 to Y4I on days 2 (OD_{600}, 0.31), and 3 (OD_{600}, 0.41) (**Figure D.4A** to **C**). Biofilm production in synthetic communities increased over time, with synthetic communities harboring the *phaI*::pKNOCK mutant showing the greatest increase in biofilm production (from OD_{600} of 0.44 to 0.92), over the course of the experiment (**Figure D.4B** and **C**). Biofilm formation in all synthetic communities increased over time compared with that of individual monoculture controls (see **Figure S.D.6** in the supplemental material).

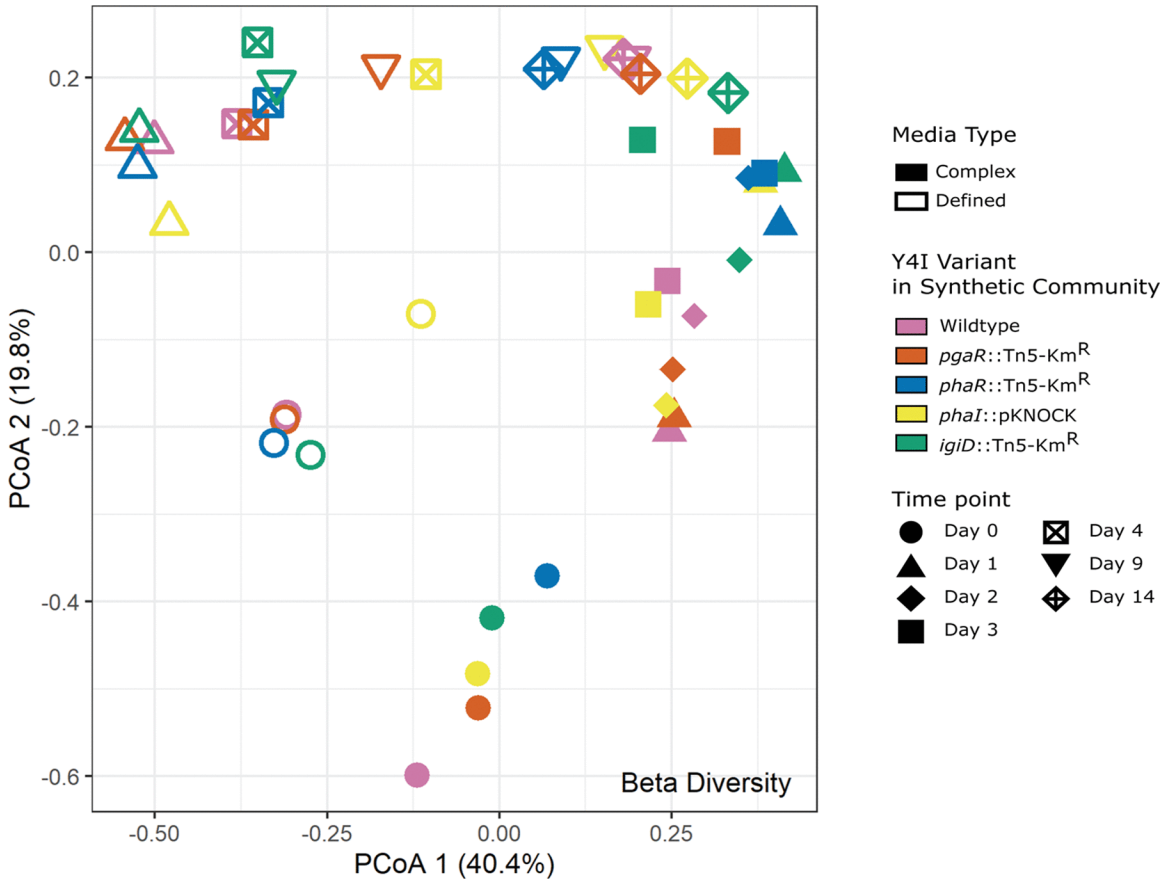

Appendix Figure D.3: PCoA plot using Bray Curtis Dissimilarity Index to determine beta diversity between each carbon source, mixed community, and time point. Media type is denoted by closed (complex medium) and open shapes (defined medium), synthetic community harboring Y4I variants are differentiated by color, and time point is denoted by shape. At day 0, synthetic communities were not significantly different ($p < 0.05$). Statistical analyses are provided in **Tables S.D.6-10**.

Similar to biofilm production observed on day 1 with the complex medium, biofilm production for all mono- and mixed cultures was comparable, with the exception of E-37, in a defined medium containing a less labile carbon source (*p*-coumaric acid). Initially, E-37 produced the least biofilm in monoculture (OD_{600}, 0.36) (**Figure D.5A**). However, the worst biofilm producer switched between ISM (OD_{600} of 0.35, day 4), and Y4I variants (wild type [OD_{600} of 0.43, day 14] and *phaR*::Tn5-Km^r [OD_{600} of 0.38 0, day 4]) at later time points (**Figure D.5B to D**). Y4I variants produced the most and least biofilm throughout this experiment. On day 1 and day 4, the wild type produced the most biofilm (OD_{600} of 0.42 and 0.45, respectively), and the *phaI* variant produced the most biofilm on day 14 (OD_{600} of 0.51) (**Figure D.5A, C, and D**). Synthetic communities harboring a *pgaR* variant produced slightly more biofilm (OD_{600} of 0.46) than the best biofilm producer in monoculture on day 4, whereas communities containing the *igiD* variant produced less biofilm ($OD600_{nm}$ = 0.41) than the worst biofilm former in monoculture on day 14 (**Figure D.5B and D**; **Table S.D.2**). Synthetic communities harboring Y4I variants produced similar amounts of biofilm compared with their monoculture counterparts, with the following exceptions: at day 4, synthetic communities containing the *pgaR* variant had significantly ($P < 0.05$) more biofilm production than its monoculture counterpart (**Figure D.5B**, see **Figure S.D.7** in the supplemental material). Conversely, the synthetic community, including the *igiD* variant showed a decrease in biofilm formation compared with its monoculture counterpart at day 14 (**Figure D.5B**, **Figure S.D.7**). In general, synthetic communities demonstrated a similar modality in biofilm production compared with their monoculture counterparts as either an increase in biofilm production over time or variations of cyclic increases and decreases in biofilm formation.

A Pearson correlation coefficient was used to analyze the growth dynamics of individual species within synthetic communities harboring Y4I variants over time. We focused on investigating interactions observed in minimal media, as the potential influence of secondary metabolite production is more evident within these communities (**Figure D.6**; see **Figure S.D.8** in the supplemental material). In synthetic communities harboring Y4I variants capable of producing indigoidine, strong negative correlations between Y4I and the community members it has been demonstrated to inhibit, namely, E-37 and EE36 ($\rho > -0.75$, $n = 3$) (see **Table S.D.5** in the supplemental material), were observed. This negative correlation was evident in both medium

Appendix Figure D.4: Biofilm production of monoculture community members and five-member synthetic communities in complex medium over time (A-C). Synthetic communities are designated by the Y4I variant in each community [Wild type Y4I, *pgaR*::Tn5-Km^R (*pgaR*$^-$), *phaR*::Tn5-Km^R (*phaR*$^-$), *phaI*::pKNOCK (*phaI*$^-$), *igiD*::Tn5-Km^R (*igiD*$^-$)]. Each data point (black dots) was collected by quantifying biomass production using a standard crystal violet assay. Error bars represent the standard error of the mean of three biological replicates and three technical replicates. Some error bars are not visible due to low variance between replicates. Gray dotted line represents biomass production of the best biofilm former in monoculture, red dotted line indicates biomass production of the worst biofilm former in monoculture at that time point.

Biologically relevant statistical significances are depicted ($p < 0.05$ [*], 0.01 [**], 0.001 [***]). For full statistical results see **Table S.D.1.**

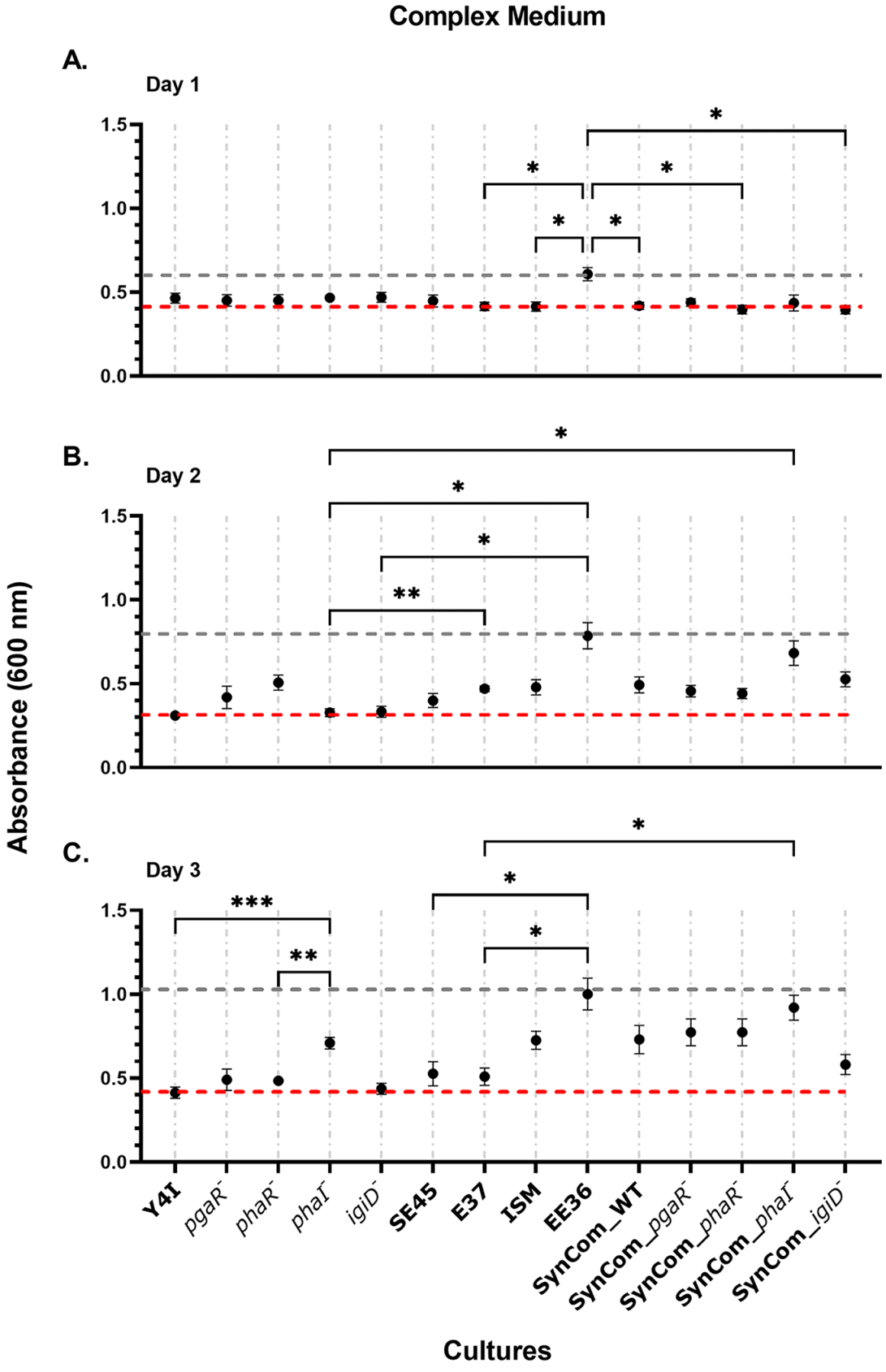
Complex Medium
A.
Day 1
B.
Day 2
C.
Day 3
Absorbance (600 nm)
1.5
1.0
0.5
0.0
*
**
***
Y4I
pgaR-
phaR-
phaI-
igiD-
SE45
E37
ISM
EE36
SynCom_WT
SynCom_pgaR-
SynCom_phaR-
SynCom_phaI-
SynCom_igiD-
Cultures

Appendix Figure D.5: Biofilm production of monoculture community members and five-member synthetic communities in defined medium over time (A-D). Synthetic communities are designated by the Y4I variant in each [Wild type Y4I, *pgaR*::Tn5-Km^R (*pgaR*$^-$), *phaR*::Tn5-Km^R (*phaR*$^-$), *phaI*::pKNOCK (*phaI*$^-$), *igiD*::Tn5-Km^R (*igiD*$^-$)]. Each data point (black dots) was collected by quantifying biomass production using a standard crystal violet assay for at least six replicates for mixed and monocultures. Error bars represent the standard error of the mean. Some error bars are not visible due to low variance between replicates. Gray dotted line represents biomass production of the best biofilm former in monoculture, red dotted line indicates biomass production of the worst biofilm former in monoculture at that time point. Asterisks represent statistical significance between cultures ($p < 0.05$ [*], 0.01 [**]). ANOVA table of significance can be found in **Table S.D.2.**

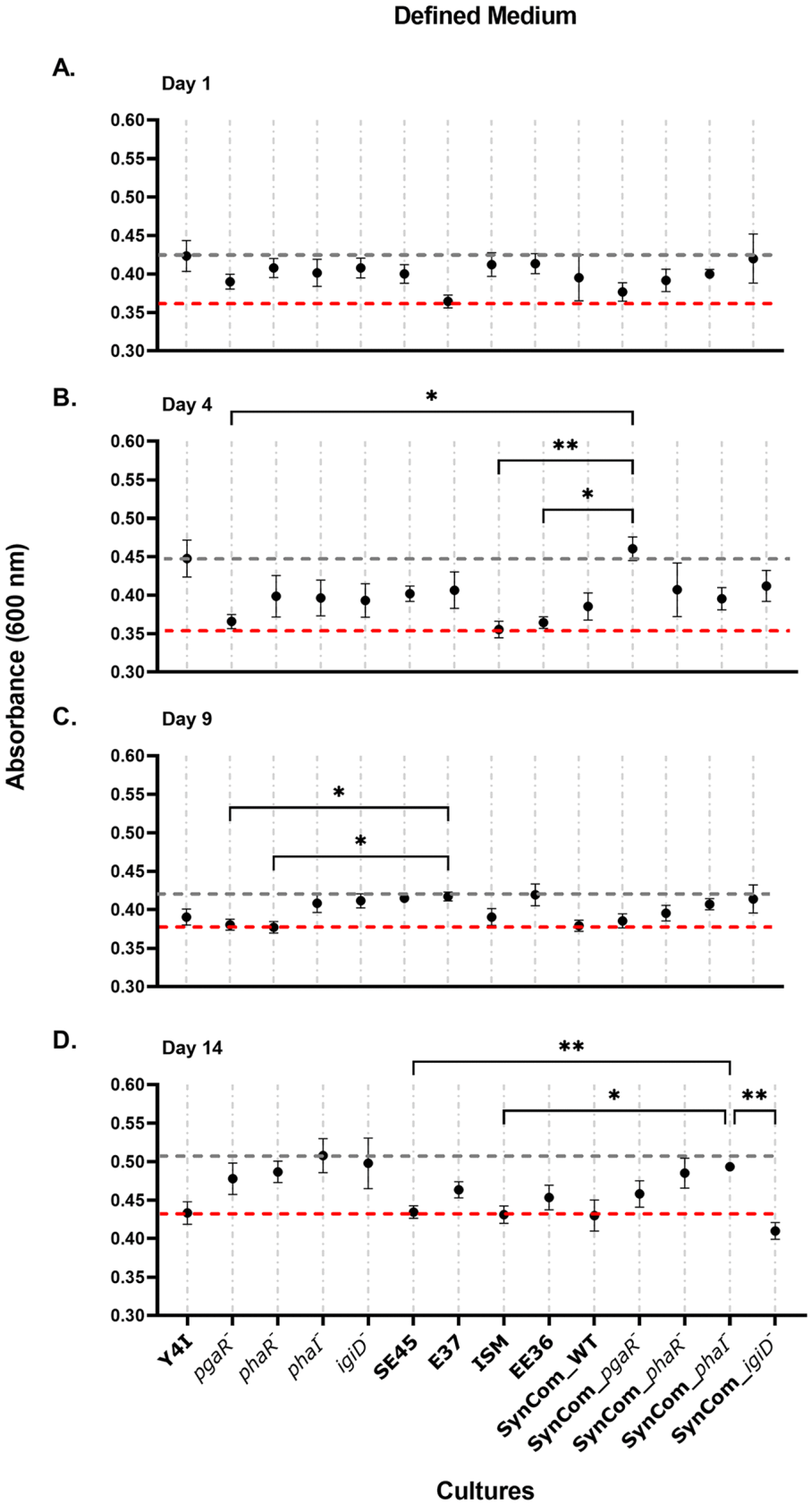
Defined Medium
A.
Day 1
B.
Day 4
C.
Day 9
D.
Day 14
Absorbance (600 nm)
0.60
0.55
0.50
0.45
0.40
0.35
0.30
*
**
Y4I
pgaR-
phaR-
phaI-
igiD-
SE45
E37
ISM
EE36
SynCom_WT
SynCom_pgaR-
SynCom_phaR-
SynCom_phaI-
SynCom_igiD-
Cultures

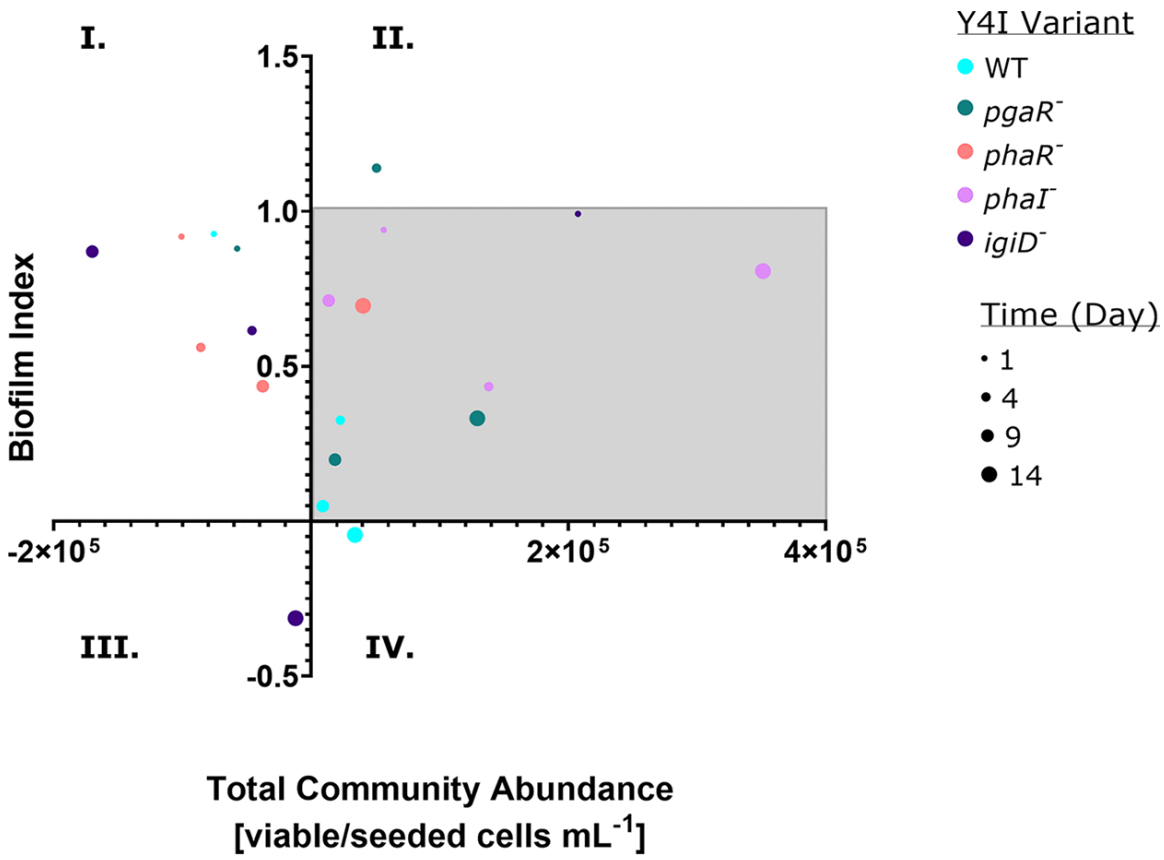

Appendix Figure D.6: Biofilm production index of synthetic communities harboring Y4I variants in defined medium over time. Y4I variants within communities are color coded according to the legend and time point varies by size of dots. Each data point represents the average of at least six replicates. Communities outside of gray box indicate greatest evidence for community cooperation (II) or competition (I, III, IV).

types. Most community members were positively correlated with each other, excluding Y4I. These positive correlations became more evident with the inclusion of Y4I variants in which secondary metabolite production was disrupted within synthetic communities. For example, ISM is positively correlated with E-37 or EE36 ($\rho > 0.65$, $n = 3$) (**Table S.D.5**) within communities harboring Y4I variant with disruptions to their QS systems. These correlations were significant ($P < 0.05$) only in synthetic communities harboring the *phaI* variant. ISM is positively correlated only with both E-37 and EE36 when the indigoidine synthase gene is disrupted ($\rho > 0.65$, $n = 3$) (**Table S.D.5**).

Discussion

Here, we assessed the effect of secondary metabolite production and growth substrate on community dynamics and composition in a five-member synthetic community. It has been hypothesized that competitive interactions shape community structure while cooperative interactions stabilize it, thereby affecting the overall function and dynamic of the biofilm (47). In order to visualize these shifts in community dynamics in response to secondary metabolite mutant variants of one strain (Y4I) within a given community, we compared biofilm production and total viable cell abundance over time. We considered an increase in biofilm formation compared with the best biofilm producer in monoculture without the loss of total cell viability in the community to represent cooperation. In contrast, a decrease in biofilm formation compared with the worst biofilm producer in monoculture, or a decrease in viability in the community, represented community competition. We found community cooperation to become increasingly evident in synthetic communities harboring various Y4I secondary metabolite mutants. When secondary metabolite production, such as QS or antimicrobials, are disrupted in Y4I by genetic manipulation, community members have more similar growth dynamics to one another over time, suggesting overall community cooperation. The influence of secondary metabolite production on community dynamics was most evident within the synthetic community where wild-type Y4I was replaced with a QS mutant (*pgaR* variant). This community shifts toward cooperation over time in the presence of either growth substrates, but it is most noticeable in the *p*-coumaric acid growth condition (**Figure D.6** and **Figure S.D.8**). The *pgaR* variant is impaired in both QS pathways harbored by the parental strain and is unable to produce indigoidine (41, 42). This information may account for the measurable shift toward community

cooperation in the synthetic community harboring this mutant when in the presence of a defined growth medium. Given access to more diverse growth substrates (i.e., complex medium), however, fewer competitive interactions were observed (**Figure S.D.8**). This finding is analogous to synthetic soil communities in which biofilms evolved to decrease negative interactions and increase cometabolism among community members (28). Further evidence of cooperation is demonstrated by communities containing a different QS mutant, the *phaI* variant. Cooperation within this synthetic community is exhibited by continual increase in biofilm formation and the stability of community member abundance over time (**Figure D.2B and D.5**). The *phaI* variant is also impaired in indigoidine production as well as in the synthesis of its cognate AHL (42). Inclusion of this mutant in synthetic communities allowed us to explore the possibility of QS cross talk between related species.

QS cross talk has been modeled to contribute to competition or cooperation in diverse microorganisms (48). Possible evidence for QS cross talk within these mixed communities is apparent within the synthetic community harboring the *phaI* variant. Three community members (E37, ISM, and EE36) that were always positively correlated in synthetic communities harboring QS mutants and were significantly correlated in the synthetic community containing *phaI* may share overlapping AHLs. Preliminary evidence indicates AHLs with masses corresponding to 3OHC10-HSL (E-37 and ISM), and C5-HSL (E-37, EE36, and ISM) as well as C12-HSL (all examined strains) (**Figure S.D.1**). The *phaI* mutant variant is unable to produce 3OHC12:1-HSL but is able to sense both AHLs predominantly produced by Y4I (C8-HSL and 3OHC12:1-HSL) (42). It is plausible the QS systems in Y4I are able to recognize AHLs with similar masses and acyl-chain lengths, including those produced by community members (e.g., C12-HSL) (**Figure S.D.1B**). Previous reviews have discussed the promiscuity of AHL ligand binding with noncognate LuxR-like regulatory proteins (49–51). Preliminary cross-talk experiments suggest that the *phaR* and *phaI* mutants produce indigoidine in response to extracellular metabolites produced by other community members. However, the exact metabolite eliciting this response is unknown. Future efforts to determine the molecular structure of these metabolites produced by community members may lead to more robust evidence for QS cross talk. Given that the *phaRI* pathway in Y4I is likely involved in regulating biofilm formation (42), the putative cross talk between strains presented here may contribute to the increased biofilm formation

observed in the synthetic community harboring the *phaI* mutant. This type of QS cross talk has been demonstrated in host-microbe models. For example, in plant-associated biofilms, cross talk among rhizosphere bacteria is hypothesized to enhance the biosynthesis of secondary metabolites, compared with nonadherent soil community counterparts, thereby increasing biofilm formation (52).

Community-level competition is evident in synthetic communities harboring either wild-type Y4I or the *igiD* variant (**Figure D.6**). Given that the *igiD* mutant is unable to inhibit community members in pairwise inhibition assays and yet possesses functional QS systems (**Table D.1**) (see references 41 and 42), interactions beyond those mediated by antimicrobials contribute to competition within these synthetic biofilms. Using a Pearson correlation analysis to investigate how every strain responded to each Y4I variant, we observed more positive correlations and fewer strongly negative correlations between community members within synthetic communities containing the *igiD* variant than communities harboring other Y4I variants. This finding suggests less competition among individual community members with those communities harboring the *igiD*-deficient strain. Overall, WT Y4I displays a strong competitive advantage against other members within synthetic communities. Each member of the synthetic community was negatively correlated with WT Y4I in the Pearson correlation coefficient matrix regardless of growth medium (see **Table S.D.4 and S.D.5** in the supplemental material). The findings presented here provide support that secondary metabolite production influences growth dynamics within a biofilm and that Y4I orchestrates community dynamics within these synthetic communities through competitive interactions. These results support previous findings that the majority of species interactions may be competitive in natural environments (53, 54).

In a previous study, primary growth substrates have been shown to impact *Roseobacteraceae* community composition (31). Another study demonstrated that nutrient availability and concentration impact microbial community interactions, specifically growth inhibition (55). Here, we show that synthetic community structures stabilize in a similar manner independent of the growth substrate. Each medium type significantly impacted community structure at day 1 and all subsequent time points. The Y4I variants experienced growth inhibition in liquid monoculture supplemented with *p*-coumaric acid. However, these strains dominate in multispecies communities provided this aromatic acid as a sole carbon substrate. The deviation

in growth dynamics between liquid monocultures and multispecies biofilms across all Y4I variants can be explained by the following two possibilities: (i) evidence for cometabolism and (ii) biofilm-mediated defense against harmful substrates. Two strains, namely, SE45 and E-37, have been reported previously to use *p*-coumaric acid as a sole carbon source. An intermediate of *p*-coumaric acid catabolism is *p*-hydroxybenzoic acid (POB), which all community members can degrade through the protocatechuate pathway (31, 39). The degradation of *p*-coumaric acid into exudate metabolites, such as POB, may explain the delayed increase in Y4I variants in these biofilm communities. Alternatively, *p*-coumaric acid is posited to be toxic at high concentrations (>5 mM) (31). It is possible that in a multispecies biofilm, Y4I is protected against the inhibitory action of these metabolites. Previous reports support the protective nature of biofilms against toxic compounds resulting in increased bacterial stress tolerance (56).

The observations presented here provide a direct link between secondary metabolite production in the form of AHLs and antimicrobials on biofilm community structure and dynamics. As AHLs and antimicrobial production are commonly associated with mixed-species biofilms, these findings have broad relevance. Our results support that primary surface colonizers, such as those in *Roseobacteraceae*, influence community interactions through their diverse metabolic capabilities, perhaps irrespective of growth substrate. This conclusion may be particularly relevant in natural systems where growth substrates fluctuate. This work lays the foundation for understanding how small diffusible molecules, including those involved in cell-to-cell communication, influence cooperative and competitive social behaviors within microbial biofilm communities in marine ecosystems.

Materials and Methods

Synthetic community bacterial strains, growth conditions, and maintenance.

A synthetic, five-member *Roseobacteraceae* community was used to assess the role of secondary metabolites on marine biofilm community structure and formation. Four of the five strains were isolated previously from southeastern United States estuaries or coastal waters (*Rhodobacterales* strain Y4I, *Sagittula stellata* sp. E-37, *Citreicella* sp. SE45, and *Sulfitobacter* sp. EE-36 [57]). The final strain, *Roseovarius nubinhibens* ISM, was isolated previously from the Caribbean Sea (46). Previously established Y4I secondary metabolite mutants *igiD*::Tn5-Km^r, *pgaR*::Tn5-Km^r, *phaR*::Tn5-Km^r, and *clpA*::Tn5-Km^r were generated

using a mini Tn5 transposon system (5, 41). The *phaI*::pKNOCK mutant was generated previously using targeted insertional mutagenesis (42). All Y4I mutant variants carry a chromosomally located kanamycin resistance gene. The growth rates of all mutants in liquid medium have been assessed previously and found to be the same as that of the wild type (5, 42), indicating no gross growth defects.

For routine maintenance, all strains were maintained on yeast extract tryptone and sea salt (YTSS) agar (per L, it included 15 g Instant Ocean [Thermo Fisher Scientific], 15 g agar [Thermo Fisher Scientific], 4 g tryptone, and 2.5 g yeast extract). Y4I strains were passaged routinely in 20% YTSS (per L, it included 15 g Instant Ocean, 0.8 g tryptone, and 0.5 g yeast extract) to reduce flocking in these strains. Each strain was passaged onto basal medium (BM; per L it included 8.7 mM KCl, 8.7 mM $CaCl_2$, 43.5 mM $MgSO_4$, and 174 mM NaCl with 225 μM K_2HPO_4, 13.35 mM NH_4Cl, 71 mM Tris-HCl [pH 7.5], 68 μM Fe-EDTA, trace metals [7.85 mM nitriloacetic acid, 0.53 mM $MnSO_4 \times H_2O$, 0.42 mM $CoCl_2 \times 6H_2O$, 0.35 mM $ZnSO_4 \times 7H_2O$, 0.038 mM $CuSO_4$, 0.11 mM $NiCl_2 \times 6H_2O$, 1.16 mM Na_2SeO_3, 0.41 mM $Na_2MoO_4 \times 2H_2O$, 0.33 mM $Na_2WO_4 \times 2H_2O$, and 0.25 mM $Na_2SiO_3 \times 9H_2O$], and trace vitamins [0.0020% vitamin H {biotin}, 0.0020% folic acid, 0.0100% pyridoxine-HCl {B6}, 0.0050% riboflavin {B2}, 0.0050% thiamine {B1}, 0.0050% nicotinic acid, 0.0050% pantothenic acid {B5}, 0.0001% cyanocobalamin {B12}, 0.0050% p-aminobenzoic acid]) containing either 10 mM sodium acetate or 2 mM p-hydroxybenzoic acid (POB). All strains were incubated at 30°C in the dark unless otherwise noted.

Surface attachment to glass beads.

Surface attachment to glass beads was assessed as described previously by Cude et al. (5). Briefly, sterilized 4-mm glass beads (Pyrex, Corning Incorporated Corning, NY) in a 96-well polystyrene plate (Costar, Corning Incorporated Corning, NY) were inoculated in triplicate with the following strains in monoculture: E-37, SE45, EE-36, ISM, wild-type Y4I, *igiD*::Tn5-Km^r, *pgaR*::Tn5-Km^r, *phaR*::Tn5-Km^r, and *phaI*::pKNOCK. Cells were allowed to attach to glass beads for 12 h, 24 h, and 48 h. Following incubation, glass beads were removed from wells, and cells were dislodged from beads as described previously (5, 42). Following extraction from glass beads, cells were serially diluted and plated onto YTSS and incubated at 25°C.

Synthetic community biofilm experiment design.

All experiments assessed interactive effects of QS by comparing viable cell counts or biofilm biomass in a mixed species community containing different Y4I variants using a complex medium (20% YTSS) or a defined medium containing 2 mM *p*-coumaric acid as the sole carbon source. Five different synthetic community mixes were assembled. Each synthetic community consisted of E-37, SE45, EE-36, ISM, and one of the following Y4I variants: wild-type Y4I, *pgaR*::Tn5-Km^r, *phaR*::Tn5-Km^r, or *phaI*::pKNOCK, *igiD*::Tn5-Km^r.

For complex medium experiments, overnight monoculture liquid YTSS cultures were diluted 10-fold in fresh YTSS and allowed to grow until mid-exponential growth was reached (~3 h). For each culture, cells were harvested by transferring 1-mL culture to a 1.5-mL centrifuge tube and spun at 8,000 rpm for 10 min. The supernatant was withdrawn, and cells were resuspended in fresh YTSS. All cultures were diluted to ~1 × 10^6 cells mL^{-1}. One milliliter of each culture was combined to establish a master mix of ~5 × 10^6 cells mL^{-1} mixed cultures containing E-37, SE45, EE-36, ISM, and a Y4I variant. Synthetic mixed cultures were then diluted to 1 × 10^6 cells mL^{-1} and used to inoculate 96-well plates with a final concentration of ~1 × 10^5 cells mL^{-1}. Final dilutions were plated to assess cell abundance of mixed cultures at the time of inoculation. Monoculture controls (~10^5 cell mL^{-1}) were included in both viable cell abundance and total biomass assays. Six replicates of each plate were made to assay viable cell abundance and total biomass on glass beads over time.

Following the inoculation of 96-well plates, each plate was wrapped with dampened cellulose fiber sheets, stored in a sealing high-density polyethylene (HDPE) bag, and incubated at 30°C. At 20 h (day 1), 44 h (day 2), and 68 h (day 3), cells were extracted from beads. Viable cells, community structure, and biofilm biomass were assessed as described below.

For defined medium containing *p*-coumaric acid, the experimental design was similar to the complex medium, with the following exceptions: all cultures were primed by inoculation into BM containing 2 mM POB and were allowed to grow overnight at 30°C. POB cultures (10 mL) were spun down and washed with BM to remove any residual carbon. BM containing *p*-coumaric acid (2 mM) was inoculated with 0.01 to 0.1 mL of culture to achieve an inoculum of 1 × 10^6 cells mL^{-1}. Cells were extracted for assaying at 24 h (day 1), 96 h (day 4), 216 h (day 9),

and 336 h (day 14). Eight replicates of each plate were made to assay viable cell abundance and total biomass on glass beads over time.

(i) Community structure.

Attached cells were extracted as described above for surface attachment assays and plated onto YTSS agar and allowed to incubate at 25°C until colony morphology was discernible (~5 days). The colony morphology of each strain was readily identifiable except for Y4I mutant variants, which lacked the blue pigmentation diagnostic of the wild-type strain (5, 31, 41, 42). Thus, all mixed cultures containing Y4I mutant variants were also plated onto YTSS containing kanamycin (50 μg/mL) as a control to differentiate between Y4I variants from other community members.

(ii) Biofilm biomass.

The total biomass on biofilm-grown cultures was assessed by performing a crystal violet stain on glass beads as described previously (42). Briefly, liquid was aspirated out of wells. Glass beads were washed with a 1.5% sea salt solution (Instant Ocean) to remove loosely attached cells. Glass beads were extracted using a vacuum apparatus and moved to a clean 96-well plate. Cells attached to glass beads were stained using a 2% crystal violet solution and solubilized with 95% EtOH. Absorbance was read at 600 nm using a microplate reader (Bio Tek Instruments, Inc.; Synergy HT multi-mode microplate reader, SN 270212).

Inhibition assays.

A factorial growth inhibition assay using synthetic community members was utilized to assess antagonistic interactions among community members. Briefly, liquid cultures of *Roseobacteraceae* strains were grown overnight in YTSS medium at 30°C with shaking. These overnight cultures were diluted 10-fold, and each of the five strains were spread evenly onto individual YTSS agar plates. All strains were grown to mid-exponential phase and then spotted (10 μL) on top of the spread plates. Y4I variants included an indigoidine null mutant (*igiD*::Tn5-Km^r) and an indigoidine hyper-producing mutant (*clpA*::Tn5-Km^r). QS mutants *pgaR*::Tn5-Km^r, *phaR*::Tn5-Km^r, and *phaI*::pKNOCK were not included in inhibition assays as they have been demonstrated previously to lack inhibitory activity (5, 41, 42). Growth inhibition assays were incubated at 30°C. Zones of clearing surrounding inhibitor organisms were assessed at 24 h postinoculation.

Data analysis.

Viable cell counts were analyzed and visualized using RStudio v1.4.1106. All viable cell count data were normalized to the mean relative abundance within replicates. Area plots were constructed based on the mean relative abundance of the strains in each mix over their respective time points for each medium type. Beta diversity analysis was performed using the bcdist() function in the ecodist package (58) for each time point for the complex medium and defined medium. Beta dispersion was calculated using the betadisper() function in the vegan package (59). The adonis() function in the vegan package was used to conduct a permutational multivariate analysis of variance (PERMANOVA) on the paired time points and on the aggregated time points for both carbon sources (59). Alpha diversity was calculated within each time point using the Shannon diversity index in the vegan package (60, 61).

Surface attachment assays and total biomass via crystal violet assays were analyzed and visualized using Prism v9.0.0 (GraphPad Software, San Diego, CA; http://www.graphpad.com). Statistical significance was calculated using a two-way analysis of variance (ANOVA). The variability of differences was corrected using Geisser-Greenhouse correction. Multiple comparisons were assessed using Dunnett's multiple comparisons for surface attachment assays and Tukey's honestly significant difference (HSD) for crystal violet assays (see **Table S.D.1** to **S.D.3** in the supplemental material).

In order to assess community dynamics of paired viable cell counts and surface attachment assays, we first generated a biofilm index for synthetic communities relative to the best and worst biofilm production in monoculture (set to 1 and 0, respectively). We then compared this biofilm index to total community abundance to visualize how the microbial community shifts over time in response to the Y4I variant included in the community. To further investigate interactions within the synthetic communities, we then assessed the correlation of each individual strain's growth dynamics over time via a Pearson correlation coefficient matrix. The Pearson correlation coefficient matrix was performed using the corr() function, subsequent visualization was done using the corrplot() function, and significance values were computed using the rcorr() function (62, 63). To compare the complex and defined medium communities, we selected correlation values that were above 0.6 or below −0.6 for both medium types to further analyze growth dynamics.

Data availability.

Code and raw data for this study are available online at https://github.com/jwalto12/RoseobacterSynComm. Bacterial strains are available upon request.

Acknowledgements

We acknowledge Hannah Edwards and Emily Bowden for technical assistance. We also thank Amanda May and Ashley Lato for their work on AHL detection and analysis.

This work was made possible by support from the NSF (Award OCE-1357242 to A.B.).

We declare no conflicts of interest.

REFERENCES

1. Leriche V, Briandet R, Carpentier B. 2003. Ecology of mixed biofilms subjected daily to a chlorinated alkaline solution: spatial distribution of bacterial species suggests a protective effect of one species to another. Environ Microbiol 5:64–71.

2. Burmølle M, Webb JS, Rao D, Hansen LH, Sørensen SJ, Kjelleberg S. 2006. Enhanced Biofilm Formation and Increased Resistance to Antimicrobial Agents and Bacterial Invasion Are Caused by Synergistic Interactions in Multispecies Biofilms †. Appl Environ Microbiol 72:3916–3923.

3. Pande S, Kaftan F, Lang S, Svatoš A, Germerodt S, Kost C. 2015. Privatization of cooperative benefits stabilizes mutualistic cross-feeding interactions in spatially structured environments. ISME J 2015 106 10:1413–1423.

4. Rao F V., Andersen OA, Vora KA, DeMartino JA, Van Aalten DMF. 2005. Methylxanthine Drugs Are Chitinase Inhibitors: Investigation of Inhibition and Binding Modes. Chem Biol 12:973–980.

5. Cude WN, Mooney J, Tavanaei AA, Hadden MK, Frank AM, Gulvik CA, May AL, Buchan A. 2012. Production of the antimicrobial secondary metabolite indigoidine contributes to competitive surface colonization by the marine roseobacter *Phaeobacter* sp. strain Y4I. Appl Environ Microbiol 78:4771–4780.

6. Guittar J, Koffel T, Shade A, Klausmeier CA, Litchman E. 2021. Resource Competition and Host Feedbacks Underlie Regime Shifts in Gut Microbiota. Am Nat 198:1–12.

7. Miller MB, Bassler BL. 2001. Quorum Sensing in Bacteria. Annu Rev Microbiol 55:165–99.

8. Case RJ, Labbate M, Kjelleberg S. 2008. AHL-driven quorum-sensing circuits: their frequency and function among the Proteobacteria. ISME J 2:345–349.

9. Fuqua C, Parsek MR, Greenberg EP. 2001. Regulation of Gene Expression by Cell-to-Cell Communication: Acyl-Homoserine Lactone Quorum Sensing. Annu Rev Genet 35:439–468.

10. Duerkop BA, Varga J, Chandler JR, Peterson SB, Herman JP, Churchill MEA, Parsek MR, Nierman WC, Greenberg EP. 2009. Quorum-Sensing Control of Antibiotic Synthesis in *Burkholderia thailandensis*. J Bacteriol 191:3909–3918.

11. Lyell NL, Stabb E V. 2013. Symbiotic characterization of *Vibrio fischeri* ES114 mutants that display enhanced luminescence in culture. Appl Environ Microbiol 79:2480–2483.
12. Su Y, Tang K, Liu J, Wang Y, Zheng Y, Zhang X-H. 2019. Quorum Sensing System of *Ruegeria mobilis* Rm01 Controls Lipase and Biofilm Formation. Front Microbiol 9:3304.
13. Pusic P, Sonnleitner E, Bläsi U. 2021. Specific and Global RNA Regulators in *Pseudomonas aeruginosa*. Int J Mol Sci 22.
14. Beyersmann PG, Tomasch JJ, Son K, Stocker R, Göker M, Wagner-Döbler I, Simon M, Brinkhoff T. 2017. Dual function of tropodithietic acid as antibiotic and signaling molecule in global gene regulation of the probiotic bacterium *Phaeobacter inhibens*. Sci Rep 7:730.
15. Ranieri MR, Whitchurch CB, Burrows LL. 2018. Mechanisms of biofilm stimulation by subinhibitory concentrations of antimicrobials. Curr Opin Microbiol 45:164–169.
16. Kaplan JB, Izano EA, Gopal P, Karwacki MT, Kim S, Bose JL, Bayles KW, Horswill AR. 2012. Low Levels of β-Lactam Antibiotics Induce Extracellular DNA Release and Biofilm Formation in *Staphylococcus aureus*. MBio 3:198–210.
17. Flemming H-C, Wingender J, Szewzyk U, Steinberg P, Rice SA, Kjelleberg S. 2016. Biofilms: an emergent form of bacterial life. Nat Rev Microbiol 14:563–575.
18. Decho AW, Gutierrez T. 2017. Microbial Extracellular Polymeric Substances (EPSs) in Ocean Systems. Front Microbiol 8:922.
19. Decho AW, Visscher PT, Ferry J, Kawaguchi T, He L, Przekop KM, Norman RS, Reid, RP. 2009. Autoinducers extracted from microbial mats reveal a surprising diversity of N - acylhomoserine lactones (AHLs) and abundance changes that may relate to diel pH. Environ Microbiol 11:409–420.
20. Yoshida S, Ogawa N, Fujii T, Tsushima S. 2009. Enhanced biofilm formation and 3-chlorobenzoate degrading activity by the bacterial consortium of *Burkholderia* sp. NK8 and *Pseudomonas aeruginosa* PAO1. J Appl Microbiol 106:790–800.
21. Adnan M, Alshammari E, Patel M, Ashraf SA, Khan S, Hadi S. 2018. Significance and potential of marine microbial natural bioactive compounds against biofilms/biofouling: necessity for green chemistry. Peer J 6:e5049.

22. Dang H, Lovell CR. 2016. Microbial Surface Colonization and Biofilm Development in Marine Environments. Microbiol Mol Biol Rev 80:91–138.
23. Dobretsov S, Teplitski M, Bayer M, Gunasekera S, Proksch P, Paul VJ. 2011. Inhibition of marine biofouling by bacterial quorum sensing inhibitors. Biofouling 27:893–905.
24. Chandler JR, Heilmann S, Mittler JE, Greenberg EP. 2012. Acyl-homoserine lactone-dependent eavesdropping promotes competition in a laboratory co-culture model. ISME J 2012 612 6:2219–2228.
25. Agogué H, Mallet C, Orvain F, De Crignis M, Mornet F, Dupuy C. 2014. Bacterial dynamics in a microphytobenthic biofilm: A tidal mesocosm approach. J Sea Res 92:36–45.
26. Smalley NE, An D, Parsek MR, Chandler JR, Dandekar AA. 2015. Quorum sensing protects *Pseudomonas aeruginosa* against cheating by other species in a laboratory coculture model. J Bacteriol 197:3154–3159.
27. Smith AC, Rice A, Sutton B, Gabrilska R, Wessel AK, Whiteley M, Rumbaugh KP. 2017. Albumin Inhibits *Pseudomonas aeruginosa* Quorum Sensing and Alters Polymicrobial Interactions. Infect Immun 85.
28. Ren D, Madsen JS, Sørensen SJ, Burmølle M. 2015. High prevalence of biofilm synergy among bacterial soil isolates in cocultures indicates bacterial interspecific cooperation. ISME J 9:81–89.
29. Quigley LNM, Edwards A, Steen AD, Buchan A, Fagervold SK. 2019. Characterization of the Interactive Effects of Labile and Recalcitrant Organic Matter on Microbial Growth and Metabolism. Front Microbiol 10:1–15.
30. de Souza RSC, Armanhi JSL, Arruda P. 2020. From Microbiome to Traits: Designing Synthetic Microbial Communities for Improved Crop Resiliency. Front Plant Sci 0:1179.
31. Kviatkovski I, Minz D. 2015. A member of the *Rhodobacteraceae* promotes initial biofilm formation via the secretion of extracellular factor(s). Aquat Microb Ecol 75:155–167.
32. Wagner-Döbler I, Thiel V, Eberl L, Allgaier M, Bodor A, Meyer S, Ebner S, Hennig A,Pukall R, Schulz S. 2005. Discovery of Complex Mixtures of Novel Long-Chain Quorum

Sensing Signals in Free-Living and Host-Associated Marine Alphaproteobacteria. ChemBioChem 6:2195–2206.
33. Buchan A, González JM, Chua MJ. 2019. Aerobic Hydrocarbon-Degrading Alphaproteobacteria: *Rhodobacteraceae* (Roseobacter), p. 1–13. In Taxonomy, Genomics and Ecophysiology of Hydrocarbon-Degrading Microbes. Springer International Publishing, Cham.
34. Dang H, Lovell CR. 2000. Bacterial primary colonization and early succession on surfaces in marine waters as determined by amplified rRNA gene restriction analysis and sequence analysis of 16S rRNA genes. Appl Environ Microbiol 66:467–75.
35. Dang H, Lovell CR. 2002. Seasonal dynamics of particle-associated and free-living marine Proteobacteria in a salt marsh tidal creek as determined using fluorescence in situ hybridization. Environ Microbiol 4:287–295.
36. Zan J, Liu Y, Fuqua C, Hill R. 2014. Acyl-Homoserine Lactone Quorum Sensing in the Roseobacter Clade. Int J Mol Sci 15:654–669.
37. Moghaddam JA, Jautzus T, Alanjary M, Beemelmanns C. 2021. Recent highlights of biosynthetic studies on marine natural products. Org Biomol Chem 19:123–140.
38. Buchan A, González JM, Moran MA. 2005. Overview of the marine Roseobacter lineage. Appl Environ Microbiol 71:5665–5677.
39. Bakenhus I, Dlugosch L, Billerbeck S, Giebel H-A, Milke F, Simon M. 2017. Composition of Total and Cell-Proliferating Bacterioplankton Community in Early Summer in the North Sea – Roseobacters Are the Most Active Component. Front Microbiol 0:1771.
40. Buchan A, Neidle EL, Moran MA. 2004. Diverse Organization of Genes of the β-Ketoadipate Pathway in Members of the Marine Roseobacter Lineage. Appl Environ Microbiol 70:1658–1668.
41. Newton RJ, Griffin LE, Bowles KM, Meile C, Gifford S, Givens CE, Howard EC, King E, Oakley CA, Reisch CR, Rinta-Kanto JM, Sharma S, Sun S, Varaljay V, Vila-Costa M, Westrich JR, Moran MA. 2010. Genome characteristics of a generalist marine bacterial lineage. ISME J 4:784–798.
42. Frank AM, Chua MJ, Gulvik CA, Buchan A. 2018. Functional Redundancy in the

Hydroxycinnamate Catabolism Pathways of the Salt Marsh Bacterium *Sagittula stellata* E-37. Appl Environ Microbiol 84.
43. Cude WN, Prevatte CW, Hadden MK, May AL, Smith RT, Swain CL, Campagna SR, Buchan A. 2015. *Phaeobacter* sp. strain Y4I utilizes two separate cell-to-cell communication systems to regulate production of the antimicrobial indigoidine. Appl Environ Microbiol 81:1417–1425.
44. Armes AC, Buchan A. 2021. Cyclic di-GMP Is Integrated Into a Hierarchal Quorum Sensing Network Regulating Antimicrobial Production and Biofilm Formation in Roseobacter Clade Member Rhodobacterales Strain Y4I. Front Mar Sci 8:1–12.
45. Slightom RN, Buchan A. 2009. Surface colonization by marine roseobacters: integrating genotype and phenotype. Appl Environ Microbiol 75:6027–37.
46. Maglangit F, Yu Y, Deng H. 2021. Bacterial pathogens: threat or treat (a review on bioactive natural products from bacterial pathogens). Nat Prod Rep 38:782–821.
47. Gonzalez JM, Mayer F, Moran MA, Hodson RE, Whitman WB. 1997. *Sagittula stellata* gen. nov., sp. nov., a Lignin-Transforming Bacterium from a Coastal Environment. Int J Syst Bacteriol 47:773–780.
48. González JM, Covert JS, Whitman WB, Henriksen JR, Mayer F, Scharf B, Schmitt R, Buchan A, Fuhrman JA, Kiene RP, Moran MA. 2003. *Silicibacter pomeroyi* sp. nov. and *Roseovarius nubinhibens* sp. nov., dimethylsulfoniopropionate-demethylating bacteria from marine environments. Int J Syst Evol Microbiol 53:1261–1269.
49. Liu W, Røder HL, Madsen JS, Bjarnsholt T, Sørensen SJ, Burmølle M. 2016. Interspecific Bacterial Interactions are Reflected in Multispecies Biofilm Spatial Organization. Front Microbiol 7:1366.
50. Valente RS, Nadal-Jimenez P, Carvalho AFP, Vieira FJD, Xavier KB. 2017. Signal Integration in Quorum Sensing Enables Cross-Species Induction of Virulence in *Pectobacterium wasabiae*. MBio 8.
51. Lazdunski AM, Ventre I, Sturgis JN. 2004. Regulatory circuits and communication in gram-negative bacteria. Nat Rev Microbiol 2:581–592.
52. Galloway WRJD, Hodgkinson JT, Bowden SD, Welch M, Spring DR. 2010. Quorum Sensing in Gram-Negative Bacteria: Small-Molecule Modulation of AHL and AI-2

Quorum Sensing Pathways. Chem Rev 111:28–67.
53. Hawver LA, Jung SA, Ng W-L. 2016. Specificity and complexity in bacterial quorum-sensing systems. FEMS Microbiol Rev 40:738–52.
54. Rieusset L, Rey M, Muller D, Vacheron J, Gerin F, Dubost A, Comte G, Prigent-Combaret C. 2020. Secondary metabolites from plant-associated *Pseudomonas* are overproduced in biofilm. Microb Biotechnol 13:1562–1580.
55. Leigh J, Fitter AH, Hodge A. 2011. Growth and symbiotic effectiveness of an arbuscular mycorrhizal fungus in organic matter in competition with soil bacteria. FEMS Microbiol Ecol 76:428–438.
56. Foster KR, Bell T. 2012. Competition, Not Cooperation, Dominates Interactions among Culturable Microbial Species. Curr Biol 22:1845–1850.
57. Ratzke C, Barrere J, Gore J. 2020. Strength of species interactions determines biodiversity and stability in microbial communities. Nat Ecol Evol 4:376–383.
58. Lee KWK, Periasamy S, Mukherjee M, Xie C, Kjelleberg S, Rice SA. 2013. Biofilm development and enhanced stress resistance of a model, mixed-species community biofilm. ISME J 2014 84 8:894–907.
59. Buchan A, Collier LS, Neidle EL, Moran MA. 2000. Key aromatic-ring-cleaving enzyme, protocatechuate 3,4-dioxygenase, in the ecologically important marine Roseobacter lineage. Appl Environ Microbiol 66:4662–4672.
60. Goslee SC, Urban DL. 2007. The ecodist Package for Dissimilarity-based Analysis of Ecological Data. J Stat Softw 22:1–19.
61. Oksanen J, Kindt R, Solymos M, Stevens HH, Wagner H. 2008. The vegan Package. 1.15-1.
62. Fisher RA, Corbet AS, Williams CB. 1943. The Relation Between the Number of Species and the Number of Individuals in a Random Sample of an Animal Population. J Anim Ecol 12:42.
63. Hurlbert SH. 1971. The Nonconcept of Species Diversity: A Critique and Alternative Parameters. Ecology 52:577–586.
64. Harrell Jr. FE, Dupont C. 2021. Hmisc: Harrell Miscellaneous. 4.6–0.
65. Wei T, Simko V. 2021. R package “corrplot”: Visualization of a Correlation Matrix. Version 0.91.

66. Cude WN, Buchan A. 2013. Acyl-homoserine lactone-based quorum sensing in the Roseobacter clade: Complex cell-to-cell communication controls multiple physiologies. Front Microbiol 4:336.

VITA

Jill Walton was born in Virginia and moved between Virginia, Maryland, and South Carolina throughout her childhood. In 2020, she obtained a Bachelor of Science degree in Microbiology from Clemson University in Clemson, SC with minors in Sustainability and Biological Science. Jill moved to Knoxville, TN in 2020 to pursue a Doctor of Philosophy in Microbiology at the University of Tennessee. Jill has currently been interning with the American Society for Microbiology working on bioeconomy policy and hopes to transition into the science policy sector after her graduation.